

ESA STUDY CONTRACT REPORT –**Deliverable D 1.1****Review of the literature and standards**

ESA Contract No: 400114452/15/ NL/NDe	SUBJECT: Milestone 2, D 1.1 Review of the literature and standards	CONTRACTOR: Riga Technical University, Institute of Materials and Structures
* ESA CR()No:	No. of Volumes:1 This is Volume No:1	CONTRACTOR'S REFERENCE: 62518 (bidder code)
ABSTRACT: <p>The aim of current deliverable on literature review is to summarise and to analyse the present state of art in analysis, testing and validation of honeycomb composite sandwich panels. The research was conducted to address several manufacturing issues - among others facing skin materials and lay-ups, honeycomb core types with different thickness, cell size and cell wall thickness proportions, adhesives used to assembly the panel. Secondly testing methods was addressed start from standard tension and compression for components up to full scale sandwich panels. This has turned out to become a core chapter describing a variety of methods, their boundary conditions, pros and cons in order to proceed with most efficient methods in project phase. Furthermore current state of art in numerical modelling has been analysed as well. Where it is required to considering intrinsic and extrinsic variables. Furthermore review on non-destructive testing techniques applicable to sandwich panels has been examined and will be further included in research process. Finally the attention was focused on previous funded research projects in order to map the key players and scientific achievements so far and to build the current project coherently on outlined findings and conclusion.</p>		
<p>The work described in this report was done under ESA Contract. Responsibility for the contents resides in the author or organisation that prepared it.</p>		
<p>Names of authors: Kaspars Kalniņš; Guntis Japiņš; Eduards Skuķis; Oļģerts Ozoliņš; Edgars Labans.</p>		
** NAME OF ESA STUDY MANAGER:	** ESA BUDGET HEADING:	
DIV: DIRECTORATE:		

Contents	
1	Summary 5
2	Introduction 5
3	Sample manufacturing 8
3.1	Facing skins 8
3.1.1	Reinforcement fibers..... 8
3.1.2	Matrix resins 13
3.1.3	Facing skin composites 15
3.1.4	Facing skin lay-up..... 16
3.2	Core 22
3.3	Sandwich panel manufacturing 31
3.3.1	Skin manufacturing 32
3.3.2	Adhesives 35
3.3.3	Honeycomb preparation 37
3.3.4	Panel assembly 39
3.3.5	Panel cutting 43
3.4	Reinforcement of specimen's ends 44
4	Experimental procedures 46
4.1	Introduction to experimental procedures 46
4.2	Variables 48
4.3	Testing of honeycomb core 52
4.3.1	Flatwise compression: ASTM C365 & MIL-STD-5.2.1 53
4.3.1	Honeycomb node tension: ASTM C363 & MIL-STD-5.1.8..... 56
4.3.2	Honeycomb shear properties: ASTM C273 57
4.4	Testing of sandwich panels 59
4.4.1	Edgewise compression: ASTM C364 & MIL-STD-401B 60
4.4.2	Compression of sandwich beam: ASTM D5467 65
4.4.3	Sandwich panel flatwise tension: ASTM C297..... 67
4.4.4	Climbing drum peel test: ASTM D1781..... 69
4.4.5	Long beam flexure test: ASTM D7249..... 71
4.4.6	Beam Shear Strength: ASTM C394..... 72
5	Estimation of damage tolerance 73
5.1	Step 1: Introduction of artificial damage 73
5.1.1	Summary 73
5.1.2	Threshold value 73
5.1.3	Damage and damage types..... 73

5.1.4	Definition of appropriate damage size	80
5.1.5	Damage resistance to a concentrated quasi-static indentation ASTM:D6264	82
5.1.6	Damage resistance to a drop-weight impact event: ASTM 7136	83
5.1.7	Damage Resistance of sandwich panels ASTM D7766.....	84
5.2	Step 2: Measurement of residual strength.....	87
5.2.1	Compression after impact summary	87
5.2.2	Compression-after-impact properties of oriented fibre-resin composites: SACMA SRM 2-88	98
5.2.3	Standard tests for toughened resin composites: NASA 1 092	98
5.2.4	Compressive Residual Strength Properties: ASTM D7137.....	99
5.2.5	Bending after impact summary	101
6	Damage & defect monitoring.....	102
7	Represent countries and departments. Foundation. Projects.....	106
8	Conclusions.....	115
9	References.....	115

List of abbreviations

BAI	bending after impact
BVID	barely visible impact damage
C	cylindrical
C/E	carbon epoxy
CAI	compression after impact
CFRP	carbon fiber reinforced plastic
Dept.	department
DW	drop weight
FE	flat edged
HOBE	honeycomb before expansion
HS	hemispherical
I	impact
LVDT	linear variable differential transformer
NASA	National Aeronautics and Space Administration
NDI	non-destructive inspection
P	Pendulum
PAS	polyarylene sulfide
PEEK	polyetheretherketone
PPS	polyphenylene-sulfide
QI	quasi-isotropic
QS	Quasi-static
Ref.	reference
RCS	residual compression strength
S	Spherical
SACMA	Suppliers of Advanced Composite Materials Association
T	Thickness
T _g	glass transition temperature
UD	unidirectional

The definition of the terms

Damage resistance – ability of material to resist destruction. Within the topic of review the damage is caused by dynamic or static out of panel's plane concentrated load usually by hemispherical indenter.

Damage tolerance – material susceptibility to damage. How large is the part of residual strength of damaged panel in comparison to intact panel.

1 Summary

The aim of current literature review is to collect information about several topics. First one is the typical sandwich panel constructions (including facing skin materials and lay-ups, honeycomb cores with different thickness, cell size and cell wall thickness, adhesives used to assembly the panel and manufacturing procedure). Second topic could be testing methods for sandwich panels. This is large chapter describing a variety of methods, their boundary conditions, pros and cons. Also there is need for considering intrinsic and extrinsic variables, review nondestructive testing techniques applicable to sandwich panels. In the end attention will be focused on financiers of reviewed researches and departments where researches were carried out.

2 Introduction

Sandwich panels, as implied by the name, are layered structures, typically featuring two thin sheets of stiff, (relatively) high-density material bonded to a thick inner core of soft, low-density material [1]. One of the high-performance sandwich structures is based on honeycomb materials which consists of array of open cells, formed from very thin sheet material by attaching many sheets one to another (Figure 2.1.) [2]. Sandwich structures are known for their high stiffness and strength to weight ratios. Nowadays these composites are widely used in various industries including aerospace industry specifically for aircraft structures and satellite launch vehicles [3, 4]. Improved manufacturing technologies with new combinations of honeycomb core-face sheet, resulted with high toughness and cost competitiveness materials [5]. Fiber usage in the commercial aerospace sector is growing. Commercial planes such as Boeing 767 and the Airbus A320 utilize two to three times more graphite fiber per plane than is used in older commercial models. The satellites ECS1 and AMSAT developed by Aerospatiale, France, feature two of the largest carbon–fiber reinforced honeycomb structures made in Europe. A sandwich structure reinforced with high modulus carbon fiber is used for the dual system capsule. The fiber, Grafil HM-S, provides exceptional dimensional rigidity for extremely low weight and matches very specific resonance characteristics required in the design. The fiber in epoxy resin is laminated to form composite skins using prepreg materials. The same grade of carbon fiber is also used in the manufacture of the actuator control struts for the second stage motor of the Ariane launcher [6].

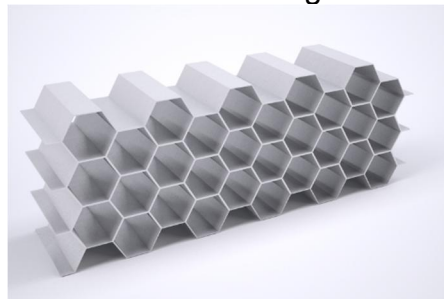


Figure 2.1. Hexagonal honeycomb cells

Figure 2.2. shows a typical honeycomb sandwich panel which is made off two facings (also called as skins), adhesive film and honeycomb core [2]. In this review focus will be on sandwich panels which consists of aluminum honeycomb core and carbon fiber reinforced plastic facings.

First aluminum honeycomb sandwich panel which also had aluminum facings has been made in 1945. It could be considered as first major breakthrough in honeycomb sandwich panel technology [2].

Apart from a number of advantages listed before, the main reason for using honeycomb constructions is to save weight [3, 2, 7,]. Table 1.1. compares the strength and stiffness values of different honeycomb structures made using a 1.6 mm thick piece of aluminum split in half as the top and bottom facings of the sandwich. The sandwich on the far right is 37 times stiffer than the flat aluminum sheet and 7 times stronger in bending strength, yet it only weighs 9% more than the solid plate [2].

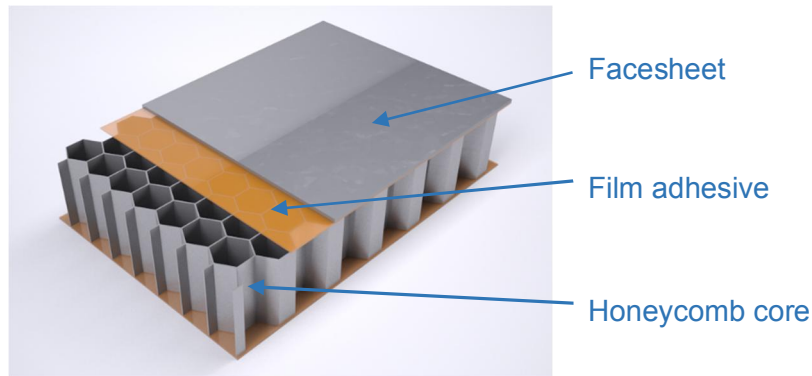


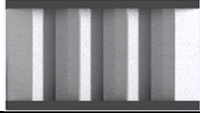


Figure 2.2. Honeycomb sandwich panel [8]

Table 2.1. Honeycomb sandwich efficiency

			
Relative thickness	1t	2t	4t
Relative stiffness	1	7	37
Relative bending strength	1	3	7
Relative weight	1	1.08	1.09
Assumes 1.626 mm aluminum, 48 kg/m ³ , 1.4 N/m ² adhesive			

Despite numerous advantages secondary difficulties are ignored. One of these secondary difficulties is the damage tolerance [9]. Current sandwich structures suffer severe strength reduction under compressive loading conditions, because they are susceptible and vulnerable to foreign object impact. Such impact may be caused by tool drop during maintenance, hail strike in service or other objects. For this reason, a significant amount of work has been done by different researchers to address the problem of low-velocity impact on sandwich structures [4, 7, 10]. Other disadvantages are the design of interface sections, the introduction of concentrated loads and the fixing of heavy equipment (these items need supplementary rings and inserts), the uncontrolled amount of adhesive, potting resin for inserts, and the interfaces of honeycomb core panels [9]. As a result, a multitude of damage mechanisms such as skin delamination and fracture, skin-core debonding, core crushing and shear failure could occur [11]. The question is how to estimate, to measure the sandwich panel's residual strength after low-velocity

impact. The majority of researchers for this purpose are using edgewise compression test. On the second place there is four-point flexure test. Test setups and conditions will be thoroughly discussed in Chapter 4.

The internal damage sustained by a composite sandwich panel under transverse loading is generally a combination of several damage mechanisms. As mentioned before the internal damage could be even undetectable by visual inspection, so there is need for advanced inspection techniques. They could be non-destructive and destructive inspections, but each NDI technique to the separate damage mechanisms is limited. In addition to the typical damage mechanisms associated with composite laminates such as matrix cracking, delamination, face sheet debonding and fiber fracture, the presence of the core material also leads to core crushing, core shear and skin-core debonding as fundamental damage mechanisms. Any combination of these damage mechanisms can lead to failure of the panel under transverse loading [7, 12].

Summarizing: chapter 3 covers all materials and manufacturing procedures for sandwich panels, in chapter 4 there are described mechanical testing methods (including test fixtures, test setups and other information), chapter 5 is about how to introduce artificial damage and estimate residual strength of the panel, chapter 6 shortly describes main non-destructive test methods for investigation of damaged panels, and chapter 7 summarizes departments where reviewed researches are carried out and organizations which gave financial support for them.

3 Sample manufacturing

3.1 Facing skins

3.1.1 Reinforcement fibers

Since Roger Bacon discovered “graphite whiskers” in 1958 at Union Carbide’s Parma Technical Center, carbon fibers have been used in high performance applications from airplanes to automobiles and from satellites to sporting goods. All high speed aircraft have carbon fiber composites in their critical parts, and in many aircraft they are used as the primary structures and skins for entire planes [13]. Fibers are produced by carbonizing in an inert atmosphere precursor fibers based on PAN, rayon, or pitch [14, 15]. Graphite carbon fibers are the predominant high-strength, high-modulus reinforcing agent used in the fabrication of high-performance polymer composites. In general, the term graphite fiber refers to fibers that have been treated above 1,700 °C and have tensile moduli of elasticity of 3,450 MPa or greater. Carbon fibers are those products that have been processed below 1,700 °C and consequently exhibit elastic moduli up to 3,450 MPa. A further distinction is that the carbon content of carbon fibers is 80%–95%; and that of graphite, above 99%. However, the industry has universally adopted the term “graphite.” however, carbon and graphite fibers are made and heat treated at different temperatures and contain different amounts of carbon [14, 15]. It will therefore be used to describe both products in review [6].

Reviewing literature it became apparent that there are some dominant types of carbon fibers. In the majority of studies are used pre-preg systems based on AS4, IM7, T300 and T700. For better understanding of topic materials were sorted according to conformity to aerospace grade and number of how many different researchers they are using. Table 3.1. summarizes composites (fiber/matrix) used in NASA articles or are related to it. Table 3.2. summarizes composites based on AS4 fibers, Table 3.3. – IM7,

Table 3.4. – T300 and Table 3.5. – other materials from many others studies.

AS4 carbon fiber is a continuous, high strength, high strain, PAN based fiber. This fiber has been surface treated and can be sized to improve its interlaminar shear properties, handling characteristics, and structural properties [16].

IM7 carbon fiber is a continuous, high performance, intermediate modulus, PAN based fiber. This fiber has been surface treated and can be sized to improve its interlaminar shear properties, handling characteristics, and structural properties [17].

T300 are the standard modulus, high strength carbon fibers. Their used in aerospace applications. These are the most cost-effective fibers as measured by tensile strength or modulus per unit cost. [18, 19]. For example, composites, such as T300/914 is a well-known aeronautical material [20].

Table 3.1. Summary of facing skins composites used in NASA articles

Ref.	Author	Material	Fabric	Ply thicknes, mm
		Fiber/matrix		
[21]	David M. McGowan	AS4/8552	UD and woven	?
[22]	McGowan D. M., Ambur D. R.	AS4/8552	UD and woven	?
[21]	McGowan, Ambur	AS4/8552	tow	?
[23]	Singh P., V. La Saponara	AS4	woven	?
[24]	A.T. Nettles	IM7/8552	UD	0.292
				0.162
[25]	Walker, 1998	IM7/5260	?	?
[26]	Tomblin	CFRP	plain weave	?
[27]	Tomblin	CFRP	plain weave	?

Table 3.2. Summary of composites based on AS4 fiber

Ref.	Author	Material	Fabric	Ply thicknes, mm
		Fiber/matrix		
[28]	Bemard, Lagace 1989	AS4/3501-6	?	?
[29]	Herup, Palazotto		?	?
[30]	Williamson, Lagace 1994		?	?
[31]	Moody, Harris, Vizzini, 2002		?	?
[32]	Wallin M		UD	?
[33]	Zonghong X., Vizzini A. J., Qingru T.		UD	?
[31]	Moody R.C., Vizzini A.		UD	?
[34]	Wu, Sun 1996		?	?
[35]	Portanova M.A., Poe C.C., Jr., and J. D. Whitcomb		Uniweave	157 g m ⁻²

[36]	Tsang, Lagace 94		plain weave	?
[37]	Lagace, Mamorini. 2000		plain weave	0.35
[21]	McGowan, Ambur. 97	AS4/8552	UD	?
[22]	McGowan D. M., Ambur D. R.		UD and woven	?
[38]	McGowan, Ambur		woven	0.125
[39]	Meo, Vignjevic, Marengo 2005		?	?
[40]	Brenda L. Buitrago		plain woven	?
[41]	Inés Ivañez, Sonia Sanchez-Saez		woven	?
[23]	Singh P., V. La Saponara	AS4	woven	?
[42]	Schubel, Luo, Daniel 2005		five harness satin weave	?
[26]	Tomblin, Lacy et al. 1999	AS4/8553-40	?	?
[7]	Gottesman, Bass, Samuel 1987	AS4/3502	?	0.135
	Kassapoglou Jonas, Abbott 1988	AS4/E7K8	UD, plain, 5 & 8 harness satin weave	?
[40]	Sanchez-Saez S., Barbero E., Zaera R., Navarro C.	woven AGP193-PW/8552 + tape AS4/3051-6	woven + ud	?

Table 3.3. Summary of composites based on IM7 fiber

Ref.	Author	Material	Fabric	Ply thickness, mm
		Fiber/matrix		
[43]	Hodge A.J., Nettles A.T., Jackson J.R.	IM7/8552-1	?	?
[44]	Tumer, Vizzini. 2004	IM7/8552	?	?
[45]	Macdonald, Vizzini. 2002		?	?
[7]	Cvitkovich, Jackson, 1999		plain weave	0.190

[12]	Czabaj et al.		UD	?
[24]	Nettles et al.		UD	0.292
	Nettles A.T., Jackson J.R.			0.162
[46]	Kassapoglou 96		directional prepreg	?
[7]	Hill		?	?
[35]	Portanova et al.		?	?
[47]	Nettles et al.		IM7/8551-7	?
[25]	Walker. 1998		?	?
[48]	Ambur, Cruz 1995	IM7/5260	?	?
[49]	Lanouette et al.	IM7/PEEK	?	0.190

Table 3.4. Summary of composites based on T300 fiber

Ref.	Author	Material	Fabric	Ply thickness, mm
		Fiber/matrix		
[50]	Zhang et al.	T300	Z-fibres	?
[51]	Jose Maria Mirazo Antolin		plain weave, 3 K tow,	?
[52]	Nettles, Hodge 1990		?	?
[20]	Petit et al.	T300/914	UD	?
[7]	Charles, Guedra-Degeorges, 1991		UD	?
[53]	Levin 1989		?	?
[50]	Zhang X., Hounslow L., Grassi M.	T300/914C	UD	0.125 mm
[7]	Zheng, Li, Wu 1998	T300/QY89 11	?	?
[54]	Ferri, Sankar, 1997	T300/BMI resin	woven roving	?
[47]	Nettles A.T., Lance D.G.	T300/934	?	?
[55]	Soutis, Spearing. 2002	T300/BMS8	plain weave	0.211

Table 3.5. Summary of composites based on other carbon fiber

Ref.	Author	Material	Fabric	Ply thickness, mm
		Fiber/matrix		
[56]	Anderson, Madenci	CF011/LTM45 EL	4x4 twill weave	0.263
[57]	Besant et al.	fiberite 7714D/XAS	UD	0.25
[39]	Meo, Vignjevic, Marengo	69/GFE 3105H	?	?
[58]	Hiel, Ishal	G40-600/5245C	?	?
[59]	Freeman et al.	F-82	plain weave	0.305
[7]	Palm	IM8/8551	?	0.1275
[60]	Hwang et al.	NB321/3K70P	plain weave	0.1905
[61]	Castanié et al.	NB321/3K70P	plain weave	?
[62]	Gustin et al.	200T/ West System z105 epoxy resin	2x2 twill weave	0.2
[63]	Tomblin J.S., Raju K.S, Acosta J.F., Smith B.L., Romine N.A	NB321/3K70P	plain weave	?

[64]	Wilfried Göttner, Michael Klaus, Hans-G.	Tenax HTA 800	UD	?
[65]	Yuichiro Aoki, Ken Yamada, Takashi Ishikawa	T800H/3633	?	?
[66]	Yunze He, GuiYun Tian, Mengchun Pan, Dixiang Chen	5HS/PPS	woven <i>TenCate</i>	0.315
[67]	Jae-Hoon Kim	TBCarbon CP200NS	?	?

3.1.2 Matrix resins

There are several matrix resins used for sandwich panel face sheet production, but mostly are used epoxy resins. The majority is thermosetting resins which cross-links to form a three-dimensional non-melting matrix. Most cured epoxy resins provide amorphous thermosets with excellent mechanical strength and toughness; outstanding chemical, moisture, and corrosion resistance; good thermal, adhesive, and electrical properties; no volatiles emission and low shrinkage upon cure; and dimensional stability – a unique combination of properties generally not found in any other plastic material. These superior performance characteristics, coupled with outstanding formulating versatility and reasonable costs, have gained epoxy resin's wide acceptance [6, 68]. A curing agent (hardener) is generally used to achieve the cross-linking. In room-temperature curing the hardener is generally an amine such as diethylene triamine or triethylenetetramine. For elevated temperature curing a number of different curing agents could be utilized, including aromatic amines and acid anhydrides. Epoxy resins first developed commercially and still completely dominating the worldwide markets are those based on 2,2-bis(4-hydroxyphenyl) propane, more commonly known as bisphenol A (as it is produced by condensation of phenol with acetone) and 1-chloro-2,3-epoxy-propane, also known as epichlorohydrin [6].

Mostly in studies are used composites based on 8552 and 3501-6 (both are an amine-cured epoxy resins [15]). Also quite often appears 8551-7, LTM45 EL, 914, 934 and other such as bismaleimide resin (BMI) (Table 3.1, Table 3.2, Table 3.3,

Table 3.4.). BMI cures via an additional/free radical mechanism resulting in a cross-linked thermoset system with no condensation by-products [69].

These all resins listed before are thermosetting, although in several studies were mentioned high performance thermoplastic resins. It is likely that thermoplastic composite could replace thermosets because thermoplastic resins offer a number of advantages over conventional thermosetting resins such as epoxies. Thermoplastics have good impact resistance, can perform in a wide range of temperatures, and have a very low level of moisture uptake. Although thermoplastics may also require different manufacturing techniques. It is often necessary to use significantly higher processing temperatures and pressures than for typical thermosetting composite materials. Since thermoplastic resins do not cure via a chemical reaction they have ultimate shelf life and they do not have to be stored in freezers. This effectively infinite shelf life is a big advantage and avoids problems with material age and storage [70].

A wide range of thermoplastics are available and in common use today. In the area of high performance thermoplastics, polyetheretherketone (PEEK) and polyphenylene-sulfide (PPS) are probably the most widely reported thermoplastic resins. Furthermore PEEK is approved as appropriate thermoplastic for space constructions [70, 49]. Most high performance thermoplastics have a semi-crystalline polymer morphology. Crystallinity is important as it has a strong influence on chemical and mechanical properties. In broad terms crystallinity tends to increase the stiffness and tensile strength while amorphous areas are more effective in absorbing impact energy. The degree of crystallinity is determined by many factors including the type of polymer and the processing conditions. In the processing of a particular polymer type, polymer crystals form during cooling from the melt state. The rate of cooling is a crucial parameter in determining the level of crystallinity [70].

PEEK thermoplastic resin is characterized by a high melting temperature (~334 °C) and high glass transition temperature (~143 °C). It forms a partly crystalline polymer morphology that has a high resistance to chemical attack, radiation and thermal oxidation. PPS has a lower glass transition (~85 °C) and melting (~285 °C) temperatures than PEEK but is extremely thermally stable, has fire retardant properties, can attain a high level of crystallinity and is resistant to many organic solvents [70]. For PPS improvement, Phillips introduced a family of high-temperature performance polyarylene sulfide (PAS) polymers. The crystalline form is said to be suitable for structural components at temperatures up to 120 °C and for nonstructural components at temperatures up to 230 °C. Amorphous form, has temperature limits of 160 °C – 200 °C for structural components and 270 °C for nonstructural components [6].

Thermoplastic resins have superior toughness compared to untoughened epoxies but it must be stressed that improved impact performance for thermoplastic resins does not necessarily translate into improved impact performance for composites made from these resins. Unreinforced thermoplastics can undergo large strains without failing but the constraint of a fibrous reinforcement tends to negate this desirable aspect to some degree. Toughened thermoset composites have been shown to have impact resistance values similar to that of thermoplastic composites, sometimes even better [70].

In spite of numerous advantages thermoplastics as composite matrix resins have disadvantages too. The temperatures required to form thermoplastics are

significantly greater than for thermosets. Typical processing temperatures for PEEK are 350°C and higher. As a result conventional manufacturing equipment such as autoclaves may not be able to reach these temperatures and different lay-up consumable materials such as bagging films and sealant tapes are also required. Due to thermoplastics at melt state still remain fairly viscous, a higher pressure is required to form and consolidate composite part. At this moment thermoplastic resins are more expensive than thermosetting, for example, the cost of thermoplastic resin prepregs can be up to four times that of comparable epoxy prepregs. Overall cost reductions can be made since shorter processing times are required and the fact that many parts can be produced using automated equipment. This itself offsets much of the raw-material expense and cost-effective parts can be made even when compared to aluminium [70].

Practical cases of in-service use of thermoplastics include a trial by Lockheed of a graphite/PEEK thermoplastic composite undercarriage door on a C-130 aircraft [70].

3.1.3 Facing skin composites

Optimal strength and stiffness of continuous fiber-reinforced polymeric composites is obtained through controlled orientation of the continuous fibers. One means to achieve this is by prepreg molding. In this process, unidirectionally oriented layers of fibers are pre-impregnated with the matrix resin and cured to an intermediate stage of polymerization. When desired, this pre-impregnated composite precursor, called a prepreg, can be laid up in the required directions for quick conversion into end components through the use of hot curing techniques. Prepregs can thus be described as preengineered laminating materials for the manufacture of fiber-reinforced composites with controlled orientation of fibers [6]. Prepregs are recommended for high quality composite parts production. Chemical reactions that take place during the cure determine the resin morphology, which, in turn, determines the properties of the cured thermoset resin [71]. It is also possible to pre-impregnate reinforcement fibers with thermoplastic resin and then obtained prepreg can be used to build parts using autoclave processing as per thermosets, furthermore it leads to decreasing of processing time, because there is no need for long curing time required by thermosets. The only complication comes when melted part has to be cooled with right cooling rate [70].

Table 3.6. summarizes mechanical properties of different aerospace grade composites. For example, composites based on IM7/8551-7 is more toughened than brittle T300/934 and AS4/3501-6, however 8551-7 is more expensive [47, 35]. IM7/8552 carbon/epoxy has a much greater glass transition temperature than T700/LTM45-EL, as results it has high temperature performance and is appropriate for high strength applications. That leads to its extensive use in wide range of aerospace applications [7]. Epoxy based composite density varies around 1.58 g/cm³ [72, 35].

Table 3.6. Properties of available CFRP composites

Type	Nomenclature	Tensile strength	Tensile modulus	Ref.
	Fiber/matrix	MPa	GPa	
Carbon/ Epoxy	AS4/8552	2205	141	[16]
	AS4/3501-6	2006	135	[15, 73, 35]

	IM7/8552	2723	164	[17]
	T300/914	1500	130	[20]
	UNIPREG	1772	116	[14]
	T300/934	1670	138	
	IM7/8551-7	2760	165	
	P75/934	930	303	
	AS4/3501-6	670	69	
	IM6/3501-6	2275	159	
Carbon/ Phenolic	FM5055	140	19	
Carbon/ PEEK	IM7/APC-2	2890	165	

3.1.4 Facing skin lay-up

Now when reinforcement fiber and matrix types are reviewed it is necessary to investigate sandwich panel facesheet composite lay-ups used by researchers. In general lay-up is a process of fabrication involving the assembly of successive layers of resin-impregnated material [15]. Obviously that panel strength and damage resistance is highly dependent on facesheet material lay-up.

Russell et al. mentions that unidirectional laminate tends to split around the bolt holes if there are such. He used [0/90/0] lay-up and for testing used clampings which required drilled holes in specimen ends [74].

Wallin et al. have made open hole compression for laminates. After he concluded that failure stresses were higher for the [0/60/-60] type laminate than for the [0/45/-45/90] type laminate except in the case of the larger circular hole [32].

Barbero et al. compared three different laminate constructions woven AGP193-PW/8552 (10 plies) and tape AS4/3051-6 with two lay-ups: cross-ply [0/90]_{3S} and quasi-isotropic [45/0/90]_s. The damage modes (matrix cracking, delamination and fiber fracture) caused by the impact varied with the laminate lay-up. In the three laminate lay-ups the absorbed energy was similar under the same impact energy, but this fact does not mean that the corresponding damaged areas were the same. In the cross-ply and quasi-isotropic laminates, the damaged area is larger than in the woven laminate. In the first two laminates, the delaminations are generated mainly by the differences between the bending stiffness of the adjacent plies, while in the woven laminate the reinforcement of all the plies has the same orientation so there is no difference between their bending stiffness. Also the weave structure of the reinforcement hinders the propagation of shear cracks and delaminations. More energy is needed to propagate cracks and consequently the damaged area in the woven laminate is smaller [73]. In Figure 3.1. there are shown delamination areas on cross-ply and woven laminates investigated by ultrasonic C-scan.

The highest value of compression strength under all the impact energies has woven laminate, and the lowest – quasi-isotropic. The better compression strength of the woven laminate is attributed to the architecture of the reinforcement which controls the spread of damage. The quasi-isotropic shows the smallest reduction of the residual strength at all impact energies. Quasi-isotropic laminates shows better damage tolerance than the other laminates, since their normalized strength reduction is the smallest at all the impact energies. This may be due to the surface

plies, which protect the load-bearing 0° plies against impact damage. The smallest damage tolerance corresponds to the cross-ply laminate, in which the non-damaged plies (90° plies) are the least stiff and therefore more unstable and liable to fail under lower stress [73].

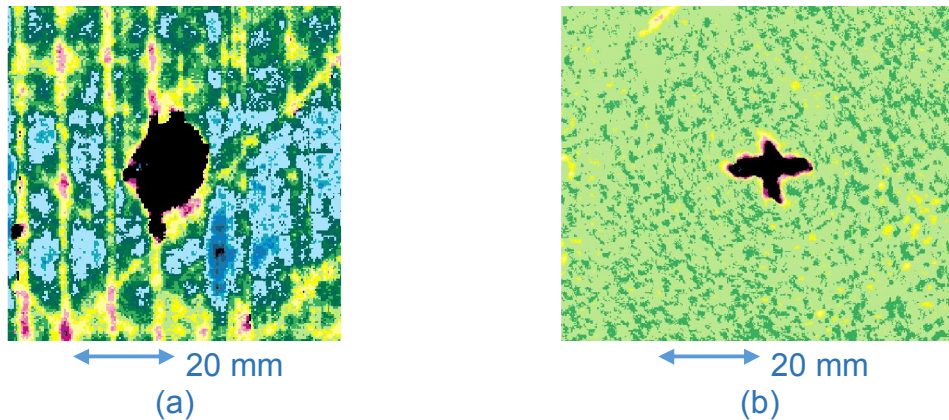


Figure 3.1. C-scan images of laminates impacted at 12 J: (a) cross ply and (b) woven fabric

A cross-ply lay-up advantages listed by Hill: a balanced symmetric simple lay-up provides good strength in both the transverse and in-plane directions. Also cross-ply laminates provide the most efficient design in terms of in-plane strength and stiffness of thin laminates where inter laminar shear is negligible in comparison with uni-directional or quasi-isotropic lay-ups. Panels with cross-ply skins had a higher compressive strength than those with angle ply skins [7].

In

Table 3.7. there are summarized facesheet layups used in researches related to NASA, in

Table 3.8. is collected information about lay-ups and number of plies used by researchers working in this field. Dominant place is taken by quasi-isotropic lay-ups, second place belongs to cross-ply lay-ups, while woven fabrics are almost unused and occurs only few times. Number of plies is also significant criteria for facesheets and it varies from 2 to 50. Most popular laminates consists of 8, 4, 6 and 2 plies.

Table 3.7. Typical lay-ups used in researchers related to NASA

Ref.	Authors	Lay-up	No of plies
[75]	Tomblin, 2001	[90/45], [90/45]2, [90/45]3	2; 4; 6
[38]	McGowan, Ambur. 97	0,90,45 & -45	36; 50
[25]	Walker. 1998	[45/-45/0/90]s	
[22]	McGowan D. M., Ambur D. R.	[Of/45/-45/0/90/-45/45/Of] Of-fabric ply	8
[76]	Shirsendu Sikdar, Sauvik Banerjee, Shaik Mahabu Subhani	[0/90/ 35/-35/0/-35/+35/0/90]	9
[24]	A.T. Nettles	[+45/0/- 45/90]2S	16
		[+45/0/- 45/0/90/0/0/90/0]S	18

Table 3.8. Typical lay-ups used by researchers

Ref.	Authors	Lay-up	No of plies
Fiber orientation 0; 90 (cross ply)			
[57]	Davies G.A.O., Hitchings D., Besant T., Clarke A., Morgan C.	[0/90]	2
[29]	Herup, Palazotto 1997		
[77]	Horrigan, Altken et al. 2000		
[55]	Soutis, Spearing. 2002		
[40]	Sanchez-Saez S., Barbero E., Zaera R., Navarro C.		
[33]	Zonghong X., Vizzini A. J., Qingru T.		
[7]	Hill, Michelle Denise	[90/0]	2
[31]	Moody R.C., Vizzini A.		
[78]	Amir Shahdina, Joseph Morlier, Laurent Mezeix, Christophe Bouvet, Yves Gourinat	[0/90]s	4
[79]	Mines, Worrall, Gibson 1998		
[30]	Williamson, Lagace 1994		
[80]	Fagerberg 2004		
[81]	Rhodes 1975		
[11]	G. Zhou and M. Hill		
[7]	Chen, Chen, Chem. 1991		
[11]	Zhou G., Hill M.		
[30]	Williamson, Lagace 1994	[0/90]10	20
[31]	Moody, Harris, Vizzini, 2002	[90/0]s	4
[45]	Macdonald, Vizzini. 2002		
[82]	Sburiati, 2002	[0 ₂ /90 ₂ /0 ₂]	6
[34]	Wu, Sun 1996		
[56]	Anderson, Madenci, 2000		
[56]	Anderson, Madenci, 2000	[0/90/0]	3
[67]	Jae-Hoon Kim	[0 ₂ /90 ₄ /0 ₂]	8
[30]	Williamson, Lagace 1994	[0/90/0]s	6
[56]	Anderson, Madenci, 2000	[0/90/0]	3
[30]	Williamson, Lagace 1994	[0/90/0/90]	4
Fiber orientation 0; 45			
[28]	Bernard, Lagace 1989	[45/-45/0]s	6
[7]	Aymerich, Prolo, and Vacca 1998	[0 ₄ /45/0 ₄ /-45/0 ₄]	14
[7]	Palm 1991	0 & +-45 fibers	-
[83]	Bull, Hallstrom 2004	[0/0/45/-45]s	8
[51]	Jose Maria Mirazo Antolin	[45/0/0]	3
[7]	Glinecki, Kodall, Curley 1982	[0/45/-45/0]	4
Fiber orientation 0; 45; 90 (quasi-isotropic)			
[7]	Cvitkovich, Jackson, 1999	[45/-45/0/90/+45]	5
		[45/-45/0/90/0/90/45/-45]	8
	Gottesman, Bass, Samuel 1987	[45/-45/0/90/0/-45/45]	7
[47]	Nettles A.T., Lance D.G.	[0/45/90/-45]s	8
[84]	Kim, Jun 1992		

[85]	Torre, Kenny 2000		
[50]	Zhang X., Hounslow L., Grassi M.	[0/45/90/-45]2S	16
		[0/45/90/-45]6S	48
[7]	Glinecki, Kodall, Curley 1982	[0/90/45/-45]	
[86]	Edgren, Asp, Bull. 2004	[0/90/45/-45]s	8
[87]	Zenkert, Shipsha, Bull, Hayman		
[86]	Edgren, Asp, Bull. 2004		
[87]	Zenkert, Shipsha, Bull, Hayman	[0/90/45/-45]3s	24
[24]	Nettles A., Jackson J.	[45/0/-45/0/90/0/0/90/0]	9
[88]	Hodge A.J., Nettles A.T., Jackson J.R.		
[88]	Nettles A.T., Hodge A.J., Jackson J.R.	[45/0/-45/0/90/0/0/90/0]S	18
[57]	Davies G.A.O., Hitchings D., Besant T., Clarke A., Morgan C.	[45/0/-45/90]	4
[35]	Portanova M.A., Poe C.C., Jr., and J. D. Whitcomb		
[24]	A.T. Nettles	[45/0/-45/90]2s	16
[12]	Michael W. Czabaj	[45/0/-45/90]s	8
[64]	Wilfried Göttner, Michael Klaus, Hans-G.		
[1]	Christopher T. James		
[89]	Takashi Ishikawa, Masamichi Matsushima, Eugene Keng Goy Lim, Yoichi Hayashi, Murray Scott	[45/0/-45/90]4s	32
[50]	Zhang X., Hounslow L., Grassi M.		
[65]	Yuichiro Aoki, Ken Yamada, Takashi Ishikawa		
[90]	Klaus M., Reimerdes H.G.	[45/90/-45/0/45/90/-45/0]	
[64]	Michael Klaus	[45/90/-45/0/45/90/-45/0]s	16
[90]	M. Klaus, H.-G. Reimerdes		
[32]	Wallin M	[0/45/45/90/90/45/45/0]3	24
[52]	Nettles, Hodge 1990	[0/45/-45/90]	4
[57]	Besant, Davies, Hitchings, 2001	[0/45/90/-45/0/0]s	12
[40]	Sanchez-Saez S., Barbero E., Zaera R., Navarro C.	[45/0/90]	3
[1]	Christopher T. James	[45/0/-45]s	6
[12]	Michael W. Czabaj	[-45/45/90/0]s	8
[26]	Tomblin, Lacy et al. 1999	[45/90/0/-45/0]3s	30
[12]	Michael W. Czabaj, Alan T. Zehnder, Barry D. Davidson, Abhendra K. Singh, David P. Eisenberg	[45/90/-45/0]s	8
[7]	Glinecki, Kodall, Curley 1982	[90/-45/45/90]	4
Different fiber orientations			
[22]	McGowan D. M., Ambur D. R.	Thick-end laminate [50 plies]: [±45/0/45/90/0/-45/0/45/90/0/-45/90/0/±45/0/-45/90/0/45/0/±45/0]; Thin-	

		end laminate [36 plies]: [$\pm 45/0/45/90/-45/0/2/[-45/90/45/0]2/45/0/2/0/[-45/0/45/90]2/-45/0/2/-45/90/45/0/+45$]	
[51]	Jose Maria Mirazo Antolin	[0/0/0/core/0/0/0]	3
[81]	Rhodes 1975	[45/-45]s	4
[22]	McGowan D. M., Ambur D. R.	[Of/45/-45/0/90/-45/45/Of] Of-fabric ply	8
[76]	Shirsendu Sikdar, Sauvik Banerjee, Shaik Mahabu Subhani	[0/90/35/-35/0/-35/+35/0/90]	9
[58]	Hiel, Ishal 1992	[0/30/-30]3s	18
[91]	Akay, Hanna 1990	5 ply front [45/90/90/90/45] 3 ply back [90/45/90]	
[92]	Thomsen, Banks. 2004	[+10/0/+10], [+45/0/+45], [+25/0/+25]	3
[20]	Petit S., Bouvet C., Bergerot A., Barrau J.J	1) [0/60/0/60/0/60/90/60/0]; 2) [0/60/0/60/0/60/90/90/60/0/60/0/60/0]	9; 14
[32]	Wallin M	[4[0/60/60/60/60/0]]	24
[59]	Freeman et al. 2005	2, 4 plain weave plies	
[93]	Vadakke, Carisson, 2004	plain weave [0/90]	2
[21]	McGowan, Ambur. 97	0,90,45 & -45 plies used 36-50 plies	

3.2 Core

The aluminum honeycomb core will be mainly described in this chapter, also some analogue core materials will be presented, for better comparison and wider understanding of topic. Honeycomb has highest strength and stiffness than other analogous constructions (Table 3.9.) and in its expanded form, is 95 to 98 percent of open space [94]. Due to honeycomb is relatively complicated construction it is necessary to define the terminology which is shown in Figure 3.2.

Honeycomb cores can be made from just about any thin, flat material over 500 kinds have already been made. The most common cell configuration is the hexagon but there are many other shapes for special applications. The basic honeycomb properties are the compressive and shear strengths and moduli. Honeycomb core costs range from relatively low to extremely high [2].

The honeycomb cell shape is normally hexagonal for optimum mechanical properties. It can also be over-expanded to produce a rectangular cell shape and provide improved drapeability for the production of curved parts [95].

In most studies reviewed were used aluminum or nomex honeycomb cores. Table 3.10. represents honeycomb cores used in articles related to NASA. Aluminum honeycomb is made primarily by the expansion method. It is simply taken aluminium foil sheets on which polyimide adhesive [96] is applied in straight lines. After that large number of sheets are bonded together. When adhesive is cured the construction is been extended. The corrugated process is most common for high density honeycomb materials more time consuming than the normal expansion method; therefore, the corrugated honeycomb is usually more expensive. The aluminum corrugated cores are made in densities from 192 to 880 kg/m³ using 0.076-0.152 mm foil thicknesses. Corrugated aluminum honeycomb is made because above 192 kg/m³ it becomes impossible to expand the HOBE (honeycomb

before expansion). The force to expand the block or slice is too great for the nodes to hold the block [2, 97]. The aluminum alloys commonly used are 3003 for commercial grade honeycomb and 5052, 5056 and 2024 for the specification grades with 5052 being the most common. The 2024 alloy is used when higher service temperatures are encountered [2]. In reviewed studies dominates 5052, 5056 and 3003 aluminium alloys honeycombs.

Table 3.11. summarizes aluminium honeycomb cores used by researchers, while in Table 3.12. are collected nomex cores and Table 3.13. consist of other core materials. Basic mechanical properties of honeycombs are collected in Table 3.14. In

Table 3.11. summarized data shows that aluminium honeycomb density varies from 29 to 192 kg/m³. Also there is no expressed density which is more common. Cell size varies from 3 to 9.5 mm and the most popular is 3.2 mm (1/8 in). Almost none of the authors mentioned cell wall thickness. According to Hexweb datasheets it varies from 0.0018 to 0.152 mm. Honeycombs with thickness ranging from 2.8 to 28.6 mm were used in studies. Benefits for aluminium honeycomb are: relatively low cost, it is best for energy absorption, greatest strength/weight ratio, thinnest cell walls, smooth cell walls, conductive heat transfer and electrical shielding [97]. Aluminium and other honeycomb materials are compared in






Table 3.15. Disadvantage of aluminium honeycomb is incensement of the degradation when it is mounted between two carbon/epoxy facesheets because of carbon conductivity which provides galvanic corrosion incensement. Therefore a more typical aeronautical composite system consisting of IM7/8552 carbon/epoxy skins is combined with 64 kg/m³ and 96 kg/m³ Nomex honeycomb core is used in addition to the aforementioned materials [7].

Nomex is a non-metallic honeycomb and is manufactured from high temperature resistant aramid paper formed into a honeycomb structure and coated with a phenolic resin. Nomex honeycomb has high mechanical strength at low density, also outstanding resistance to corrosive attack by chemicals, excellent resistance to impact damage and moisture, fire retardant and self-extinguishing, good dielectric properties, transparent to radio and radar waves [95]. Nomex honeycomb cores used by researchers are summarized in Table 3.12. Nomex honeycombs which are used by researchers have density ranging from 14.7 to 144 kg/m³, with absolutely dominant density 48 kg/m³, cell size varies from 2 to 15 mm and core thickness is similar to aluminium honeycomb cores specifically from 3 to 28.6 mm.

Also were found some studies which used honeycombs made off other materials such as titanium, glass/phenolic and honeycomb with trade name KOREX which is made from aramid paper dipped in a heat-resistant phenolic resin to achieve the final density. KOREX honeycomb offers improved strength-to-weight ratios and/or lower moisture absorption than Nomex honeycomb of a similar configuration [97].

Hill in her literature review mentioned that no significant research has been found for the effect of varying the honeycomb cell size. Also Hill writes that Williamson et al. (1994) performed the largest study into the effect of core thickness on damage resistance. In this study it was found that increasing the core thickness increased the amount of skin and core damage. This observation has also been repeated in other researches (Bernand, 1989; Ambur, 1995; Akay, 1990) though the opposite was found by Tomblin et al. [75, 7].

Table 3.9. Structural comparisons for structures of equivalent weight

Design	Relative strength	Relative stiffness
 Honeycomb sandwich	100%	100%
 Foam sandwich	26%	68%
 Structural extrusion	62%	99%
 Sheet and stringer	64%	86%
 Plywood	3%	17%

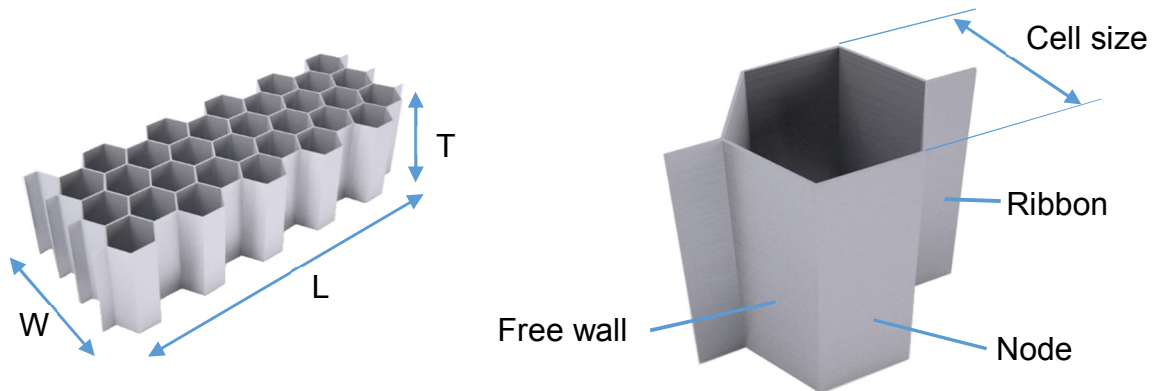


Figure 3.2. Honeycomb terminology

Table 3.10. Summary of honeycomb core materials used in NASA articles

Ref.	Author	Honeycomb	Density	Cell size	Thickness
			kg/m ³	mm	mm
[76]	Shirsendu Sikdar, Sauvik Banerjee, Shaik Mahabu Subhani	5052 aluminium alloy	32	1.59	12
[24]	A.T. Nettles	aluminum	50	3.18	28.65
[25]	Walker. 1998	titanium	96	4.76	25.4
[75]	Tomblin, 2001	Nomex	48	4.76	9.5; 19.05
				7.76	19.05
[21]	McGowan, Ambur. 97	Phenolic (HRP)	192	4.76	varying
[21]	McGowan D. M., Ambur D. R.	Korex	72.1	?	3.2

Table 3.11. Summary of aluminium honeycomb core materials

Ref.	Author	Honeycomb	Density	Cell size	Thickness
			kg/m ³	mm	mm
[43]	Nettles A.T., Hodge A.J., Jackson J.R.	perforated 5052 aluminum	49.7	?	28.6
[11]	Zhou & Hill - 2009	5052 (4.4-3/16-15) aluminum	70	?	12.7
[12]	Michael W. Czabaj	HexWeb® CR-III 5052-H39 aluminum	49.7; 72.1	3.2	25.4; 16.5
[1]	Christopher T. James	HexWEB CRIII 3/16 5052 4.4 aluminium	?	?	12.7
[12]	Michael W. Czabaj, Alan T. Zehnder, Barry D. Davidson, Abhendra K. Singh, David P. Eisenberg	HexWeb® CR-III	49.7; 72.1	3.2	25.4; 16.5
[57]	Davies G.A.O., Hitchings D., Besant T., Clarke A., Morgan C.	4.5-1/8-10(5052) aluminium light alloy	72	3	10; 25
[11]	G. Zhou and M. Hill	5052 aluminium (4.4-3/16-15)	70; 64	?	14.7
[7]	Hill, Michelle Denise	5052 aluminium alloy	50; 70; 90	?	12.7

[57]	Besant, Davies, Hitchings, 2001	Aluminium 4.5-1/8-10(5052)T	72	3.2	10
[76]	Shirsendu Sikdar, Sauvik Banerjee, Shaik Mahabu Subhani	5056 aluminium alloy	32	3.2	12
[98]	Nguyen et al. 2005	5056 aluminium alloy	?	?	25.4
[92]	Thomsen, Banks. 2004	Aluminium 3/8-5056-0.0007	?	9.53	10
[41]	Inés Ivañez, Sonia Sanchez-Saez	3003 aluminium alloy	77	?	20
[99]	Thayambalil Kim 1999	A3003-H19 aluminium	54.5; 83.2	6.35	25.4; 12.7
[100]	Akil Hazjzan, Cantwell 2003	3003 aluminium alloy	84	6	13; 25
[101]	A. Abbadi	3003 aluminium alloy (ECM)	?	?	?
[40]	Brenda L. Buitrago	3003 aluminium alloy	77	4.8	20
[7]	Chen, Chen, Chem. 1991	aluminium	70	6.35	?
	Palm 1991	aluminium	32; 61; 29; 48	?	12.7
[28]	Bemard, Lagace 1989	aluminium	80	?	6.4; 9.6
[102][Tsotsis, Lee 1996	aluminium	96; 136	?	3; 4
[53]	Levin 1989	aluminium	72; 130; 192	3.2	?
[7]	Gottesman, Bass, Samuel 1987	aluminium	130	3.2	?
[103]	Kiratisaevee, Cantwell 2005	aluminium	?	?	10
[43, 88]	Hodge A.J., Nettles A.T., Jackson J.R.	aluminium	49.7; 97.7; 39.85; 49.7	3.2	2.9; 28.6

Table 3.12. Summary of Nomex honeycomb core materials

Ref.	Author	Honeycomb	Density	Cell size	Thickness
			kg/m ³	mm	mm
[77]	Horrigan, Altken et al. 2000	Nomex HRH-10-1/8-3.0	48	3.2	25.4

[39]	Meo, Vignjevic, Marengo 2005	Nomex HRH10-1/8	29; 96	3.2	6.35, 15.24
[29]	Herup, Palazotto 1997	Nomex HRH-10-1/8-9.0	144	3.2	12.7
[61]	Aminanda Y., Castanier B., Barrau J.-J., Thevenet P.	Nomex HRH 78,1/ 4,3 Hauteur	?	15	15
[60]	Hwang & Lacy (2007)	Nomex HC (PN2-3/16-3.0)	48.1		19.05
[61]	Castanié B., Aminanda Y., Bouvet C., Barrau J.J.	Nomex (E - 137.9 MPa)	48	4.76	?
[56]	Anderson, Madenci, 2000	HRH-10 Nomex	48; 96	3.2	12.7
[7]	Zheng, Li, Wu, 1998	NRH-2-80-(0.08) Nomex	80	2	?
[63]	Tomblin J.S., Raju K.S, Acosta J.F., Smith B.L., Romine N.A	Plascore Nomex	48.1; 72.1; 96.1	?	?
[31]	Moody R.C., Vizzini A.	phenolic (Nomex)	48	3	?
[33]	Zonghong X., Vizzini A. J., Qingru T.	Phenolic (Nomex)	?	3	?
[67]	Jae-Hoon Kim	Nomex (Aerocell CACH 1/8-3.)	48	3.2	10; 20
[104]	Mirazo J.M., Toribio M.G., Spearing S.M	NomexTM	48	?	?
[75]	Raju, Tomblin, 2001	Nomex	48	4.76	9.525; 19.05
[102]	Tsotsis, Lee 1996			80, 144, 184	3; 4
[30]	Williamson, Lagace 1994		48	3.2	6.4, 9.5, 25.4
[84]	Kim, Jun 1992		48; 128	3.2	
[81]	Rhodes 1975		48		25
[11]	Zhou G., Hill M.D.		70; 64		12.7
[7]	Charles, Guedra-Degeorges, 1991		?	?	15
[75]	Tomblin, 2001		48	4.76	9.5; 19.05
[31]	Moody, Harris, Vizzini, 2002		48	3.2	25.4
[7]	Cvitkovich, Jackson, 1999		48	3.2	25.4

[91]	Akay, Hanna 1990		48	3.1	12.5
[36]	Tsang, Lagace 94		48	3.2	25.4
[37]	Lagace, Mamorini. 2000		48	3.2	25.4
[46]	Kassapoglou Jonas, Abbott 1988		14.7; 29	?	25.4; 19.05
[44]	Tumer, Vizzini. 2004		48	3.1	25.4
[45]	Macdonald, Vizzini. 2002		48	3.1	25.4
[7]	Glinecki, Kodall, Curley 1982		48	3.2	8.38
[55]	Soutis, Spearing. 2002		?	?	25.4
[105]	Toribio, Spearing 2001		48	?	25.4
[57]	G.A.O. Davies, D. Hitchings, T. Besant, A. Clarke, C. Morgan		32	?	20
[51]	Jose Maria Mirazo Antolin		?	?	?
[60]	Lacy T. E., Hwang Y.		48.1; 72.1; 96.1	4.76	9.5, 19.1, 28.6
[106]	N. Baral, D.D.R. Cartié, I.K. Partridge, C. Baley		64	5	12
[107]	Ratcliffe J., Jackson W., Schaff J.		48.1	3.2	?
[10]	Thomas D. McQuigg		?	?	?
[108]	Daniel O. Adams		?	?	?
[7]	Caidwell, Borris, Falabella 1990		48; 64; 80; 88; 96	3.2, 4.8, 6.4	12.7

Table 3.13. Summary of other honeycomb core materials

Ref.	Author	Honeycomb	Density	Cell size	Thickness
			kg/m ³	mm	mm
[22]	McGowan D. M., Ambur D. R.	Korex	72.1	3.2	?
[26]	Tomblin, Lacy et al. 1999	glass/phenolic	88	4.76	22.86

[52]	Nettles, Hodge 1990		32	4.76	35
[48]	Ambur, Cruz 1995		48; 88; 128	?	6.35; 9.5; 12,7
[25]	Walker. 1998	Titanium	96	4.76	25.4

Table 3.14. Typical mechanical properties of aluminium honeycomb cores at room temperature [2]

Core	Density	Compression		L shear		W shear	
		Strength	Modulus	Strength	Modulus	Strength	Modulus
	kg/m ³	MPa	GPa	MPa	GPa	MPa	GPa
5052	16	0.38	0.07	0.31	0.08	0.21	0.05
Alu	192	19.99	6.21	13.38	1.45	9.86	0.52
5056	16	0.41	0.10	0.37	0.10	0.24	0.05
Alu	130	13.10	3.00	6.52	0.99	3.86	0.35
3003	21	0.48	0.11	0.37	0.10	0.27	0.05
Alu	77	4.34	1.02	2.31	0.43	1.48	0.21

Table 3.15. Comparison between honeycomb cores

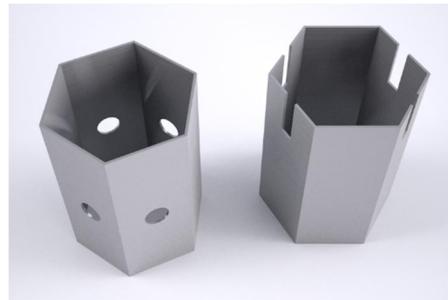
Honeycomb material	Density kg/m ³	Compression		Shear	
		Strength MPa	Modulus GPa	Strength MPa	Modulus GPa
Aluminium	49.66	2.07	0.52	1.45	0.31
Nomex	48.06	2.24	0.14	1.21	0.04
Fiberglass	48.06	2.83	0.16	1.34	0.13

In some space applications the honeycomb cells must be vented to allow the entrapped air to escape. In launch situations the air is rapidly heated to rather high temperatures. Usually very thin facings are used on the honeycomb core as light weight is crucial. If the cells are not vented the pressure buildup at high temperature may peel the thin facing from the core, causing the sandwich panel to fail. Another reason why air may not be wanted in the honeycomb cells is because the vacuum in space would suck out any air that was present when the facings were bonded on. The air escaping in space could contaminate mirror surfaces or other delicate equipment. There are several methods used to vent the honeycomb cores. Aluminum honeycomb can have the foil perforated. Here the foil is punctured by needles on a cylinder which rolls over the flat foil. This operation is done after the node glue lines have been printed onto the foil. After perforation, hard rubber rollers flatten out the metal that was upset during perforation. The needles on the roller taper from 0.46 mm diameter to a point. This results in holes in the aluminum foil 0.13 to 0.38 mm in diameter. The holes in the nodes tend to be blocked by the node adhesive when the block is pressed and cured. The needles are in diagonal rows around the roll. The space between needles is typically 3.2 mm and the rows are 5.1 mm apart [2].

There are two specifications that have honeycomb perforation requirements, Mil-C-7438 and AMS-4175. These are as follows [2].

Non-metallic honeycomb cores cannot be perforated as they are dipped in resin after being expanded, and the resin would fill the perforations. These cores

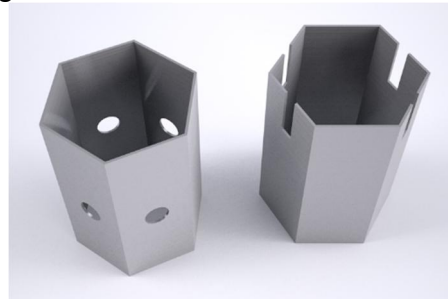
are slotted or drilled. This can also be done to aluminum honeycomb. The nodes or free walls are slotted or drilled as shown in



Drilled

Sloted

Figure 3.3. It is best to slot or drill only the free walls as this does not affect the core properties very much and it will allow the core to vent in both the L and W directions. Slotting is the most widely used venting technique and it can be used on both corrugated and expanded cores. The minimum slot width is 0.79 mm and the maximum depth cannot be greater than two times the slot width [2].



Drilled

Sloted

Figure 3.3. Vented honeycomb core

3.3 Sandwich panel manufacturing

Sandwich panel manufacturing is complex process including several operational steps. In Figure 3.4. there is flowchart representing best offered sandwich panel manufacturing process for the research. More detailed information of each step is reviewed in further paragraphs.

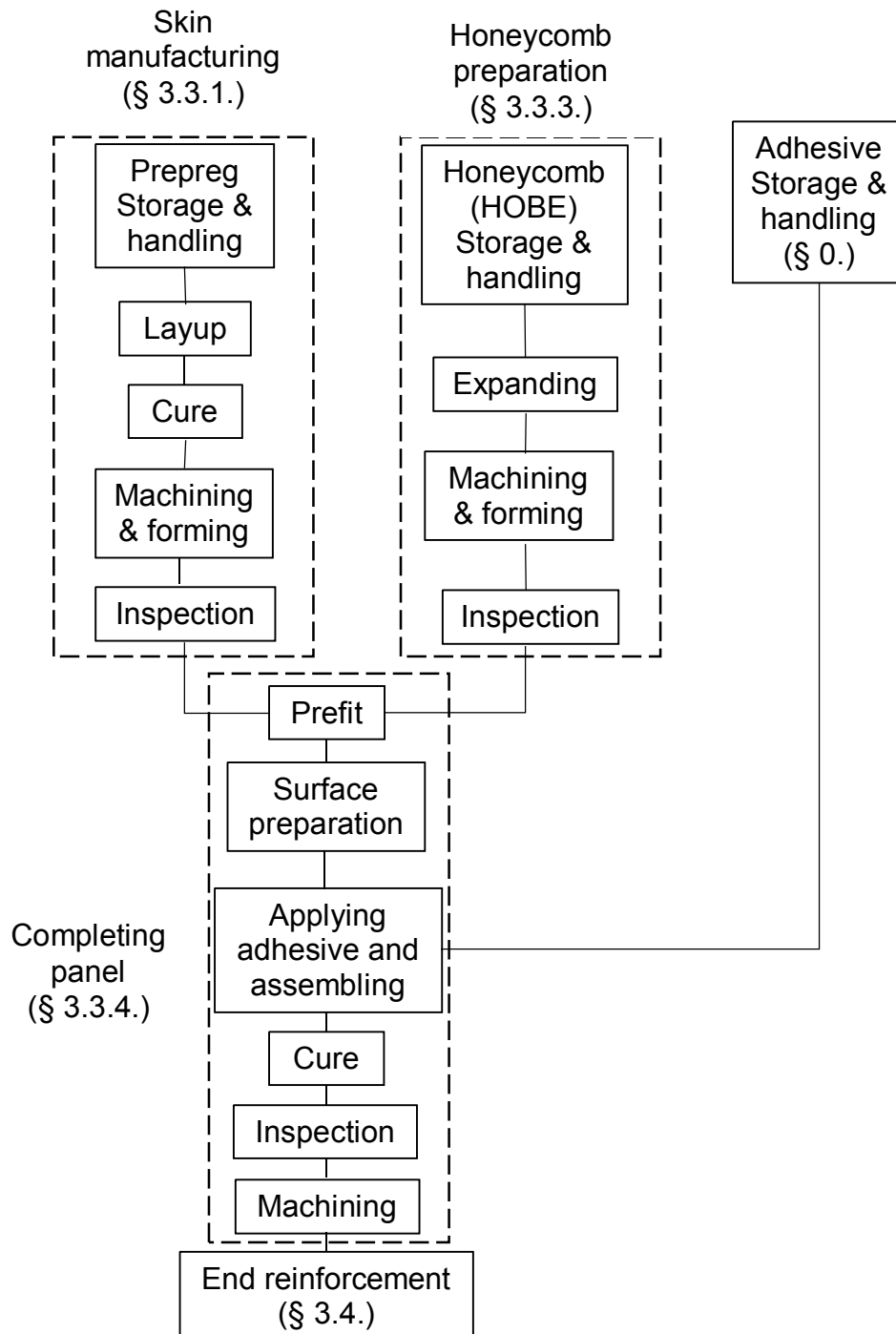


Figure 3.4. Manufacturing process flow chart (In brackets given number of paragraph containing discussion about the specific topic)

3.3.1 Skin manufacturing

Prepregs should be stored, as received, in a freezer at -18°C . Typically prepregs have a guaranteed shelf life at -18°C for 12 months from date of manufacture. The exact -18°C shelf life and room temperature life are printed on the prepreg box labels. Tack life and out life at 23°C are matrix dependent and are defined on the relevant product data sheet [109]. Handle all prepreg using clean gloves. Use sharp, precision equipment when cutting or paneling prepreg. Treat all prepreg as being very fragile. Upon receipt, all prepreg should be immediately moved from the receiving area to a controlled environment. All prepreg should be used as soon as possible [110].

Sandwich panel facesheets are made by hand lay-up – a process in which components are applied either to a flat working surface, and the successive plies are built up and worked by hand. Also it is predetermined and designed for specific purpose laminate orientation – a configuration of a cross plied composite laminate with regard to the angles of cross plying, the number of laminate at each angle, and the exact sequence of the lamina lay-up [15].

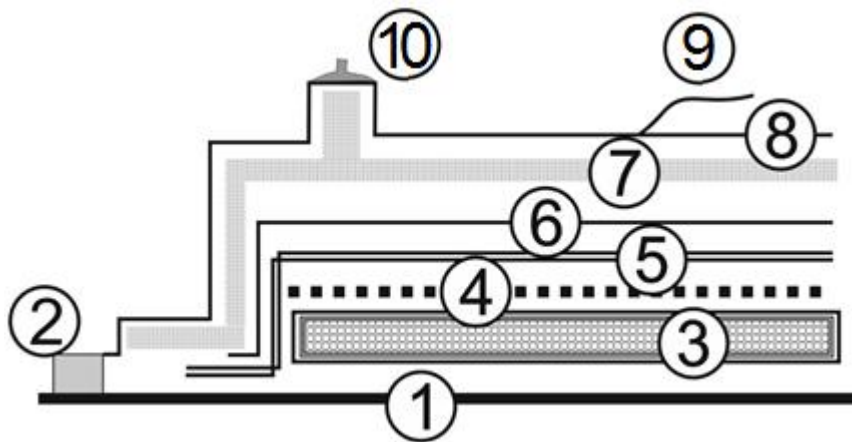
During lay-up, adhesives, bonding and support tools are used to properly align and assemble the components into an assembly for curing. This operation is to be performed with gloved hands in a controlled contamination area [111]. The general procedure for assembly lay-up is:

1. After removing prepreg from the refrigerator it should be left to warm-up to room temperature to prevent moisture condensation inside the sealed moisture-proof bag for at least 3 1/2 hours or until visible moisture has vanished from the outside of the bag [7, 112, 113].
2. Cutting and lay-up. The prepreg is laid on the cutting table and cut to the desired size and orientation. White, lint-free cotton gloves are required for hand / personal protection. Talc-free latex or nitrile gloves are acceptable alternates. No cutting of prepreg materials is permitted on the tool [7, 113].
3. Lay-up surface shall be cleaned prior to lay-up, using non-contaminating cleaners, such as acetone or alcohol. Mold preparation shall be performed outside the lay-up room. After cleaning, each mold shall be treated with non-contaminating release agents. The recommended approach is using caul plates which are smooth metal plates, free of surface defects, the same size and shape as a composite lay-up, used immediately in contact with the lay-up during the curing process to transmit and distribute normal pressure and to provide a smooth surface on the finished laminate [7, 15, 113].
4. Next step is laying up the prepreg on flat surface after removing all adhesive separator materials. Once more time there is need to make sure that all surfaces of skins and caul plates are clean since the small contamination particles could cause a mark-off [7]. Entrapped air between prepreg sheets is removed by using a squeezing roller after applying each prepreg sheet. Lay-up operations must be completed with sufficient time remaining to bag and initiate cure of the assembly before the out time for the adhesive(s) has been exceeded. Room temperature exposure of adhesives causes them to advance chemically cure, which can lead to inadequate flow during the curing operation and weak bonds [111, 112].
5. After applying all the prepreg sheets, next step is vacuum bagging. It is made by applying release film, bleeder, barrier film, breather, and bagging materials. Recommended shop supplies of all bagging materials are

collected in Table 3.16. In Figure 3.5. shown vacuum bagging lay-up in cross section. The process is described below step by step:

- a. The release film is a perforated, thin film that allows entrapped air, excess resins, and volatiles to escape. It is produced from nonstick materials, such as fluorinated polymers, PVC, etc. In general they are interleaved between any adhesive film, resin, potting compounds, or sealant and a surface not intended to be bonded [15, 112].
 - b. The function of the bleeder – porous cloth – is to absorb moisture and excess resin coming from the stack of prepregs [15, 112].
 - c. Apply barrier film on top of the bleeder. The film is similar to release film except that it is not perforated or porous [112].
 - d. Apply breather layer, a porous fabric similar to the bleeder. The function of the breather is to create even pressure around the part and at the same time allowing air and volatiles to escape [112].
 - e. The final layer is a vacuum bag. It is an impervious plastic film, made of expendable (PA, PVC, Mylar, PVF, etc.) or reusable elastomer material, that completely envelopes the entire assembly. It is usually 0.05 to 0.1 mm in thickness and is discarded after each cure cycle because the plasticizers in the film are affected by heat, causing cracking and leaks [15]. The film is sealed on all sides of the stacked prepreg using seal tape (“tacky tape”). It is possible to enclose the entire mold inside the vacuum bag. A nozzle is inserted into the vacuum bag and connected to a vacuum hose for creating vacuum inside the bag [112].
6. The entire assembly is then placed into the autoclave or oven. Appropriate temperature for resin curing is installed. The pressure is created in two ways: using the vacuum bag for oven as well as the pressure inside the autoclave and venting the sealed parts to the external atmosphere. The vacuum bag creates a vacuum inside the bagging material and thus helps in proper consolidation. To create vacuum inside the bag, the nozzle in the bagging system is connected to the vacuum pump using a hose. This procedure is essential to obtain a bonding pressure by sealing assembly from ambient environment. The heat for curing comes from heated air in oven or pressurized gas inside the autoclave [114, 112].
 7. During the cooling stage after the cure of the composites, residual thermal stress is related to the difference between the cure temperature and ambient temperature, and the thermal expansion behavior of the composite material. A post-cure process is usually applied to the structure to relieve the induced thermal stress. After cooling, the vacuum bagging materials are removed and the part is taken out [112].

After cured laminate is removed from vacuum bagging system it should be inspected for any defects. Non-destructive inspection by visual means is by far oldest and most economical method. Consequently, visual inspection is performed routinely for damage assessment. In some instances aids such as microscopes, borescopes, magnifying glasses and other optical devices are used to inspect areas for defects that are either inaccessible or cannot be seen with the unaided eye. For more deep inspection ultrasonic C-scan could be used [114]. Much more information about NDI is gathered in chapter 6.



1. Tool surface
2. "Tacky tape" rubberized sealant tape
3. Prepreg laminate
4. Release film (peel ply porous Teflon or equivalent)
5. Bleeder
6. (optional) 0.05 mm non-porous Teflon or equivalent
7. N-10 Airweave breather cloth
8. 0.05 mm vacuum bagging film

Figure 3.5. Vacuum bagging lay-up cross section [113]

Table 3.16. Recommended shop supplies [113]

Item	Part no. or specification	Supplier
Acetone	2-propanone (Acetone) purity 99.5%	Sun Chemical, Dow, Ashland, Union Carbide
Denatured Alcohol	Ethanol - min 190% proof	Ashland, Sofecia, Union Carbide, Eastman Chemical
Release Film	WL4600 (non-porous) WL5200 (non-porous) A4000R (non-porous) A5000 (non-porous) 200 TFNP-Brown Teflon 234 TFNP-Brown Teflon or Equivalent	Airtech International Airtech International Airtech International Richmond Richmond Airtech International
Release Agent	A-3000 Airweave N10 or Equivalent	Richmond Products Airtech International
Breather	7781 woven fiberglass cloth or Equivalent	JPS Industries Inc., BGF Industries Inc., Hexcel-Schwebel

Bleeder	7781 woven fiberglass cloth or Equivalent	JPS Industries Inc., BGF Industries Inc., Hexcel-Schwebel
Peel Ply	200TFP (porous) - Teflon 234TFP (porous) - Teflon Release Ply B – Nylon or Equivalent	Richmond Airtech International Airtech International
Sealant Tape	GS 100 SM5126 or Equivalen	Circuit Supply Scnee-Morehead
Silicon Rubber	Silicon Rubber minimum 190°C use temperature	Airtech International, Inc., Richmond Aircraft Products, Inc. De-Comp Composites, Inc
Bagging Sheet Film	HS6262 WL7400 WL8400 or Equivalent	Richmond Products Airtech International Airtech International

3.3.2 Adhesives

Film adhesives

Films and tapes are the most popular forms of adhesive used in the aerospace industry. They provide several advantages, including positive bond-line control, thickness uniformity, and ease of storage. The film form ensures an optimum and controlled weight of adhesive containing exact proportions of resin and hardener. Film adhesives therefore require no mixing of components. During the heating cycle the film liquefies and flows enough to wet the adherend surfaces, displaces any entrapped air, and then cures to an infusible solid. They require no special application equipment and provide ready-to-use convenience. However, they are restricted to a limited range of available weights, are difficult to handle in light weights, and are high in cost. Reticulating films, which have recently become popular, offer the same advantages, plus an extra advantage. They have the possibility of optimum utilization of adhesive or honeycomb cell applications. The application of powders to both flat sheet stock and honeycomb cell edge by electrostatic spray and fluidized-bed techniques has been suggested by one company, but the development has been dropped due to lack of interest, probably because of the high cost of capital equipment [94, 115].

Also reviewing literature was found standard specification for structural film adhesives for honeycomb sandwich panels ASTM E865-82. This specification covers film adhesives for bonding of honeycomb sandwich panels used in tactical shelters. The adhesives are for use in bonding aluminum alloy facing to non-metallic core, inserts, edge attachments and other components of a sandwich panel. The adhesive covers thermosetting films only [94].

For example, if using Redux adhesives, for good overall properties and bonding to honeycomb core, areal weights of film adhesives in the range 150-400

g/m² should be used. Where weight is critical lightweight film (60-150 g/m²) can be adequate when close tolerance joints are achievable [115].

Pastes

One hundred percent solid adhesives offer many advantages, including those of solvent-free systems, low cost and good performance. On the debit side, some special processing equipment is needed, including a roller coater, material handling and metering end mixing equipment. Roller coating with paste adhesive has been used to apply adhesive to flat skin materials and honeycomb cell edge at ambient and elevated temperatures. The choice of an adhesive for this technique depends on adhesive rheology, viscosity and use life at the application temperature. The latter parameter restricts, to some extent, the use of ambient-curing adhesives. Because of the relatively short pot lives that most paste adhesives have, application temperatures of 49-71°C are used with curing temperatures 121°C [94].

Only few authors mentioned which specific adhesive they were using. One thing is clear, as mentioned before, film adhesives dominates. Several times occurred VTA260, FM300, Hysol and Redux adhesives. They all are based on epoxy resin. Hysol trademark adhesives in reviewed literature are used only in panels with nomex core. Table 3.17. summarizes adhesives used by different authors for aluminium honeycomb core bonding to facesheets.

VTA®260 is a variable cure temperature film adhesive suitable for bonding both composite substrates and aluminium to themselves or to honeycomb and foam core materials [116].

FM®300 is a modified epoxy film adhesive used in aerospace industry. It has high elongation, toughness and shear strength. This makes it particularly suitable for redistributing the high shear stress concentrations of graphite epoxy-to-metal bonds, and allows it to accommodate the low inter laminar shear strength of the composite [117].

3M™Scotch-Weld™Structural Adhesive Film AF 555 is a thermosetting, modified epoxy adhesive film. It was designed for bonding of composites in conjunction with honeycomb or in a monolithic structure. Scotch-Weld AF 555 Film can be co-cured, co-bonded with composite prepregs, or used to bond cured composite [118].

The Redux® trademark adhesive is suitable for aerospace bonding needs, including Redux 609 and 312 which are epoxy film adhesives appropriate for sandwich constructions with a variety of skins and cores [119, 119, 115].

If the facesheets are made of thermoplastic matrix the adhesive bonding requires a suitable surface treatment, adhesive and application method. Thermoplastic polymers have lower surface energies when compared to epoxies which makes it difficult for adhesives to wet the adherend surface and create a good bond. Correct adhesive choices are therefore critical in order to produce strong and durable bonds. Since thermoplastic resins can withstand temperatures common to many aerospace graphite/epoxy prepregs (177°C), it is possible to use common aerospace epoxy, acrylic and other thermoset adhesives. Adhesives that have been used successfully include FM300 for both PPS and PEEK, FM 377 and FM 87, Hysol 9309.3, FM73M, Permabond F241, F245, F246 and V501, and Bostik M890, M896. [70].

In order to be prepared to carry out qualitative tests the facing thickness should be measured prior to bonding, because accurate measurement of facing thickness is difficult after bonding or co-curing of the facings and core. Although for co-cured facings, the thicknesses are generally calculated using nominal per ply thickness values [120].

Table 3.17. Adhesives used for aluminium honeycomb core bonding to facesheets

Ref.	Author	Adhesive	CFRP Facesheets	Core
[76]	Shirsendu Sikdar, Sauvik Banerjee, Shaik Mahabu Subhani	Hexcel 212-Na	-	5056 aluminum
[24]*	A.T. Nettles	FM-300K	IM7/8552	aluminum
[1]	Christopher T. James	Redux 609	T700	5052 aluminium CRIII 3/16
[11]	G. Zhou and M. Hill	VTA260	T700/LTM45	5052 aluminium
			T700/LTM45-EL	
[7]	Hill, Michelle Denise	Redux 312; VTA260	T700/LTM45-EL; IM7/8552	5052 aluminium
[88]	Hodge A.J., Nettles A.T., Jackson J.R.	FM300K	IM7/8552-1	perforated 5052 aluminum
			IM7/8552	
[12]	Michael W. Czabaj, Alan T. Zehnder, Barry D. Davidson, Abhendra K. Singh, David P. Eisenberg	3MTM AF-555; 3MTM EW-5000	IM7/8552	HexWeb® CR-III
[67]	Jae-Hoon Kim	EA 9696(HYSOL)	CP200NS	Nomex (Aerocell CACH 1/8-3.)
[31]	Moody R.C., Vizzini A.	FM - 300 film	AS4/3501-6	phenolic (Nomex)
[106]	N. Baral, D.D.R. Cartié, I.K. Partridge, C. Baley	ST1035; SA80	R367-2	Nomex
[27]	Tomblin J.S., Suresh Raju K., Arosteguy G.	Hysol 9628.060 PSF NW film	NB321/3K70 plain weave	Plascore PN2-3/16-3.0 Nomex

* Article related to NASA

3.3.3 Honeycomb preparation

Care of honeycomb is taken throughout the process not to contaminate it [2]. Mostly aluminium honeycomb is supplied in sliced form (HOBE). Obviously before sandwiching it between CFRP skins it is need to expand the HOBE. To achieve best results appropriate equipment should be used. Figure 3.6. shows machine for HOBE expansion which in general is table like device with several pins to grab honeycomb's cells which are arranged along the edge and pull them for whole HOBE expansion (Figure 3.7.).

Unless there are obvious signs of contamination, aluminium honeycomb does not require pretreatment prior to bonding. However, any oil or grease contamination should be evidenced, then the affected slice should be immersed in the vapor of a suitable hydrocarbon solvent in a vapor degreasing unit. After

immersion, always sufficient time for the honeycomb core to drain dry should be allowed. This is particularly important as liquid solvent held in the corners of the honeycomb cell can be very difficult to detect and must be removed before bonding [115, 7]. Drying temperature up to 180 °C and drying time up to 2 hours may be necessary to completely remove the vapor degreasing fluid from thick, spliced core with closed cells. Handle core with clean dry white lint-free cotton gloves so as not to get finger oils on the core surfaces. Take care to avoid damaging the core [115, 2].

If the core is not going to be used right away protect it by wrapping it with a clean covering, for example with protective bubble wrap [2, 7].

For cutting best solution is horizontal or vertical band saw using special honeycomb blades. This saw must have vacuum systems because of the large amount of core material dust generated [2]. Band saw and other tools for honeycomb and sandwich panel cutting and machining is shown in Figure 3.8.

If the core becomes contaminated during shipping or in the plant, it can be cleaned. Cores can be vapour degreased, solvent flushed, or wiped with a lint-free cloth moistened with trichloroethane. After cleaning, if possible, the core should be dried in an oven at 66°C maximum. A hot air gun can be used, but be sure the air temperature is below 66 °C. If neither of these methods can be used, at least allow the solvents to evaporate from the honeycomb at room temperature. Any solvents on the core when it is layed up and bonded to the facings can cause poor adhesive bond [2].



Figure 3.6. Aluminium honeycomb expansion machine [121]

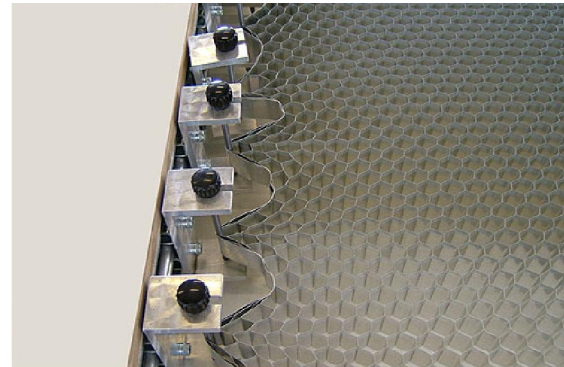


Figure 3.7. Fixing pins for honeycomb expansion [121]



Band saw



Jig saw



Pillar drill



Circular saw



Oscillating saw

Figure 3.8. Some of the hand tools used in the fabrication of honeycomb sandwich panels [122]

3.3.4 Panel assembly

When facesheets are manufactured and HOBE expanded, it is time to assembly sandwich panel.

Only minority of authors mentioned which technology and adhesive their used for facesheet bonding to honeycomb core. There are two general approaches to manufacture CFRP/honeycomb core sandwich panels. First is one step technology. Co-curing¹ two facesheets prepregs with core simultaneously, producing complete sandwich panel (Figure 3.9.). This technique seems to be easier, cheaper and faster but in many cases authors did not used it, maybe because it is impossible to distribute adhesive (which is contained by prepreg) uniformly on whole sheet surface and amount of adhesive probably is to small. Co-curing of the laminate to the core is rarely used as the bond line strength can be considerably less than with the use of a separate adhesive, and skin-core debonding can become a major issue, especially under in-plane loading [7]. To overcome this issue and still obtain a good core-to-facing bond is to use a prepreg with a higher resin content next to the core. For example, the ply next to the core may have a 50% resin content while the other plies may have a normal 40% content [2]. Second approach – two steps technology is more often used (Figure 3.10.). First step the laying-up and curing of the laminate skins, and second the bonding of the laminate skins to the honeycomb core [7]. So the separate adhesive is used. Most film adhesives used for this purpose weigh about 290 g/m². On thin panels the adhesive

¹ Cocuring is the act of curing a composite laminate and simultaneously bonding it to some other prepared surface during the same cure cycle [15]

can be a very large percentage of the total sandwich weight. To overcome this unwanted added weight, the only way is using mentioned before one step technology – composite skins co-curing to the honeycomb [2].

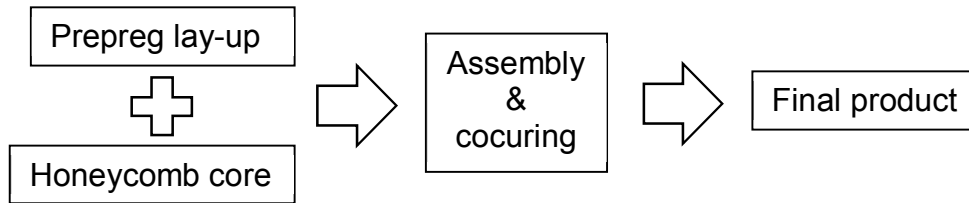


Figure 3.9. Sandwich panel manufacturing with one step technology

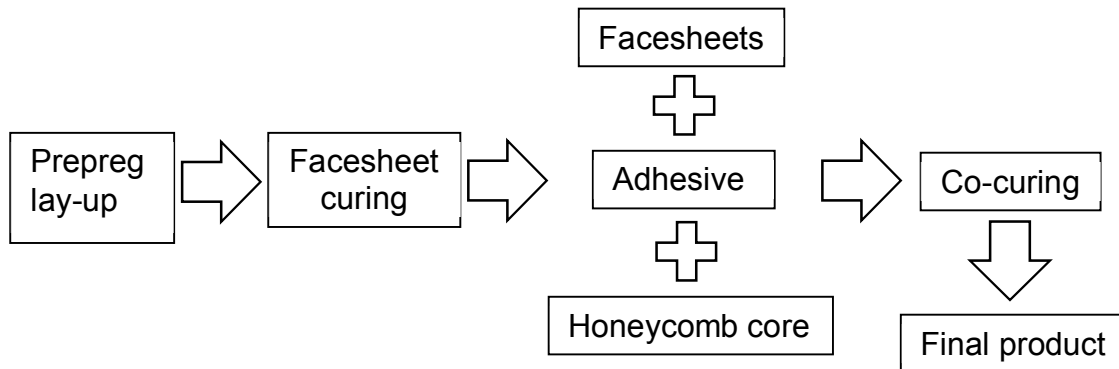


Figure 3.10. Sandwich panel manufacturing with two steps technology

The facing is bonded to the honeycomb cell wall primarily on the sides as shown in Figure 3.11. Due to adhesive is wetting aluminium surface the fillets are forming. If there were no fillets and the facing was bonded only to the flat contact area of the cell wall the bond strength would not be very high. Honeycomb is only 1-5% of the area present. The depth of the fillet is important as if it is not enough the core will fail right at its sawn edge at a much lower load. The usual way of measuring this facing-to-core bond is the flatwise tension test (§ 4.4.3.) [2]. So the honeycomb side of the adhesive should provide good filleting the skin side should provide high peel strength. Fillet size is the most important physical factor in obtaining the maximum properties of honeycomb and sandwich constructions. For example, a small-fillet 440 g/m² modified epoxy adhesive, was found to give the core less effective strength and “effective stiffness” than the medium-fillet 660 g/m² epoxy-phenolic adhesive weight and fillet size are related. This is generally true for the same, or same type adhesive, assuming that adhesive manufacturing, use processing, and aging effects can be held Constant. When comparing two different adhesives types, the most important characteristic is the fillet size. The weight of the adhesive within each type is also important, but not so much as the fillet size [94].

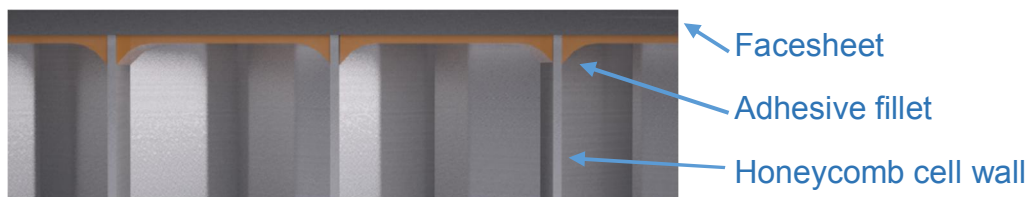


Figure 3.11. Honeycomb bonded to face sheet showing location of adhesive fillet

As two step sandwich panel manufacturing is most commonly practiced [94], therefore it will be described more detailed.

Normally the sandwich panels are laid up in a clean room where the temperature and relative humidity are controlled and the wearing of white cotton gloves is suggested [2]. Handle core and thin skins with extreme care as they could be easily damaged [111].

1. Clean the surfaces of the laminate skin with acetone to remove dust and grease [7].
2. Cut honeycomb block to required dimension. Appropriate tool for this operation is a sharp knife [7], also handbook suggests die cutters, band saws, serrated blade knives and razor blade knives [2]. When ready to bond the honeycomb to the skin gently blow the surface to remove any dust using clean air with no oil present [7, 2]. Acetone can be used to remove grease but extreme care must be taken to prevent fibers from the cleaning cloth sticking to the honeycomb cell walls [7].
3. Remove the adhesive roll from the freezer and allow to thoroughly defrost prior to unbagging and unrolling, so as not to damage the bonds and mesh material within the adhesive which are brittle when frozen [7].
4. Cut 2 sheets of adhesive using a pair of sharp scissors. Return one sheet to the freezer wrapped in an airtight plastic bag [7].
5. As writes Hill minimum bond pressure for film adhesives is 100 kPa higher pressures is not advisable due to the comparatively low crushing strength of the core [7], but the higher available pressures nominally provide a superior quality bond line. Although there is one conflicting fact that most honeycombs can withstand 480 kPa with no problem [2]. As mentioned in other sources honeycomb assemblies are typically cured from 241 to 310 kPa in autoclave. [2, 114]. Pressure can be applied in two ways: with vacuum bag or with pressing assembly by putting on weight or placing in pressing machine. It is highly recommended to glue skins separately. Put adhesive film on skin than honeycomb core. To prevent damage during the curing of one side place the second skin on top of the honeycomb [7].
 - a. Than simplest way to apply pressure is put steel caul plate on the assembly [7].
 - b. One other way that is in-between the aerospace and handyman methods is vacuum bagging the panel and then curing it in an oven while holding the vacuum. Pressure obtained by the vacuum method is up to about 100 kPa. Vacuum procedure provides satisfactory bond. For that reason and other difficulties vacuum bag usually is used only for curved constructions [2, 114].
6. Next, put the system in oven or autoclave where adhesive curing by hot air will be provided. Once curing is complete, leave the oven to cool for 1-2 hours before removing the panel, as the cured adhesive must be cooled slowly to prevent damage occurring due to rapid cooling [7].
7. Trim off the excess honeycomb with a Stanley knife taking care not to damage the cell walls. This will make it easier to align the second skin directly above the first skin [7].
8. Once bonded the sandwich panel edge can be trimmed and individual specimens cut using the diamond edged tile cutter [7].

The panel assembling and curing in autoclave or oven by using vacuum bag is quite similar to prepreg curing described in § 3.3.1., but due to specific properties of honeycomb the following rules must be applied:

- Very important detail in vacuum bagging and autoclave curing is to make sure that honeycomb edge do not exposes to any side pressure. Honeycomb cannot withstand any side pressure and will cave inwards; therefore seals must be used as shown in Figure 3.12. [2, 114].

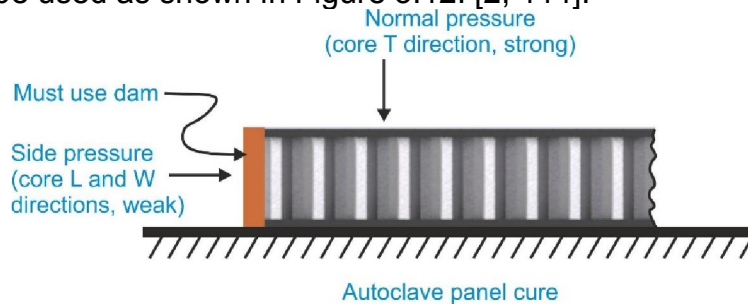


Figure 3.12. Preventing side pressure influence on honeycomb core edge

- When the assembly is to be left under vacuum for an extended period of time, for example overnight, the pressure should be reduced to 34 to 41 kPa.
- When vacuum is applied to an assembly to be cured in autoclave, the autoclave pressure is raised to 136 to 170 kPa release the vacuum on the assembly by venting it to the exterior atmosphere [114].

In conclusion of this paragraph some aircraft typical sandwich constructions are presented in Figure 3.13., Figure 3.14., Figure 3.15. They are made by hand lay-up or by automated fiber placement in autoclave or in oven [26].

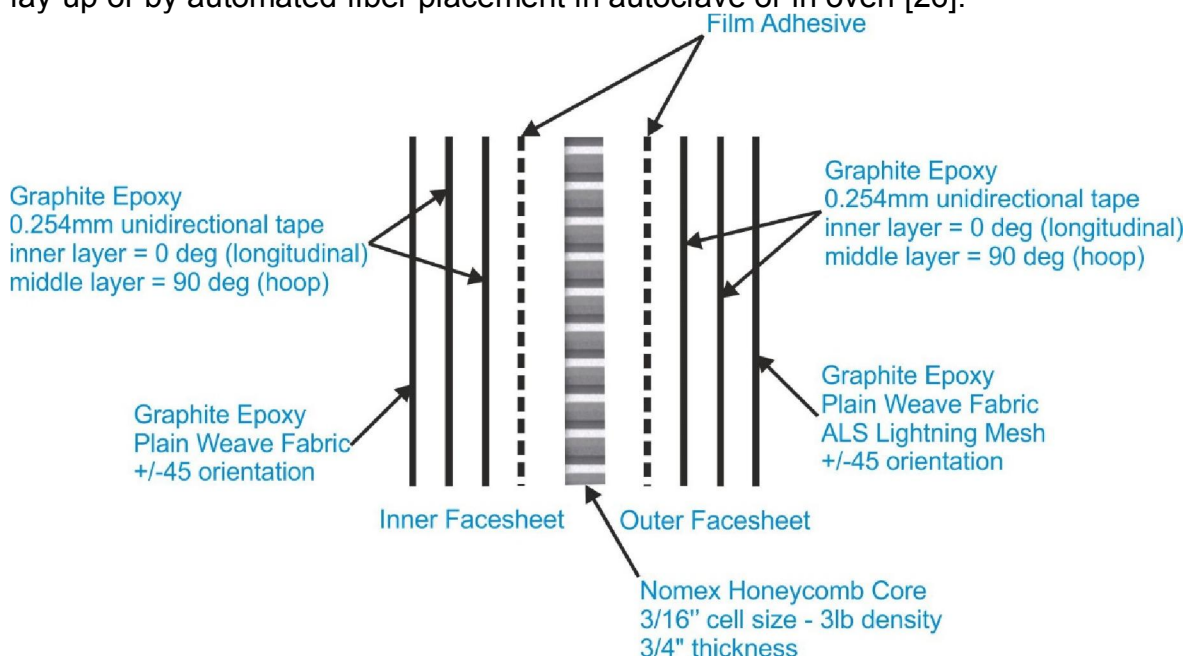


Figure 3.13. Typical layup configuration for Beech Starship

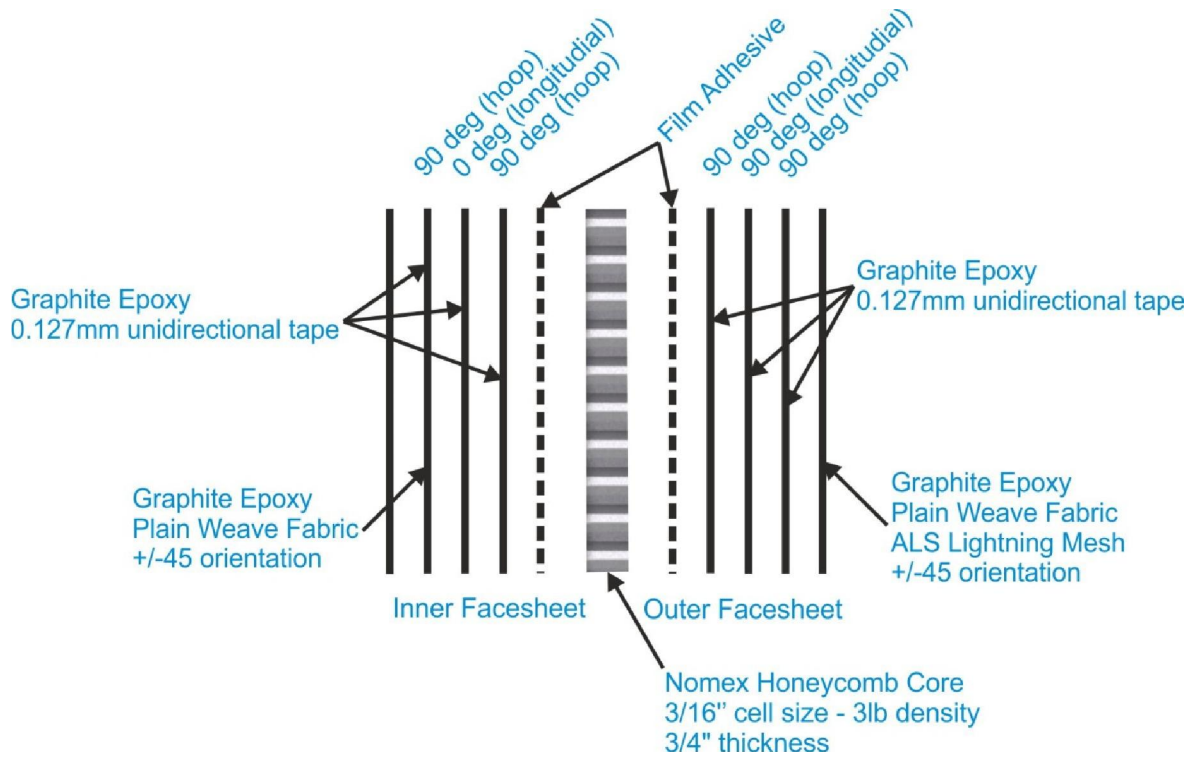


Figure 3.14. Typical layup configuration for Premier I

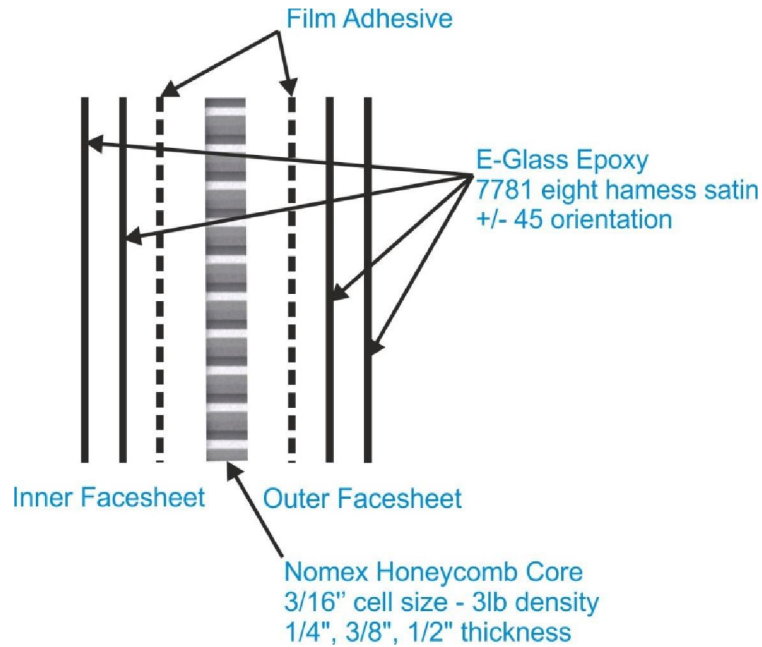


Figure 3.15. Typical layup configuration for Columbia 300

3.3.5 Panel cutting

Carbide or diamond blades appropriate for carbon and fiberglass facings, fine tooth blade for metal facings, and an inverted tooth blade for Kevlar [2]. (Also see Figure 3.8.)

3.4 Reinforcement of specimen's ends

The most important aspect of compression test is to get flat, parallel loading surfaces. The best way to do this is to cut the specimen ends on a milling machine. For thick metallic skins, potting the core is not necessary, but for thin metallic facings and nonmetallic skins the core should be potted [2]. Also need for specimen's ends reinforcement is to prevent some undesirable effects such as end-brooming failure and skin buckling near specimen ends [22]. In this section there will be summarized approaches which are used to solve these problems.

Typically specimens with free unloaded edges are mechanically clamped. Clamping force should be high enough to prevent slipping, but core maybe not able to carry that force and crush, so the loaded ends can be reinforced. Commonly reinforcement is in the form of high density aluminium honeycomb (350kg/m^3) or solid metal blocks with completely same thickness integrated in place of core in the clamping region (Figure 3.16.). Glass epoxy or aluminium tabs can also be bonded to the outer surface in the clamping region [7, 42, 26, 108].

As popular alternative for mechanical clamping, many authors used a potting of the loaded panel ends in epoxy resin or other potting compounds such as metal alloys with low melting temperature. In addition, potting can be done in several ways: potting panel ends with epoxy using the frame (Figure 3.17.), second approach is to remove core in the potting place and that pot with resin filled for example with chopped fiberglass strands, third – fill honeycomb with epoxy resin. Using metal as potting agent have advantage, because after test potted ends is possible to melt and reuse. Potted specimens also can be mechanically clamped or the ends should be machined to provide a uniform load on surfaces. Less frequently used method is setting the specimen in U shaped aluminium or steel blocks (Figure 3.18.) [4, 7, 10, 22, 57, 108, 123, 124,125].

In four-point flexure test places in panel where load will be applied should be reinforced analogically as compression specimens, for example, by potting honeycomb with epoxy resin (Figure 3.19.) [126].

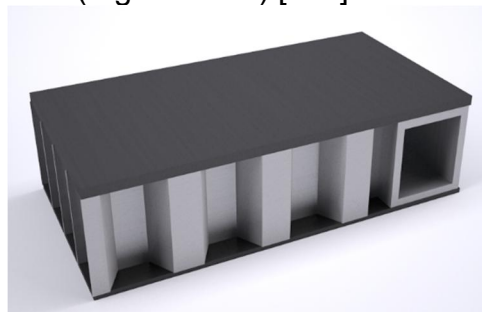


Figure 3.16. Core replacing at specimen end by steel insert

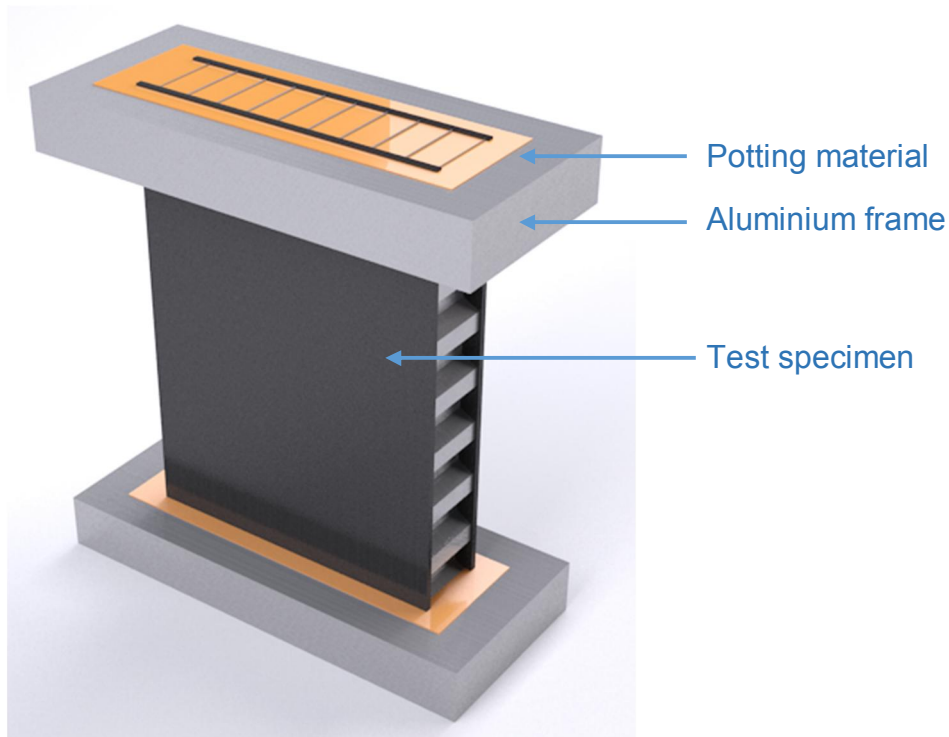


Figure 3.17. Specimen ends potting in frame

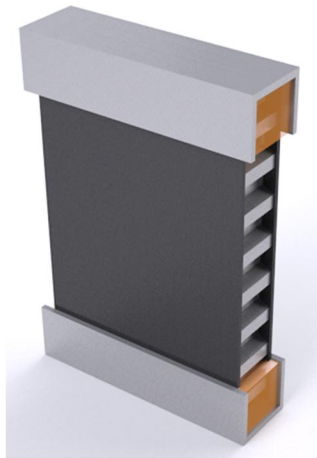


Figure 3.18. Bonded „U” section

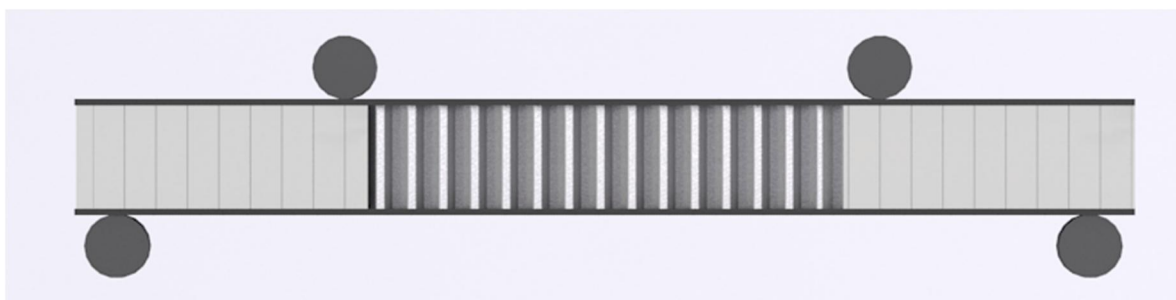


Figure 3.19. Four-point flexure test with reinforced ends

4 Experimental procedures

4.1 Introduction to experimental procedures

Various mechanical tests have been designed to ensure the integrity of honeycomb sandwich structures. These tests evaluate various critical properties of the panel [111]. The basic honeycomb core and sandwich panel tests are contained in: ASTM Standards Test Methods Volume 15.03 (Space Simulation, Aerospace and Aircraft, High Modulus Fibers and Composites) and the Military Standard 401B (Sandwich Constructions and Core Materials). Also, all the major aircraft companies have their own internal honeycomb specification requirements [2], for example, SACMA SRM 2-88, NASA 1 092, Composites Research Advisory Group (CRAG), Boeing and others.

The relatively complexed structure of honeycomb sandwich panel and variety of test methods makes difficulties to create simple and understandable framework of all methods to be logically divided into groups. There is need to review all standards which are related to honeycomb sandwich panels and also for it's separate components (facings and core) and finally to develop method for damaged panel's residual strength estimation, because, as mentioned before, so far there isn't any. Test methods, more or less connected to topic of this review are collected in flowchart shown in Figure 4.1.

Every method is appropriate only for specific information obtaining. In Table 4.1. is summarized information about sensitivity of different methods for different faults estimation.

Tests commonly used for quality control of honeycomb sandwich composites are:

- Flatwise tensile
- Beam shear
- Peel (T-peel and climbing drum peel)
- Lab shear
- Wedge-crack [111].

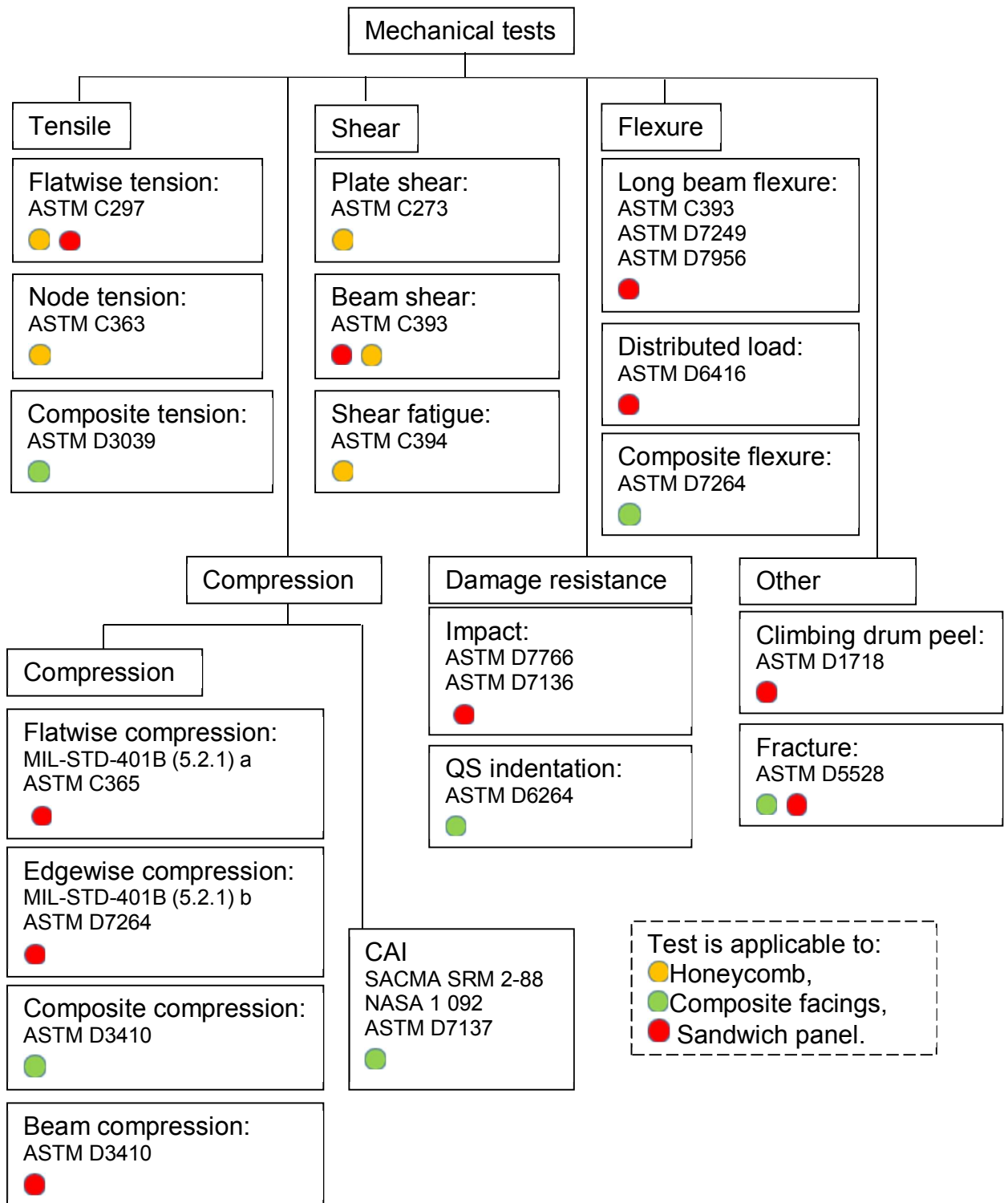


Figure 4.1. Test methods related to CFRP/honeycomb sandwich damage tolerance estimation

Table 4.1. Mechanical tests. Estimation of sensitivity of standard tests to specified faults [111]

Core Defect	Shear Flatwise (ASTM C273)	Tension Flatwise (ASTM C297)	Compression Flatwise (ASTM C365)	Compression Edgewise (ASTM C364)	Flexure Flatwise (ASTM C393)	Shear fatigue Flatwise (ASTM C394)	Drum Peel Test (ASTM D1718)
Gap between core and edge member	N/A	N/A	N/A	High	N/A	N/A	N/A
Unbonded nodes	High load perp. To ribbon dir.	Low	Low	Low	High moment parallel to ribbon	High load perp. To ribbon dir.	Low
Core splice exceeding separation limit	Low	Low	Low	Low	Low	Low	Low
Gaps machined core/stepped skin	Low	Low	Low	Low	Medium moment parallel to step	Low	N/A
Crushed core at edge member	N/A	N/A	N/A	Low	N/A	N/A	N/A
Mismatched nodes (coagurated)	High load perp. To bond line	Low	Low	Medium	High moment parallel to bond line	High load perp. to bond line	Low
Blown core	Medium	Medium	Medium	Medium	Medium	Medium	N/A
Incomplete edge seal	N/A	N/A	N/A	N/A	N/A	N/A	N/A
Diagonal line of collapsed cells	Low	Low	Low	Low	Low	Low	N/A
Over expanded core	Medium	Low	Low	Medium	Medium	Medium	Low
Drilled vent hole in skin	Low	Low	Low	Low	Low	Low	Low
Sideways condensed core	N/A	N/A	N/A	Low	N/A	N/A	N/A
Incomplete core splice	Low	Low	Low	Low	Low	Low	Low
Nested cell (corrugated)	Low	Low	Low	Low	Low	Low	Low
Misaligned ribbon	Low	Low	Low	Low	Low	Low	Low

4.2 Variables

Damage tolerance is affected by a multitude of factors including the facesheet layup configuration and thickness, core material and thickness, interface properties between facesheet and core, fabrication techniques, impact velocity and energy, indenter shape, temperature, boundary conditions, and environmental factors. These factors could be divided in two groups: intrinsic and extrinsic variables are

affecting the impact damage response of the panels [26], nevertheless reviewing literature became apparent that many authors paid limited attention for all this variables. Many researches were focused only on few variables investigation. Also was situations when researchers used only small amount of specimens and from statistical point of view these are not reliable results. Hill [7] reports that much of the previous research had not deeply investigated effect of both intrinsic and extrinsic variables. The number of variations for each parameter was typically restricted to two, such that only limited conclusions could be drawn. In other published research often two parameters were changed simultaneously, again restricting the identification of the individual effects of each variable [7]. Tomblin et al. writes that majority of experimental studies found in the literature considered relatively few sandwich configurations and examined the effect of projectile parameters (mass, shape, impact energy, etc.) on the impact damage induced. The results from many of these studies often were in conflict with each other. Consideration of a small number of panel configurations, however, does not allow for adequate treatment of the complex coupling between facing and core that largely dictates the impact damage development for a given loading [26]. In Table 4.2. are summarized intrinsic and extrinsic variables which should be taken in consideration in damage tolerance tests.

Table 4.2. Main intrinsic and extrinsic variables in damage tolerance tests [7, 22, 26]

Intrinsic variables	Extrinsic variables
fiber type	impactor diameter
matrix type	drop-weight
fiber volume	impact type (drop weight, air gun)
skin layup	impact location
skin thickness	indenter stiffness
core thicknesses	impact energy
core density	indenter shape
skin and core materials	temperature
specimen's dimensions	specimen support conditions
	indenter geometry
	loading speed

Influence of skin thickness

Indentation depth decreases by increasing of skin thickness, also decreases fiber failure average width [26]. Also thicker skinned panels have a higher compressive strength than thinner skinned panels with the compressive strength approximately doubling for 2 to 4 ply skins and trebling for 8 to 24 ply skins [7].

Failure modes also changed, with thinner skinned panels typically failing due to compressive failure of the skins as the skins were not strong enough to crush the core, whilst thicker skinned panels failed due to the catastrophic inward growth and propagation of the residual indentation [7].

Increasing the facesheet thickness does not necessarily improve the impact resistance of a given sandwich structure and may result in surface damage below the threshold of detectability for a particular impact [26].

The absorbed energy/impact energy ratio and contact duration decrease with the face-sheet thickness, while the peak load increases [4].

For sandwich configurations with thin facesheets, the residual strength increased with panel width. However, this increase was not observed for sandwich configurations with thicker facesheets [108].

Skin lay-up

Panels with different skin lay-ups but constant thickness do not change the basic failure mechanism although the compressive strength is varying. Panels with cross-ply skins had a higher compressive strength than those with angle ply skins [7].

Matrix type

Tougher matrix materials decrease local matrix damage area [26].

Core

Panels with thick low density cores are often prone to local buckling, whilst high density cores provide greater stability to the skins and consequently fails due to compressive skin. The increase in compressive strength with core density is significant for low to medium density cores but is minimal for further increases in core density. This is likely to be due to the change in failure mode from local buckling to compressive skin failure. Generally the aluminium panels shows less sensitivity to the impact damage with lower local strain concentrations and a slightly higher residual compressive strength than the nomex panels. Although the failure modes for both types of panel are similar, the nomex panels shows some growth of the residual indentation whereas the aluminium panels do not [7].

It was determined that a thicker core produced a higher CAI strength for a given impact energy [4].

Indenter

The residual compressive strength decreases when the indenter diameter increases up to a diameter of 12.7mm. Further increases in indenter diameter above 12.7 mm marginally increases the residual compressive strength. This trend is suggested to be due to indenter diameters of 12.7 mm and below causing fiber fracture of the impacted skin, whereas larger indenters only causes residual indentation of the skin. Tomblin et al. found the failure modes associated with 25.4 mm and 76.2 mm indenters to be different and panels loaded with the small indenter to generally have a higher residual compressive strength for a given impact energy. The small indenter causes a large residual dent but small damage area, which led to a compressive skin failure emanating from the damage site under in-plane compression [7].

The absorbed energy/impact energy ratio and contact duration decrease with the indenter size, while the peak load increases [4].

Influence of impact location

Impact location, can affect the impact deformation and damage formation behavior of the specimens significantly. Also results can be affected if the impact force is not applied perpendicular to the plane of the laminated plate [127].

Let's see this difference on an example. Tomblin et al. [27] have made research where impacted panel in different locations. The impact testing was conducted at two energy levels, using a 76.2 mm diameter indenter. The off-center impacts (Figure 4.2.) were conducted at distances of 50.8 mm ($a/8$) and 101.6 ($a/4$) from the supported edge. It was observed that the peak impact force increases as the impact location approaches the boundary supports due to the increased flexural stiffness of the panel closer to the supports. Thus, in an airframe, the locations close to the underlying frames or bulkheads will increase the stiffness of the panel, resulting in higher impact forces [27].

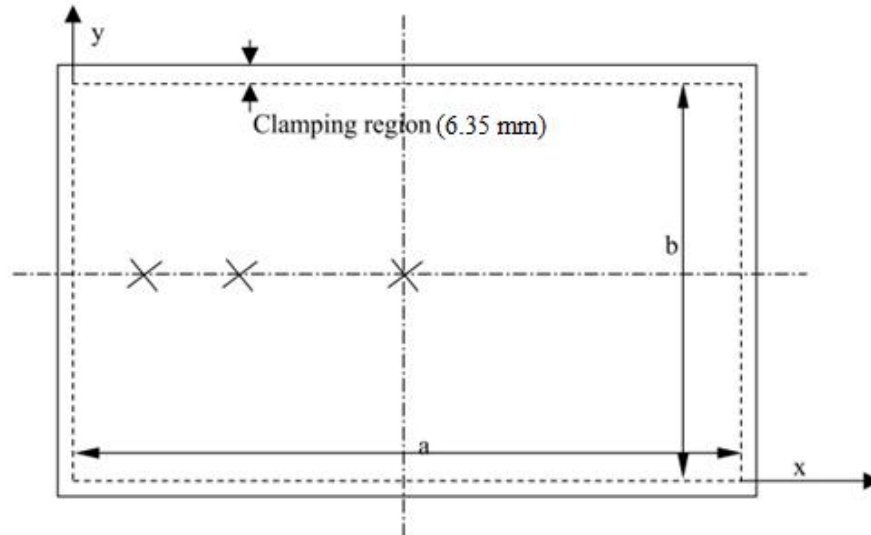


Figure 4.2. Specimen geometry and impact locations used

Impact velocity

Zenkert et al. found panels subjected to quasi-static indentation whilst resting on a solid base to suffer propagation of the residual dent prior to compressive skin failure. However, for unsupported panels subjected to low velocity impact there was no growth of the residual indentation with catastrophic compressive skin failure. In the study by McGowan where impact damage was inflicted by both drop weight and airgun apparatus, a subsequent variation in RCS could be seen. Below the BVID threshold this difference was small but above the threshold the RCS of the panels impacted with the airgun was 14% lower than for the panels impacted with drop weight rig despite the residual dent depths being similar. This variation was due to the internal damage caused by the airgun impact being more severe and highlights the problems of using dent depth alone as a measure of impact damage and subsequent residual compression strength [7, 22, 128].

Impact Energy

Higher energies increase the indentation, increase local matrix damage area. Also higher energies had fiber failures concentrate towards the back surface in the fiber failure through-thickness distribution [26].

Force increases with impact energy until facesheet fracture is occurring. The impact parameters, such as peak load, absorbed energy/impact energy ratio and contact duration increases with impact energy [4].

Both the planar damage diameter and indentation depth increases with the impact energy, but decreases with the face-sheet thickness [4].

Impact type

The residual strength of the panels impacted using drop weight and airgun methods is similar to each other for low-energy-level impacts. However, as the impact energy level increases, the residual strength of the airgun-impacted panels is less than that of the dropped-weight-impacted panels [22].

Temperature

Higher temperatures increases indentation [26].

Dimensions

Hill made comparisons between the impact damage of small 200 mm x 400 mm panels and large 800 mm x 800 mm panels. For the same level of impact energy the smaller panels were seen to suffer fiber fracture and delamination of the top skin whilst the larger panels had some delamination and core damage but no fiber breakage. This is suggested to be due to more energy being absorbed elastically through the greater amount of global deflection and induced membrane action in the large panels, leaving less energy to be absorbed through creating permanent damage [7].

Effects of scaling on the impact damage resistance and damage tolerance of sandwich panels with thin quasi-isotropic facesheets and honeycomb cores studied by Tomblin et al [27]. The effects of scaling were characterized in terms of the impact response, planar damage size, and the residual dent depth. The experimental results indicated that the impact force decreased when both the planar dimensions of the panel were increased. However, the increase of a single dimension did not significantly change the impact response. The scaling of planar dimensions on the planar damage size exhibited trends similar to that of the impact force, with the exception of the sandwich specimens with rigid-base supports, which suffered more residual indentation than planar damage. The effects of varying the ratio of specimen width to planar damage diameter, for a fixed damage size, were studied by conducting compression tests. No significant trend was however observed for sandwich specimens with 4-ply facesheets. The displacement and strain distributions showed contrasting behavior of impact damage as the specimen width was increased. The results indicated higher component of facesheet bending within the damage region for narrow specimens when compared with the wider specimens [27].

Clearly an increase in panel thickness will increase the flexural rigidity and therefore alter the bending response [7].

4.3 Testing of honeycomb core

The basic honeycomb core mechanical tests are compression, plate shear and tensile-node bond strength.

Compression

The compression tests consist of two types: the bare compression method and the stabilized compression method. The bare compression is performed on just bare honeycomb without facings. It is used only as a quick quality assurance test and only the bare compressive strength is obtained. The bare compressive strength

should be used when investigating the core pressure from curing [2]. Flatwise compressive strength and modulus are fundamental mechanical properties of sandwich cores that are used in designing sandwich panels [129].

Tensile-node bond strength

The honeycomb tensile-node bond strength is a fundamental property that can be used in determining whether honeycomb cores can be handled during cutting, machining and forming without the nodes breaking. The tensile-node bond strength is the tensile stress that causes failure of the honeycomb by rupture of the bond between the nodes. It is usually a peeling-type failure [130].

Plate shear test

From this test the honeycomb shear strengths and moduli are determined. In most designs these are the critical core properties. There are two ways of performing this test: compressive plate shear or tensile plate shear. Here the honeycomb is bonded to thick steel plates. Both of these tests give the same results. The compressive method may be quicker and it is easier to load the specimen on the test machine; however, the tensile method may be safer as the steel blocks cannot fly off the test machine at failure (this rarely happens). The specimen length should be equal to or greater than 12 times the core thickness [2].

Beam shear test

Another type of shear test is the beam shear test. This test is normally used on heavy density cores over 160 kg/m^2 as some of these cores will not fail when tested by the plate shear method as the core-to-plate adhesive fails first. Important that load required to fail the honeycomb core in shear does not stress the facings above their yield stress. Because the facings do take some of the shear load as the honeycomb yields, the core beam shear strengths are higher than the plate shear values and can be significantly greater, especially on Nomex cores [2].

4.3.1 Flatwise compression: ASTM C365 & MIL-STD-5.2.1

Summary

This test method covers the determination of compressive strength and modulus of sandwich cores, including honeycomb. Test setup shown in Figure 4.3. [129].



Figure 4.3. ASTM C365 Honeycomb flatwise compression test setup

Specimens

Test specimens shall have a square or circular cross-section. The specimen's cross-sectional area is defined in the facing plane, in regard to the orientation that the core would be placed in a structural sandwich construction [129].

The required facing area of the specimen is dependent upon the cell size, to ensure a minimum number of cells are tested. Minimum facing areas are recommended in Table 4.3. for the more common cell sizes. These are intended to provide approximately 60 cells minimum in the test specimen. The largest facing area listed in the table (5625 mm²) is a practical maximum for this test method. Cores with cell sizes larger than 9 mm may require a smaller number of cells to be tested in the specimen. For example, for a honeycomb core the cross-sectional area is defined in the plane of the cells, which is perpendicular to the orientation of the cell walls [129].

Table 4.3. Recommended minimum specimen cross-sectional area [129]

Minimum cell size, mm	Maximum cell size, mm	Minimum Cross-Sectional Area, mm ²	Square specimen dimensions, mm
-	3	625	25 × 25
3	6	2500	50 × 50
6	9	5625	75 × 75

* Maximum cell size should not exceed area equal to 10 000 mm².

Preparing of the specimens should be done as the loaded surfaces shall be parallel to each other and perpendicular to the sides of the specimen. When cutting specimens from large sheets of core to notches, undercuts, and rough or uneven surfaces must be avoided [129].

Test set-up

Force shall be introduced into the specimen using one fixed flat platen and one spherical self-aligning seat platen. The platens shall be well-aligned and shall not apply eccentric forces. A satisfactory type of apparatus is shown in Figure 4.3. The platen surfaces shall extend beyond the test specimen periphery [129].

Specimens must be aligned well between the platens, in order to distribute the applied force as uniformly as possible over the entire loading surface. Non-uniform loading often results in failures that are confined to one corner or one edge of the specimen [129].

Specimen is loaded until failure, or until the measured LVDT/compressometer deflection equals 2 % of the initial core thickness [129].

Facing plane stabilization

In order to prevent local crushing of some honeycomb cores, it is often desirable to stabilize the facing plane surfaces with a suitable material, by dipping in a thin layer of resin or bonding to thin facings [129]. In both cases adhesive fillet stabilizes the honeycomb cell walls and produces slightly higher results than the bare compression test [2].

Speed of Testing

Speed of testing should be in the interval to produce failure within 3 to 6 min. The suggested standard head displacement rate is 0.50 mm/min [129].

Displacement

For displacement measurement acceptable are using a machine crosshead movement indicator, LVDT, compressometer, or similar device with 61 % precision on displacement. Although it is not good practice to use the test machine cross-head travel to obtain the specimen's deformation. The modulus values determined this way will normally be quite low, as little as one-third the actual value [2].

Failure

Uniform compressive failure of the sandwich core is the only acceptable failure mode. Compressive failures confined to one corner or edge of the specimen shall be considered invalid [129].

Calculation

Ultimate flatwise compressive strength calculation by equation:

$$F_z^{fcu} = \frac{P_{\max}}{A}$$

where:

F_z^{fcu} – Ultimate flatwise compressive strength, MPa;

P_{\max} – Ultimate force prior to failure, N;

A – cross-sectional area, mm².

Deflection Stress. If 2 % deflection is achieved prior to stopping the test, calculate the flatwise compressive stress at 2 % deflection using equation:

$$\sigma_z^{fc0.02} = \frac{P_{0.02}}{A}$$

where:

$\sigma_z^{fc0.02}$ – flatwise compressive stress at 2 % deflection, MPa;

$P_{0.02}$ – applied force corresponding to $\delta_{0.02}$, N;

$\delta_{0.02}$ – recorded deflection value such that δ/t is closest to 0.02;

t – measured thickness of core specimen prior to loading, mm.

Calculation of the flatwise compressive chord modulus by using equation:

$$E_z^{fc} = \frac{(P_{0.003} - P_{0.001}) \cdot t}{(\delta_{0.003} - \delta_{0.001}) \cdot A}$$

where:

E_z^{fc} – core flatwise compressive chord modulus, MPa;

$P_{0.003}$ – applied force corresponding to $\delta_{0.003}$, N;

$P_{0.001}$ – applied force corresponding to $\delta_{0.001}$, N;

$\delta_{0.003}$ – recorded deflection value such that δ/t is closest to 0.003,

$\delta_{0.001}$ – recorded deflection value such that δ/t is closest to 0.001.

The deflection values selected are intended to represent the lower half of the core's stress-strain curve. For core materials which fall below $\delta/t = 0.006$, a deflection range of 25 to 50 % of ultimate is recommended [129].

4.3.1 Honeycomb node tension: ASTM C363 & MIL-STD-5.1.8

Summary

The honeycomb tensile-node bond strength test also known as core delamination test covers the determination of the tensile-node bond strength of honeycomb core materials. Honeycomb construction is subjected to a uniaxial tensile force parallel to the plane of the honeycomb [130, 2].

Specimens

The test specimens shall be 130 ± 5 mm wide. The test specimens shall have a minimum length of 260 with a minimum test section outside the grips of 200 mm. The standard thickness of the core slice shall be 16 ± 1 mm for metallic cores [130].

Specimens shall be cut such that the number of cells along the width is constant along the specimen length. The length being defined as the specimen dimension parallel to the application of the force. The specimen width shall be parallel to the node bond areas [130].

Test set-up

The force is transmitted to the honeycomb through pins, which are placed in cell rows on the top and bottom portions of one specimen. Pins should have the largest diameters that will easily fit into the honeycomb cells. Figure 4.4. shows a fixture that has been satisfactorily used to hold and load the pins. Specimen is loaded until it is completely torn into two pieces or an unacceptable failure mode occurred [130].

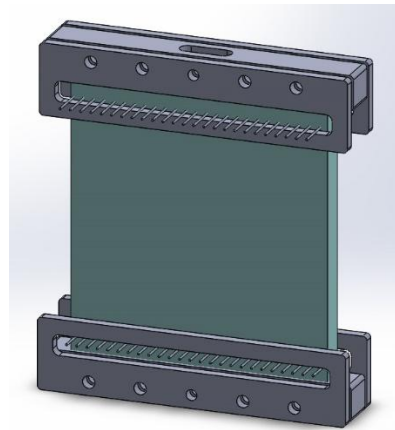


Figure 4.4. Honeycomb core tensile-node bond strength test setup

Speed of Testing

Applied testing speed should produce failure within 3 to 6 min. The suggested standard head displacement rate is 25 mm/min [130].

Failure

The only acceptable failure mode is the tensile failure of the node-to-node honeycomb bond within the body of the honeycomb specimen in other words failure mode is a peeling of the nodes. Failure of the honeycomb material at the loading pin location is not a valid failure mode [130].

Excessive bending will cause premature failure. Every effort should be made to eliminate excess bending from the test system. Bending may occur as a result of misaligned grips, poor specimen preparation, or poor alignment of the loading fixture [130].

Calculation

Node bond strength of the core could be calculated by using following equation:

$$\sigma = \frac{P_{\max}}{bt}$$

where:

P_{\max} – ultimate tensile force, N;

b – initial width of specimen, mm

t – thickness of specimen, mm [130]

4.3.2 Honeycomb shear properties: ASTM C273

Summary

This test method covers the determination of shear properties of sandwich construction core materials associated with shear distortion of planes parallel to the facings. The core shear properties are fundamental properties that are used in the design of sandwich panels. This test method provides information on the force-deflection behavior of sandwich constructions or cores when loaded in shear parallel to the plane of the facings [131].

Specimens

The test specimens shall have a thickness equal to the thickness of the sandwich, a width not less than 50 mm, and a length not less than twelve times the thickness [131].

Test set-up

Either a tensile or compressive loading mode may be used. In either case, the test specimen shall be rigidly supported by means of steel plates bonded to the facings. The thickness of the plates may be varied in accordance with the strength of the sandwich, but the plate length shall be such that the line of action of the direct tensile or compressive force shall pass through the diagonally opposite corners of the core/sandwich as shown in Figure 4.5. A correct line of load action may also be obtained by modifying the core length to thickness ratio provided the specimen dimensional requirements [131]. A LVDT transducer is mounted near the center of the specimen to measure the relative displacement between the steel plates. The core can be oriented with the L or W direction in the loading direction, depending on which core shear property is being determined [2].

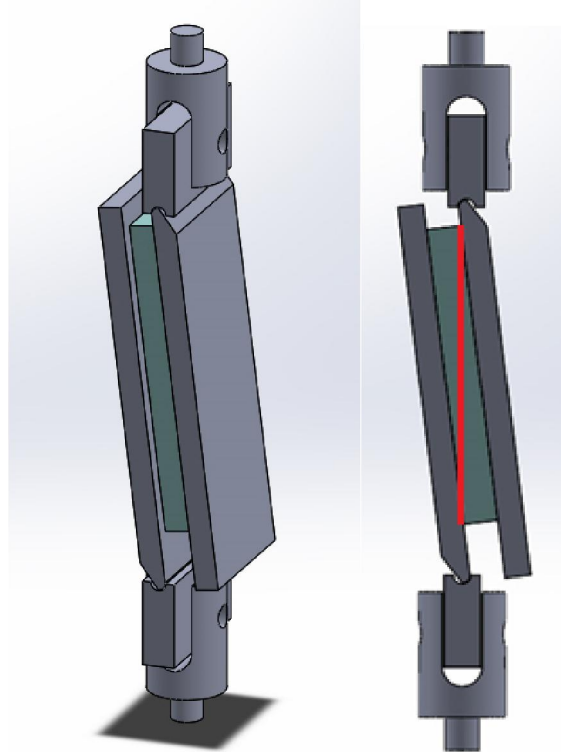


Figure 4.5. Plate shear test (compression mode)

Speed of Testing

Speed of testing should be appropriate to produce failure within 3 to 6 min. The suggested standard head displacement rate is 0.50 mm/min [131].

Failure

Adhesive or cohesive failures, or both, at the core-to-facesheet, facesheet-to-load-plate, or (if no facesheets are used) core-to-load-plate interface are not acceptable failure modes and the data shall be noted as invalid. The core shear failure mode is considered to be acceptable [131].

Calculation

Shear stress is calculated as follows:

$$\tau = \frac{P}{L \cdot b}$$

where:

- τ – core shear stress, MPa;
- P – instantaneous force on specimen, N;
- L – length of specimen, mm;
- b – width of specimen, mm.

Instantaneous effective core shear strain calculated as follows:

$$\gamma = \frac{u}{t}$$

where:

- γ – core engineering shear strain, mm/mm;
- u – instantaneous displacement between loading plates, mm;
- t – thickness of core, mm.

Effective core shear modulus is calculated as follows:

$$G = (\Delta P / \Delta u) \cdot t / (L \cdot b)$$

where:

$\Delta P / \Delta u = (P_b - P_a) / (u_b - u_a)$ = Slope of the linear portion of the force-displacement curve, in N/mm, from u_a mm to u_b mm where u_a and u_b may be chosen on either a specimen- or dataset-basis [131].

4.4 Testing of sandwich panels

There are several tests for properties determination of honeycomb sandwich panels. Flatwise tension and climbing drum peel test are good ways of evaluating the integrity of a honeycomb sandwich panel and how well the skins are bonded to the honeycomb, flatwise compression, plate shear, flexural shear (all the same as the honeycomb tests), edgewise compression and long beam flexure. Here the test specimens must be obtained from the panel for which the properties are desired [2].

The edgewise compression test consists of compressively loading the panel parallel to the facing plane. All the honeycomb should do is stabilize the skins from the local buckling mode failures and provide a thick enough panel so overall buckling or shear crimping does not occur [2]. In general there are two methods for sandwich panel compression test. They are ASTM C364 and Military Standard's 401B section 5.2.1. Both are related so they will be discussed simultaneously [120].

The flatwise tensile test is conducted to determine the tensile strength of the core or the tensile strength of the adhesive bond between the core and the face sheet of a honeycomb sandwich assembly [111].

Beam shear test is often used to evaluate the overall sandwich performance. Values obtained using this test generally depend on the facing thickness, facing material and loading condition [111].

4.4.1 Edgewise compression: ASTM C364 & MIL-STD-401B

Summary

The edgewise compression sandwich test covers a procedure for determining compressive properties of sandwich constructions in a direction parallel the plane of a sheet of sandwich. The edgewise compressive strength of short sandwich construction specimens provides a basis for judging the load carrying capacity of the construction in terms of developed facing stress. It is particularly appropriate for honeycomb [120, 132]. Test setup shown in Figure 4.6. Procedure is for in-plane compression only and does not include or consider impact damage. Unlike the other test methods (SACMA, NASA, D7137) ASTM C364 does not offer support to the unloaded edges of the panel, so 'column compression' is induced [7].

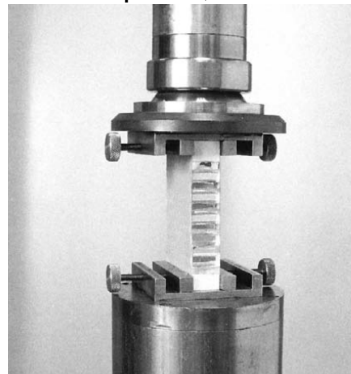


Figure 4.6. Edgewise compression test [120]

Specimens

Care shall be taken in preparing the test specimens to insure smooth end surfaces, free of burrs. The dimensions of the specimens shall be measured to at least the nearest 0.5 percent in [132]. The specimen size can be any reasonable dimensions as long as they conform to the ASTM and Military Standard 401B limitations. Normally a 76.2 mm by 127 mm sample will be adequate; however, sometimes a 50.8 mm by 50.8 mm specimen is required to obtain the highest test values [2]. MIL-STD-401B postulating that specimen shall be at least 5 cm wide, but not less than twice the sandwich thickness, not less than the width of two complete core cells. The unsupported specimen length (dimension parallel to direction of applied load) shall be not greater than eight times the sandwich thickness [132]. Recommended dimension range by ASTM is given in Table 4.4.

Table 4.4. Recommended dimension range [120]

Dimension	Recommended Range
Length, L (mm)	$L \leq 8 \times t$
Width, W (mm)	$50 \leq W \leq L$; $W \geq 2 \times t$; $W \geq 4 \times \text{cell widths}$

Lateral end supports

Unintended loading eccentricities will cause premature failure. Such eccentricities may occur as a result of misaligned grips, poor specimen preparation, or poor alignment of the loading fixture [120]. The facings of the sandwich shall be supported against lateral buckling at the specimen ends [132]. There are three ways to support specimen ends:

1. Via clamps made of rectangular steel bars fastened together so as to clamp the specimen lightly between them (the cross-sectional dimensions of each of these bars shall be not less than 6 mm, such as that shown in Figure 4.7. [120]. Since the panels tested are usually not all the same thickness, this is one fixture that works well. Here the bars are movable and the fixture can accommodate panels of different thicknesses [2];
2. Fitting the specimen snugly into a lengthwise slot in a round steel bar, where such bars shall have a diameter not less than the thickness of the sandwich plus 6 mm, and are suitably retained on the spherical bearing block (preferably of the suspended, self-aligning type) surfaces [120, 132];
3. Casting the ends of the specimens in resin or other suitable molding material. The cast ends of the specimen should be ground flat and parallel [120, 132].

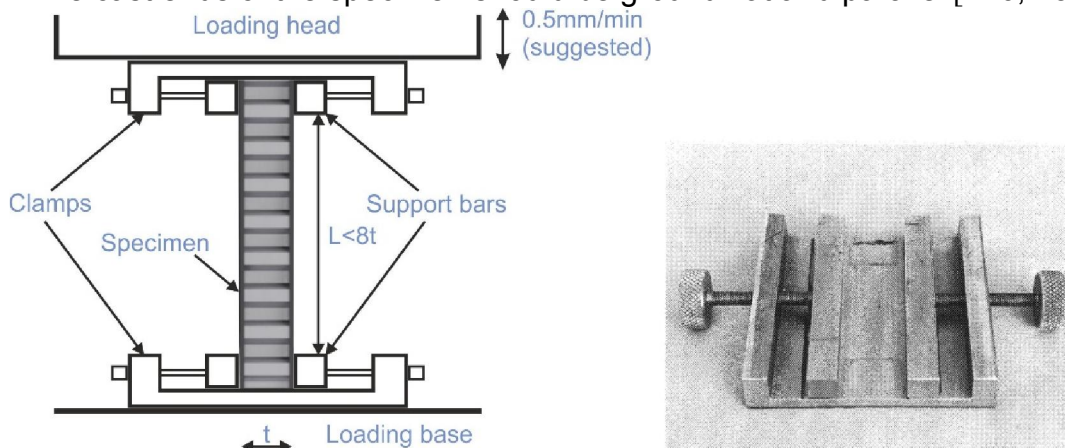


Figure 4.7. Adjustable for different panel thickness edgewise compression test fixture [2, 7]

Speed of Testing

Appropriate speed of testing should produce failure within 3 to 6 min. For use as a guide in obtaining the proper testing machine speed ASTM suggests standard head displacement rate is 0.50 mm/min [120], MIL-STD-401B suggests rate of head movement is 0.3 percent of specimen length per minute [132].

Strain

The load shall be applied to the specimen through apparatus, properly centered on the specimen to distribute the load equally into each facing. It is essential that strains be measured to avoid widely varying results, due to different effective eccentricities, which occur if strains are not properly balanced [132].

Strain gage capable of measuring strain to at least 0.0001 mm/mm and having a gage length not greater than two thirds of the unsupported length of the specimens to be tested, not less than three unit cells if the facesheet is a composite fabric material form. A minimum of two axial strain gages, centrally located on opposite faces of the test specimen, is required. If more complete shear and bending information is desired, four to twelve gage configurations may be used. Apply compressive force to the specimen, until approximately 10% of the anticipated ultimate force is achieved. Reduce the compressive force to 150 N at an equivalent unloading rate and check strain gage output for proper alignment per the following step [120].

Review the recorded strain gage data for evidence of specimen bending. A difference in the stress-strain or force-strain slope from opposite faces of the specimen indicates bending in the specimen. Determination of percent bending at the maximum applied force for each of the back-to-back gage locations is carried out by using equation:

$$B_y = \frac{\varepsilon_1 - \varepsilon_2}{\varepsilon_1 + \varepsilon_2} \cdot 100$$

where:

B_y – percent bending,

ε_1 – indicated strain from gage on one face,

ε_2 – indicated strain from gage on opposite face [120].

The sign of the calculated percent bending indicates the direction in which the bending is occurring. This information is useful in determining if the bending is being introduced by a systematic error in the test specimen, testing apparatus, or test procedure, rather than by random effects from test to test. Rapid divergence of the strain readings on the opposite faces of the specimen, or rapid increase in percent bending, is indicative of the onset of panel instability. If either of these conditions is found to exist in the strain gage data, or if percent bending at the maximum applied force exceeds 10%, the fixture, specimen and load platens must be examined for conditions which may promote specimen bending, such as the presence of gaps, loose fixture components, or platen misalignment. In such situation test should be readjusted and repeated [120].

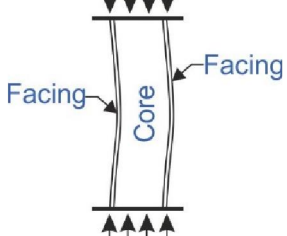
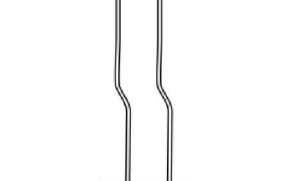
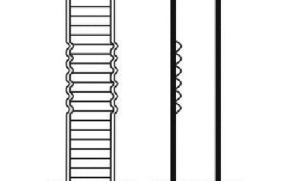
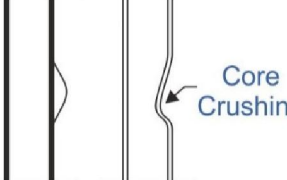
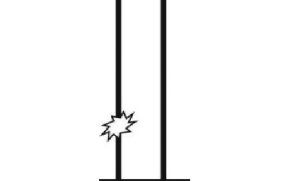
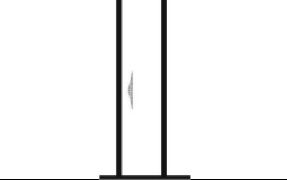
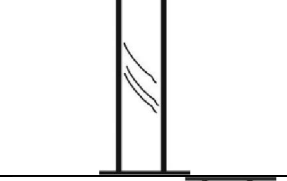
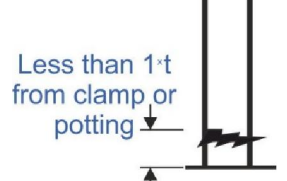
Failure (*Failure modes also discussed in chapter 5.2.1.)

The only acceptable failure modes for edgewise compressive strength of sandwich constructions are those occurring away from the supported ends. The sandwich column, no matter how short, usually is subjected to a buckling type of failure unless the facings are so thick that they themselves are in the short column class. The failure of the facings manifests itself by wrinkling of the facing, in which the core deforms to the wavy shape of the facings; by dimpling of the facings into the honeycomb cells; by bending of the sandwich, resulting in crimping near the ends as a result of shear failure of the core or by failure in the facing-to-core bond and associated facesheet buckling [120].

The sandwich column, no matter how short, is usually subject to a buckling type of failure. This failure manifests itself by wrinkling of the facing, shear crimping, dimpling of facings or general buckling, in which case, the core deforms to the wavy shape of the facings; by dimpling of the facings into the cell of honeycomb-like cores; or by bending of the sandwich resulting in crimping near the end, due to core shear failure or perhaps failure of the core-to-facing bond (see

Table 4.5) [132]. Failure modes listed before are considered to be acceptable [120]. It is rare to achieve the actual ultimate compressive strength of the facing material, but the results should be close [2].

Table 4.5. Sandwich panel edgewise compression failure modes

Type of failure	Idealized picture
<p>General buckling [132]</p>	
<p>Shear crimping [132]</p>	
<p>Dimpling of facings — In honeycomb panels, intracell dimpling of the facesheet(s). [120, 132]</p>	
<p>Facesheet buckling — One or both facesheets exhibit a buckling type of failure, often initiated by facesheet-to-core debonding or core crushing [120, 132]</p>	
<p>Facesheet compression — Short-column compression failure of one or both facesheets prior to any core or bondline failure, often followed by global buckling of sandwich panel [120].</p>	
<p>Core compressive failure — Out-of-plane facesheet deformation initiates local core crushing, often followed by global buckling of sandwich panel [120].</p>	
<p>Core shear failure — Out-of-plane facesheet deformation initiates local core shear failure, often followed by global buckling of sandwich panel [120].</p>	
<p>End failures – occurring at the bond to the loading blocks or within one specimen-thickness of the end-clamps. These are not acceptable failure modes and the data shall be noted as invalid [120].</p>	

Calculation

For ultimate edgewise compressive strength calculation is used following equation:

$$\sigma = \frac{P_{max}}{w(2t_{fs})}$$

where:

σ – ultimate edgewise compressive strength, MPa

P_{max} – ultimate force prior to failure, N

w – width of specimen, mm;

t_{fs} – thickness of a single facesheet, mm [120].

4.4.2 Compression of sandwich beam: ASTM D5467

Summary

This test procedure introduces compressive load into a thin skin bonded to a thick honeycomb core with the compressive load transmitted into the sample by subjecting the beam to four-point bending [133].

Specimens

A sandwich beam composed of two prepreg facesheets separated by a relatively deep honeycomb core [133], recommended facesheet and beam core geometry and material specifications for carbon reinforced test coupons are provided in Table 4.6. [120]. The main component of the compression test specimen is the face sheet that is loaded in compression during flexure, with the material direction of interest oriented along the length of the beam. The other facesheet is of a material and size carefully selected to preclude its influence on the test results. The ultimate compressive strength of the material is determined from the load at which the test facesheet of the sandwich beam fails in an acceptable compression failure mode [133].

Individual test specimens may be machined from fabricated larger panels. Care should be taken to avoid damaging the edge of the laminate since the compression strength is sensitive to edge damage. All edges should be visually examined for damage [120].

Test set-up

Test setup shown in Figure 4.8. Rubber pads may be used to distribute the load at the specimen/fixture contact points. Pads shall cover the full width of the beam, with a nominal length of 25 mm for the test facesheet and 38 mm for the opposite facesheet [120].

If the strain values from gages on sandwich specimen differ more than 10 %, so then the test results are not valid [120].

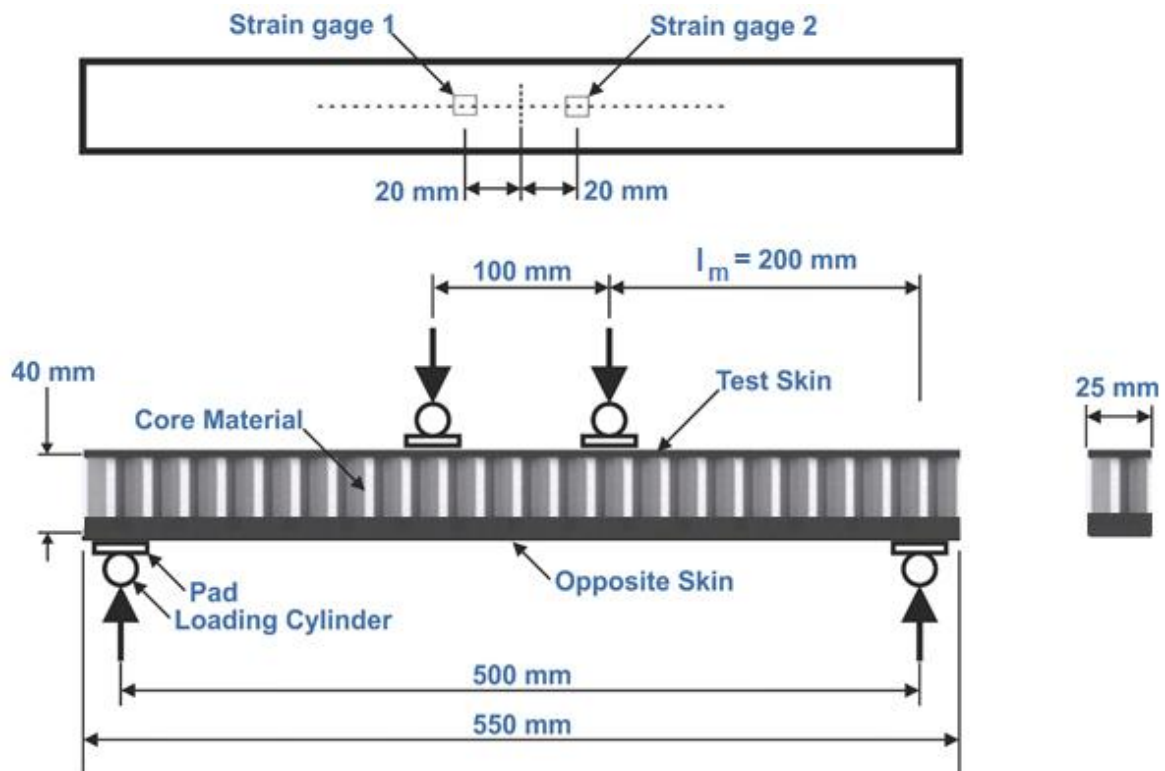


Figure 4.8. Longitudinal compression sandwich beam test setup [133]

Table 4.6. Recommended nominal specifications for carbon tape test facesheets [120]

Dimension	Configuration [0] mm	Configuration [90] mm
facing skin thickness	0.8	1.2
core thickness	40	13
opposite skin thickness	1.2	1.6
l_m	200	50
width	25	25

Materials:

Core	3 to 4 mm hexagonal cell size. Aluminium honeycomb, W/L axis in span direction	
Opposite facesheet	Same as test facesheet	2024 Aluminum
Core density	368 kg/m ³	130 kg/m ³

Speed of Testing

Speed of testing should be enough to produce failure within 1 to 10 min from the beginning of load application. The suggested standard speeds are: strain-controlled tests (0.01 min⁻¹) and constant head-speed tests (1.5 mm/min) [120].

Strain

If the specimen strain is monitored with strain or deflection transducers then the stress-strain response of the material can be determined, from which can be derived the compressive modulus of elasticity for this configuration [120].

Strain data shall be determined by means of strain gages. Strain gages should have an active grid length of 3 mm or less; (1.5 mm is preferable). Resistances of 350 Ω or higher are preferred [120].

If strain is to be measured for the [0] configuration, apply two longitudinal strain gages to the specimen test facesheet as shown in Figure 4.8. Apply one longitudinal gage if strain is to be measured for the [90] configuration in center of beam, like between this two strain gages mentioned before [120].

Failure

The objective of this test method is to load the sandwich beam in four point flexure and fail the upper (compressively loaded) facesheet in compression. Therefore, the acceptable failure modes for this test method are those that occur in the compressively loaded face. Unacceptable failure modes include core shear, core crushing, local wrinkling, or separation of the core from the facesheet. The acceptable failure area is within the central 50 mm of the gage section of the test facesheet [120].

4.4.3 Sandwich panel flatwise tension: ASTM C297

Summary

This test method determines the flatwise tensile strength of the core, the core-to-facing bond, or the facing of an assembled sandwich panel. Sandwich construction is subjected to a uniaxial tensile force normal to the plane of the sandwich. This test method can be used to provide information on the strength and quality of core-to-facing bonds, also it can be used to produce flatwise tensile strength data for the core material [134].

Specimens

Test specimens shall have a square or circular cross section. The required facing area of the specimen is dependent upon the cell size, to ensure a minimum number of cells are tested. These are intended to provide approximately 60 cells minimum in the test specimen. Cores with cell sizes larger than 9 mm may require a smaller number of cells to be tested in the specimen. Table 4.7. summarises minimum specimen facing area for common cell sizes [134].

Table 4.7. Recommended minimum specimen facing area and loading block dimensions [134]

Minimum Cell Size, mm	Maximum Cell Size, mm	Minimum Loading Block Dimension, mm	Minimum Facing Area, mm ²
-	3	25	625
3	6	50	2500
6	9	75	5625

When cutting specimens from large panels it is very important to avoid notches, undercuts, rough or uneven surfaces, or delaminations due to inappropriate machining methods [134].

The loading blocks shall be bonded to the core or facings of the test specimen using a suitable adhesive. The assembly bonding pressure shall not be greater than

the original facing-to-core bonding pressure [134]. The top and bottom surfaces of the sandwich sample should be well sanded and cleaned to assure a good bond to the blocks. The blocks should also have good bonding surfaces as this bond must not fail during the test. This test is also done on bare honeycomb with the core bonded directly to the metal blocks. The blocks should be free to rotate so the load applied to the specimen is in pure tension and there is not any peeling occurring. This can drastically lower the ultimate failure load [2].

Test set-up

The force is transmitted to the sandwich through thick loading blocks, which are bonded to the sandwich facings or directly to the core. An improved type of apparatus is shown in Figure 4.9. It has two positioning rods to make sure that blocks are bonded to honeycomb (or panel) and perfectly oriented 0/90 to each other. Also it has positioning frame to make easier sample bonding exactly in the middle of fixture. Universal joint is attached to each loading block to minimize any moments imparted to the test specimen [134].

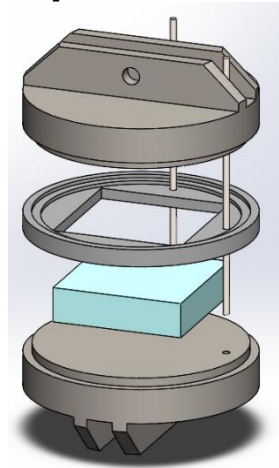


Figure 4.9. Improved flatwise tension test setup

Speed of Testing

Appropriate speed of testing must produce failure within 3 to 6 min. The suggested standard head displacement rate is 0.50 mm/min [134].

Failure

The modes of failure are the following: core tearing, adhesion-to-core, adhesion-to-facing and cohesion of the adhesive. When examining the failed specimen there are two types of core tearing failures. The one desired is to tear the core near the middle of the honeycomb. This will give the highest core mode failure load. Sometimes when an adhesive is used that does not have a deep fillet on the honeycomb cell walls the core will fail right at the cell edge where it was sawn, which usually gives a lower load. If the honeycomb is not failed and does not have any adhesive on it, this is an adhesion-to-core failure and is caused by the core surface being contaminated [2]. Summarizing the only acceptable failure modes for flatwise tensile strength are those which are internal to the sandwich construction (see Table 4.8.). Failure of the loading block-to-sandwich bond is not an acceptable failure mode [134].

Table 4.8. Sandwich panel flatwise tension test acceptable failure modes

Core failure	Adhesive failure of core-facing adhesive	Cohesive failure of core-facing adhesive	Facing tensile failure
Tensile failure of the sandwich core. Pieces of the core may remain in the adhesive that bonds the core to the block or facing.	Failure in the adhesive layer used to bond the facing to the core, with adhesive generally remaining on either the facing or the core surface, but not both.	Failure in the adhesive layer used to bond the facing to the core, with adhesive generally remaining on both the facing and core surfaces.	Tensile failure of the facing, usually by delamination of the composite plies in the case of a fiber-reinforced composite facing.

Calculation

Calculation of ultimate flatwise tensile strength is carried out by using equation:

$$F_z^{ftu} = \frac{P_{\max}}{A}$$

where:

F_z^{ftu} – ultimate flatwise tensile strength, MPa;

P_{\max} – ultimate force prior to failure, N;

A – cross-sectional area, mm².

4.4.4 Climbing drum peel test: ASTM D1781

Summary

Climbing drum peel test is carried out by using ASTM D1781 test method [111] or EN2243 DIN53295 [135]. The climbing drum peel test should only be performed on sandwich panels with relatively thin skins. The maximum thicknesses should be approximately 0.813 mm for aluminum, 0.508 mm for steel and 1.016 mm for fiberglass. The reason that these maximum thicknesses are required is that the facing must be wrapped around 101.6 mm diameter drum in ASTM standard and 100 mm in EN standard, and if the facing is too stiff it takes a large force just to bend the skin. This causes the failure mode of the sandwich to be slightly different as the peeling of the skin from the honeycomb does not start in the desired location. Normally a 0.508 mm aluminum facing with 6.35-5052-126 aluminum honeycomb is used to evaluate different adhesives [2].

Test results are expressed in torque, inch-pounds per inch (in.·lb/in.) or inch-pounds per 3 inch width (in.·lb/3 in.), and can include the torque to bend facings and rotate the drum or these values can be subtracted giving just the torque to peel the skin from the core [2].

Specimens

The test panel dimensions from different sources differ: 254 by 305 mm, with the core ribbon direction remaining parallel to the 305 mm dimension [111] and 76.2 by 356 mm [2]. Usually the honeycomb L orientation is in the long direction (this gives a more uniform peel load and just slightly higher values), [2].

Test setup

The honeycomb climbing drum peel apparatus is shown in Figure 4.10. By pulling down on the drum straps, the drum rotates and travels upward, bending the facing and peeling the facing off the core [2].

Speed of testing

The test specimen is loaded at a rate of head travel of 12.7 mm/min [111].

Failure

The failure modes in the climbing drum peel test are similar to those in the flatwise tensile test: cohesive failure of the adhesive, adhesion to the facing or honeycomb, void, or core tearing [2, 111].

Calculation

The peel strength is calculated as follows:

$$T_p = (R_o - R_i) \cdot (L - C)$$

where

T_p – peel strength, inch-pounds.

T_o – outer radius of drum

R_i – inner radius of drum

L – average load, pounds

C – correction load, pounds.

The correction load “C” is the sum of the load necessary to overcome the weight of the drum plus the load required to wrap the peeling member around the

drum. The correction load “C” may vary with each piece of equipment due to slight differences in the weight of the drum [11]. To obtain “C” a flexible piece of plain fiberglass should be tested, then a piece of the facing by itself should be tested to obtain the force to bend the facing [2].

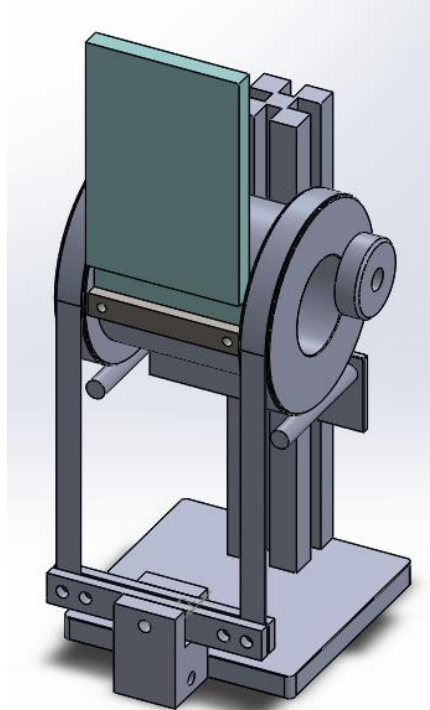


Figure 4.10. Climbing drum peel test

4.4.5 Long beam flexure test: ASTM D7249

Another test commonly performed on sandwich panels is the flexural beam test. Here the span is usually 457 mm or 508 mm with a single or double point loading. The beams are normally 76.2 mm wide and 101.6 mm longer than the span [2].

The beam can fail in several different ways: compressive or tensile failures of the facings, face wrinkling of thin compressive skins, core shear or localized core compressive failure under the load or support pads, or core-to-facing bond failures. The span and loading arrangement will dictate which failure mode will occur. The longer the span the more likely it is that a facing failure will happen, and the shorter the span the more likely it is that a core shear failure will occur. The load and support pads should be wide enough to prevent local core crushing failures. It helps to put thin pieces of rubber under the loading pads to reduce load concentration under the load pad edges and prevent the load pad edges from crushing into the core. It is best to use the four point bending test instead of the three point bending test as on the four point setup the load pads can rotate as the beam deflects, while in the three point it cannot. Core-to-facing delaminations are warnings that something is wrong with the sandwich and should be corrected; contaminated facings or core, too little resin on the inter prepreg ply, or inadequate adhesive [2].

The facing compressive or tensile modulus can be determined by bonding on a strain gauge to the top or bottom skin. The panel stiffness can be obtained by measuring the deflection at the mid span. Remember that this deflection is made up of the bending deflection and shear deflection [2].

4.4.6 Beam Shear Strength: ASTM C394

This method is limited to assemblies having a constant core thickness and is usually only used on flat assemblies. Specimen size is 203 by 76.2 mm. The core ribbon should either be parallel or perpendicular to the length. The test specimen should be supported for testing as shown in Figure 4.11. The end support plates should be 6.35 by 25.4 by 76.2 mm, machined from steel with grooves for alignment on the test apparatus. Loading surfaces should have the edges rounded to 1.5 mm radius. The reaction span should be 152.4 mm. The load should be applied through round loading bars, 12.7 mm in diameter and 76.2 mm long. It is permissible to place thin narrow plates at load points to prevent local bending of the sandwich faces. Such plates should not exceed 6.35 mm in width. The load should be applied at a rate of 0.38-0.51 mm per minute. Maximum load values should be obtained to determine the shear strength of the sandwich specimen. Tests should be conducted at ambient (room) temperature. Sandwich shear strength is calculated from the following equation:

$$SC = P_{\max} / W(T + T_c)$$

where

SC - shear strength, MPa

P_{\max} - maximum load, N

W - specimen width, mm

T - specimen thickness, mm

T_c - core thickness, mm

L, L' - load points

R, R' - reaction points [111].

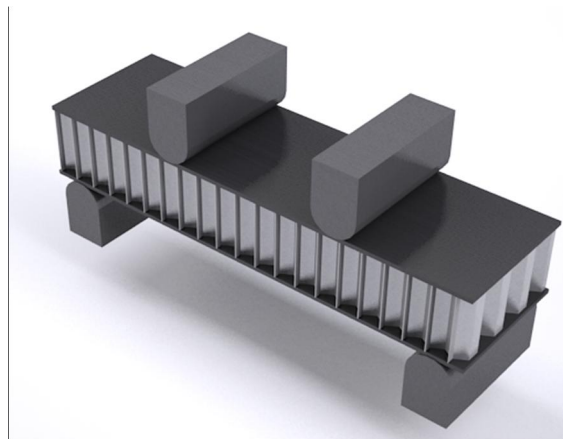


Figure 4.11. Beam shear test

5 Estimation of damage tolerance

5.1 Step 1: Introduction of artificial damage

5.1.1 Summary

It is hard to produce qualitative method for introduction of artificial impact damage, because it is not enough to test each sample with single energy, it would just not clarify the material behavior [73].

There isn't any single system not only for testing but also for article writing. Different researchers presented different information. Only minority of authors gives as much parameters as possible, including impact energies, drop weight, drop height, impactor diameter and shape. As result it is difficult to analyze and systematize data from large amount of articles.

5.1.2 Threshold value

Numerous experiments have shown that low velocity impact damage in sandwich structures results in significant reductions in the residual strength in tension, compression, shear, and bending [87]. Typically, the strength after impact is unaffected until the impact energy exceeds a threshold value after which there is a marked reduction from the virgin strength. It is highly desirable that impact damage resulting in an unacceptable reduction in mechanical properties be detectable via standard inspection techniques [26].

5.1.3 Damage and damage types

The size, shape, and location of damage can affect the deformation and strength behavior of the specimens significantly. Edge effects, boundary constraints, and the damaged stress/strain field can interact if the damage size becomes too large relative to the length and width dimensions of the plate [136].

In these events, impact energy is transformed into the energy of plastic deformation and it is absorbed through the large compressive stroke. The honeycomb core exhibits the cyclic plastic buckling deformation. The energy absorption characteristic in impact crush deformation is strongly influenced not only by the mechanical properties of the honeycomb material and the thickness of cell wall but also by the geometric configuration of the honeycomb cell [3].

Few ways can be used to introduce artificial damage in specimens: by using impact (drop weight or gas gun) event, by using quasi-static loading and third – by drilling hole in one of the facesheets. Each method described below.

Impact damage is typically confined to the top facing, the core-top facing interface, and the core. The lower facing remains generally undamaged. Low-velocity impact can cause the following damage modes in core sandwich panels:

- permanent indentations having semi-spherical shapes under the impactor,
- matrix crushing due to compression,
- inter-ply and intra-ply matrix cracks,
- fiber failures, similar to that observed in laminates,
- core crushing or buckling of cell walls in a region surrounding the impact point under the face-sheet,
- overall residual deformation of the whole panel [4, 7, 26].

Numerous researchers have reported that skin damage in sandwich structures increases almost linearly with impact energy until a maximum value is reached [26]. Table 5.1. contains information about impact damage introduction test parameters used in articles related to NASA, Table 5.2. – test parameters from many other sources.

Quasi-static testing, typically at loading rates between 1-10mm/min. Static indentation is a controlled, easily repeatable method of causing damage in composite sandwich panels. The controlled loading speed allows the test to be stopped at any moment, facilitating the identification of damage mechanisms and propagation. Accurate data for the load-displacement response is also obtained much easier than in impact testing. However, as the loading speed is very slow the analogy of the quasi-static response to the impact response is often questioned due to strain rate sensitivity [7, 10]. Indenter shape, loading speed and other QS damage introduction parameters collected in Table 5.3.

For the most severe damage the contact force gradually increases and induces the progressive breaks and matrix crushing in the face-sheet, a sudden load drop appears corresponding to the face-sheet fracture along the perimeter of the impactor [4].

Some researcher used **drilled hole** instead of damage induced by spherical indenter (Table 5.4.). Results shown that there is no any significant difference between these two approaches. Instead the influence of drilled hole on panel's residual strength is much easier to predict and simulate. The failure modes and residual strength of the sandwich composite were analogous to those of an undamaged panel with an open circular hole of comparable size. Hence, the residual strength of the facing may be estimated using available methods for predicting the residual strength of open-hole composites [26], however this approach with drilled hole in facesheet cannot completely replace real impact damage, because often a small residual dent with core crushing can result in a more catastrophic reduction in residual strength of the panel than if the panel contained a through-the-thickness hole of the same diameter [4].

Table 5.1. Impact types, impactor types, impactor diameters used in articles related to NASA

Reference	Skin material	Honeycomb core material	Core density (kg/m ³)	Honeycomb cell size (mm)	Core thickness (mm)	Length x With (mm)	Impact type, impactor type & diameter (mm)
[24]	IM7/8552 prepreg	aluminum	49.65	3.17	28.58	304.8× 76.2	HS 6.35, 12.7, 38.1

[21, 38]	prepreg AS4/8552 graphite-epoxy tape and woven fabric materials	Korex	?	?	3.17	254×127	DW HS 25.4 & 12.7
	AS4/8552 graphite-epoxy	?	192	4.75	?	254×127	S 12.7 - 25.4
	tow AS4/8552	Phenolic (HRP)	192	4.76	?	254×127	DW HS 25.4
	CFRP tow AS4/8552	Phenolic (HRP)	192	4.76	?	1676×254, 356	DW HS 25.4
[23]	woven AS4 carbon fiber with fiber orientation equal to 0 and 90 deg	Last-A-Foam 6704; Stitches: Kevlar yarn of 400/4 ply	64.1	?	19.05	254×127	47.75
[75]	Carbon plain weave	Nomex	48	4.76	9.5 & 19.05	267×216	DW HS 25.4 & 76.2

Table 5.2. Impact types, impactor types, impactor diameters used in articles reviewed

Reference	Skin material	Skin thickness (mm)	Honeycomb core material	Honeycomb density (kg/m ³)	Honeycomb cell size (mm)	Core thickness (mm)	Length × Width (mm)	Impactor type & diameter (mm)
[57]	FIBERITE 7714 D/XAS U-D C/E prepreg	1; 2	5052 alu	?	3	10; 25	496×490	20
[91]	CFRP plain & 8 harness weave	1.97 front 0.63 back	Nomex	48	3.1	12.5	127×76	DW HS 12.7
[48]	IM7/5260 (BMI resin)	?	Glass/phenolic	48, 88, 128	?	6.35, 9.5, 12.7	254×127	DW HS 12.7
[56]	CFRP, 4x4 twill weave - CF0111/LTM45-EL	0.79	HRH-10 Nomex	48; 96	3.1 75	12.7	76.2 × 76.2	DW HS 25.4
[28]	CFRP AS4/3501-6	?	Aluminium	80		6.4 & 9.6	178×152	AG HS 12.7
[57]	CFRP fiberite 7714D/XAS	?	Alu 4.5-1/8-10(5052)T	72	3.2	10	600×175	DW FE 20
[40]	plain woven AS4/8552	2	3003 alu	77	4.8	20	140×	AG S

							140	7.5
[7]	E-glass fabric 7781/F185	1.52	Nomex, glass, carbon	48, 64, 80, 88, 96	3.2, 4.8, 6.4	12.7	203× 203	HS 12.7
[61]	NB321/3K70P Plain wave carbon fabric	?	Nomex	48	4.7 6	?	127× 101. 6	25.4, 76.2
[7]	CFRP	?	Aluminium	70	6.3 5	?	127× 76.2	DW HS 12.7, 6.25- 50.8
[1]	UD prepregs; T700S 12K roving	0.853; 0.644	HexWE B CRIII 3/16 5052 4.4	?	?	12.7	150× 100	HS 16
[7]	IM7/8552 plain weave		Nomex	48	3.1 8	25.4	152× 152	DW HS 12.7
[108]	G11 glass/epoxy		NOMEX	?	?	?	267× 216	?
[59]	Plain weave carbon fibre F-82 epoxy resin	0.61	Honeycomb filled with foam	106, 164	?	?	304. 8× 76.2	DW HS 12.7
[57]	Al2024-T3 alu	1; 1.5	Nomex	32		20- 19	496× 490	20
[7]	AS4/3502	0.675	Aluminium	130	3.1 75		405× 100	DW HS 25.4
[62]	carbon fiber	0.3048 , 0.254, 0.305	?	112	?	25.4	100× 100	HS 12.7
[29]	C/E AS4/3501-6		HRH- 10-1/8- 9.0 Nomex	144	3.1 75	12.7	178× 178	HS 12.7
[7]	T700/LTM45-EL; IM7/8552	0.5; 1; 1.5; 2	5052 alu	50; 70; 90		12.7	150× 150	HS 20
[88]	IM7/8552-1 140 g/m ²	?	alu	49.7, 97.7	3.1 7 mm (1/8 -in)	?	152× 102	?
[77]	Glass epoxy 8 harness station	?	Nomex HRH- 10-1/8- 3.0	48	3.1 75	25.4	720× 320	HS 69
[60]	plain weave fabric NB321/3K70P	0.762	Nomex (PN2- 3/16- 3.0)	48.1	?	19.0 5	254× 203	HS 25.4, 76.2
[41]	woven carbon-fibre reinforced epoxy AS4/8552	2	3003 alloy	77	?	20	480× 50	cilindric al

[62]	200 T 2x2 twill weave carbon fabric (200 g/m ²) / West System Z105 epoxy resin	1	?	31	6.4	12	100× 100	12.7
[67]	TBCarbon CP200NS; glass/epoxy TBCarbon SGP125NS	?	Nomex (Aerocel I CACH 1/8-3.)	48	3.2 mm	10; 20	250× 80	HS 6.35
[46]	CFRP plain weave IM7/8552	0.571, 0.762, 0.381	HFT-3/16-3.0	48	4.7 6	25.4	152× 152	DW HS 12.7
[46]	CFRP AS4/E7K8 UD, plain, 5 & 8 harness satin weave	?	Nomex	14.7, 29	?	25.4, 19.0 5	229× 154	pendulum HS 12.7, 38.1
[137]	Chopped strand mat and E glass	3.5	?	?	?	40	500× 500	HS 50
[84]	CFRP	?	Nomex	48 or 128	3.1 75	?	76.2 × 76.2	DW HS 12.7
[90]	CFRP laminate	2	Nomex	137. 5	?	20	400× 91	S
[103]	UD or woven glass fibre and aluminium layers	2	Aluminium foam	?	?	10	170× 170	DW HS 12.7
[37]	CFRP plain weave AS4/3501-6	0.35	Nomex	48	3.1 8	25.4	350× 89	
[53]	CFRP T300/914C	?	Aluminium	72, 130, 192	3.2		1000 × 160	DW HS 30
[45]	IM7/8552	?	Nomex	48	3.1	25.4	356× 83	HS 25
[22]	CFRP ud and woven AS4/8552	1	korex	72	3.1 75	12.7	254× 127	DW AG HS 12.7, 25.4
[39]	CFRP 69/GFE 3105H	?	Nomex HRH10-1/8	29, 96	3.1 75	6.35, 15.2 4	361× 305	DW HS 16; 50
[64]	CFRP	2	NOMEX	137. 5		20	400× 91	S 25.4
[12]	HexPly® IM7/8552 UD	?	HexWeb® CR-III 5052-H39 alu	49.7; 72.1	3.2 mm	25.4; 16.5	17.8 × 5.1	S 25.4
[79]	GFRP plain weave	0.48	?	?	?	?	500× 500	HS 50
[31]	AS4/3501-6	?	Nomex	48	3.2	25.4	356 152 356× 305 358× 83	DW HS 25.4
[43]	IM7/8552	2.92	perforated 5052 alu	49.7	?	28.6	152. 4× 101. 6	HS 12.7
[47]	IM7/8552 QI; IM7/8552; T300/934; IM7/8551-7	?	alu	49.7		28.6	152. 4×	

					3.1 7 mm		101. 6 178× 76	6.35, 12.7, 38.1
[52]	T300/fiber		Glass/p henolic	32	4.7 6	35	114× 114 292× 76	DW HS 12.7
[98]	Alu 2024-T8	0.81 top 0.51 bottom	Aluminiu m 5056	?	?	25.4	152× 101	DW HS 25
[7]	IM8/8551	1.02	aluminu m	32, 61, 29, 48	?	12.7	127× 76	DW HS 12.7
[20]	T300/914 UD	?	?	?	?	?	150× 100	HS 16
[107]	C/E fabric	0.6	Nomex	48.1	3.1 75 mm	?	140× 140	12.7
[81]	CFRP; kevlar/epoxy (hybrids)	?	Nomex	48	?	25	150× 80	AG, DW HS 12.7
[81, 40]	CFRP; kevlar/epoxy (hybrids); AGP193-PW/8552 + tape AS4/ 3051-6	?	Nomex	48	?	25	560× 80 560× 80 78× 78	AG, DW HS HS 12.7 20
[10]	woven E-glass; woven S2- glass;	?	Nomex	?	?	?	152. 4× 152. 4	HS 12.7
[63]	NB321/3K70P Plain Weave carbon prepreg; NB321/7781 Satin Weave E-glass prepreg	?	Nomex; Divinyce II Foam cores	48.1, 72.1, 96.1; 41.6, 67.3, 88.1	?	?	267× 216	?
[27]	NB321/3K70 plain weave CF prepreg	?	PN2- 3/16-3.0 Nomex	?	?	75	267× 165 317× 216 419× 317	HS 76.2
[26]	CFRP AS4/8553-40	2	glass/ polyimid e	88	4.7 6	22.8 6	100× 100	DW 25.4, 50
[102]	S2-glass UD	?	Nomex	?	80, 144 , 184	?	305× 305	HS 15.88
[44]	IM7/8552	?	Nomex	48	3.1	25.4	356× 152	DW HS 25.4
[32]	AS4/35016 C/E prepreg	?	?	?	?	?	150× 100	HS 16

[30]	CFRP AS4/350t-6	?	Nomex	48	3.2	6.4, 9.5, 25.4	358× 89	HS 12.7, 25.4, 38.1
[65]	T800H/3633	?	?	?	?	?	150× 100	HS 15.9
[50]	T300/914C UD; T300/BMI	?	?	?	?	?	150× 100	HS 20
[11]	T700/LTM45	1.024	5052 Al (4.4- 3/16-15)	70	?	12.7	200× 150	HS 20
[33]	AS4/3501-6 UD	?	Phenolic (Nomex)	?	3	?	365× 82	HS 25

Table 5.3. Quasi-static damage introduction

Reference	Skin material	Honeycomb core material	Honeycomb density (kg/m ³)	Honeycomb cell size (mm)	Core thickness (mm)	Length × With (mm)	Indenter type & diameter (mm)
[29]	CFRP AS4/3501-6	HRH-10-1/8-9.0 Nomex	144	3.175	12.7	178×178	HS 12.7
[137]	Chopped strand mat and E glass	?	?	?	40	500×500	HS 51
[79]	GFRP plain weave	?	?	?	?	500×500	HS 50
[102]	S2-glass UD	Nomex	?	80, 144, 184	3; 4	305×305	FE 6.35 & 12.7
[30]	CFRP AS4/350t-6	Nomex	48	3.2	6.4, 9.5, 25.4	358×89	HS 12.7, 25.4, 38.1
[56]	CFRP 4x4 twill weave - CF0111/LTM45-EL	Foam core				76.2×76.2	HS 25.4
[138]	E glass woven roving polyester resin					500×200 1000×800	HS 25.4
[54]	CFRP woven roving, T300/BMI resin					125×125 250×250 125×125 250×250	HS 25.4
[139]	E glass woven roving (two types) polyester resin (top skin only)					300×300	HS 20
[82]	CFRP CF011/LTM45 EL 4x4 twill					76.2×76.2	HS 25.4
[42]						279×279	HS 12.7

	CFRP AS4 carbon five harness satin weave		175×25.4	HS 13.7
--	---	--	----------	---------

Table 5.4. Notched specimens

Ref.	Skin material	Core material	Length (mm)	Width (mm)	Notch diameter (mm)
[51]	plain weave, 3K tow, T-300 Graphite fiber fabric embedded in an Epoxy matrix	Nomex	152.4	50.8	6.35
[86]	CFRP NCF [0/90] & [45/-45]	Foam	300	300	12.5

5.1.4 Definition of appropriate damage size

There is need to set reasonable range of energies, which is based on specific sandwich panel properties. Lowest energy threshold could be defined as barely visible impact damage, which is hardly detectable by unarmored eye. The highest energy threshold could be impactor penetration through the facing.

Different sandwich constructions (thicknesses, facesheet lay-ups and core densities), different test conditions and aims of researches used by authors contributed to using of different impact energies, different impactor diameters and shapes.

Every author used his or her own criteria of BVID estimation, like dent depth, impact energy, drop height and others. Obviously for different materials values of these parameters could vary in wide range and not every separate approach could be considered as absolutely reliable, for example, use of dent depth only as a measure of the extent of damage in an impacted structure might not always be reliable or realistic [26]. In Table 5.5. is given information, how researchers had chosen criteria for damage which correspond to BVID.

The only test method for out-of-plane indentation on sandwich panel is ASTM 7766 (§ 5.1.7.). This practice supplements test methods D6264 (for quasi-static indentation testing for laminates, § 5.1.5) and D7136 (for drop-weight impact testing for laminates, § 5.1.6) with provisions for testing sandwich specimens [140]. In contrast in laminates areas of delamination in sandwich panels are much smaller than laminate plates impacted similarly [4]. Several important test specimen parameters (for example, facing thickness, core thickness and core density) are not mandated by this practice. Susceptibility to damage from concentrated out-of-plane forces is one of the major design concerns of many structures made using sandwich constructions [140]. Each method is described separately in paragraphs below.

Indenter type

Hemispherical indenters are the most common in existing research. In reviewed researches they take part of 88%, but the few studies into indenter geometry suggest indenter shape to have a significant effect on the damage mechanisms, with flat ended indenters simulating much larger hemispherical indenters [7]. In

Table 5.6. are summarized diameters of indenters used in researches. Most common are 12.7 mm (0.5 in) and 25.4 mm (1 in) indenters. Also spherical impactors as airgun bullets are used [40, 49]. Furthermore was found one research using cylindrical indenter [41] for beam like specimens.

Table 5.5. Definition of BVID by different authors

Czabaj et al. [12]			Residual strength measurement method	
Sandwich construction		BVID load threshold		
Facesheet layups	Core		1) 25.4 mm indenter, QS load 1300 N, max permanent dent depth 0.5 mm 2) 76.2 mm indenter, QS load 2800 N, max permanent dent depth 1.0 mm	
	mm	kg/m ³		
[45/0/-45/90]s	25.4	49.7		
[45/-45/0/90]s	16.5	49.7		
[-45/45/90/0]s				
[45/90/-45/0]s	25.4	72.1		
McGowan et al. [22]			Residual strength measurement method	
Facesheet	Core	BVID load threshold		
AS4/8552 8-ply-thick [O _f /45/-45/0/90/-45/45/O _f]	Korex honeycomb, 3.17 mm cells, 72.1 kg/m ³	The criterion is dent depth at the impact site 1.27 mm. Drop weight & gas gun, Impactors 12.7 and 25.4 mm. Impact-energy 7 J.	Compression after impact	
Klaus et al. [141]			Residual strength measurement method	
Facesheet	Core	BVID load threshold		
2 mm, [45/90/-45 /0/45/90/-45/0]s	20 mm, 137.5 kg/m ³ , aramid fibre paper impregnated with phenolic resin	Impactor 25.4 mm, drop weight 1.56 kg.	Bending after impact	
		5 J		BVID
		20 J		clear visible dent with first fibre fractures
		40 J		fibre fractures in all plies

Table 5.6. Indenter diameters used for impact damage introduction in sandwich panels (arrangement by diameter)

Impactor diameter		Usage in researches, %	Impact type
mm	in		
5.25	0.21	0.6	QS
6.35	0.25	4.2	QS, DW
7.5	0.30	0.6	AG
7.9	0.31	1.2	DW
10	0.39	1.2	DW
12.7	0.50	31.3	DW, AG, QS, P
15.9	0.63	2.4	DW
16	0.63	3.0	DW
20	0.79	8.4	DW, QS
25	0.98	3.6	DW
25.4	1.00	24.7	DW, QS, AG
30	1.18	0.6	DW
38.1	1.50	6.0	QS, DW, P
47.75	1.88	0.6	
50	1.97	6.0	DW, QS, AG
51	2.01	0.6	QS
69	2.72	0.6	
76.2	3.00	4.2	DW

5.1.5 Damage resistance to a concentrated quasi-static indentation ASTM:D6264

Summary

A flat, square composite plate is subjected to an out-of-plane, concentrated force by slowly pressing a hemispherical indenter into the surface. The damage resistance is quantified in terms of a critical contact force to cause a specific size and type of damage in the specimen [142].

Specimens

Specimens shall be 150 by 150 mm square, flat, and of constant thickness. For comparison screening of the damage resistance of different materials, the standard specimen thickness shall be 4.0 to 6.0 mm and the laminate shall consist of unidirectional plies with a stacking sequence of $[45/0/-45/90]_n$ where n is a whole number [142].

Test setup

The damage resistance may be determined for a specimen that is edge supported or rigidly backed. Hemispherical indenter diameter shall be 13 mm in diameter. For both configurations, the specimen's face shall be held normal to the axis of the indenter. Edge supported configuration shall consist of a single plate with a 125 mm diameter opening made from a structural metal such as aluminum or steel. The top rim of the opening shall be rounded with a radius of 0.75 mm. The plate shall be sufficiently large to support the entire lower surface of the specimen,

excluding the circular opening. The thickness of the plate shall be a minimum of 25 mm and greater than the expected maximum indenter displacement [142].

Testing speed

The speed of testing should be appropriate to reach the maximum force within 1 to 10 min. The suggested standard crosshead displacement rates are 1.25 mm/min [142].

Calculations

The energy at any indenter displacement δ may be calculated from the contact force versus indenter displacement curve using equation:

$$E(\delta) = \int_{\delta_0}^{\delta} F(\delta) d\delta$$

E – energy at displacement δ , N-m;

δ – indenter displacement during the test, m;

δ_0 – indenter displacement at initial specimen contact, m;

F – measured contact force at indenter displacement δ , N.

For energy calculation which used to reach maximum displacement, the integral higher border δ is changed by δ_{\max} – maximum indenter displacement, for absorbed energy calculation is used indenter's displacement at the end of the unloading cycle δ_f [142].

5.1.6 Damage resistance to a drop-weight impact event: ASTM 7136

Summary

A flat, rectangular composite plate is subjected to an out-of-plane, concentrated impact using a drop-weight device with a hemispherical impactor. The potential energy of the drop-weight, as defined by the mass and drop height of the impactor, is specified prior to test. Equipment and procedures are provided for optional measurement of contact force and velocity during the impact event. The damage resistance is quantified in terms of the resulting size and type of damage in the specimen [127].

A drop-weight impact test is performed using a balanced, symmetric laminated plate. Damage is imparted through out-of-plane, concentrated impact (perpendicular to the plane of the laminated plate) using a drop weight with a hemispherical striker tip. The damage resistance is quantified in terms of the resulting size and type of damage in the specimen. The damage response is a function of the test configuration; comparisons cannot be made between materials unless identical test configurations, test conditions, and so forth are used [127].

Specimens

The standard specimen is 100 by 150 mm in with thickness from 4.0 to 6.0 mm with a target thickness of 5.0 mm and the laminate must have appropriate number of unidirectional plies to achieve a total cured thickness nearest to 5.0 mm with a stacking sequence of [45/0/-45/90]_n where n is a whole number. The laminated plate layup is to be defined such that the 0° fiber orientation is aligned with the lengthwise (long) dimension [127].

Test setup

The impact support fixture, shown in Figure 5.1., shall utilize a plate at least 20 mm thick constructed from either aluminum or steel. The cut-out in the plate shall be 75 mm by 125 mm. Four clamps shall be used to restrain the specimen during impact. The clamps shall have a minimum holding capacity of 1100 N [127].

The impactor shall have a mass of 5.5 kg and shall have a smooth hemispherical striker tip with a diameter of 16 mm and a hardness of 60 to 62 HRC. Alternative impactors may be used to study relationships between visible damage geometry (e.g., dent depth, dent diameter) and the internal damage state [127].

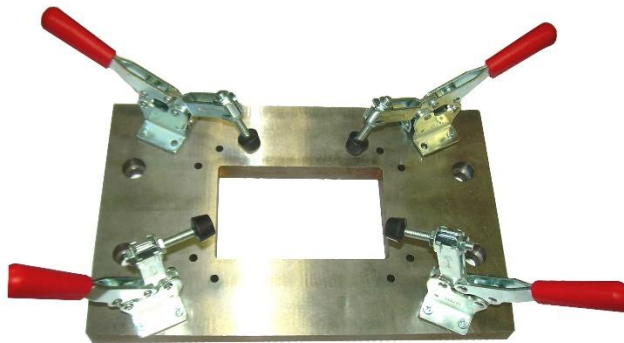


Figure 5.1. Impact support fixture according to ASTM D7136

Testing speed

In this method there is no such term as testing speed. An alternative criterion is the drop height, which is directly proportional to speed/velocity and is determined by following two steps using few equations:

1. Impact Energy Calculation:

$$E = C_E h$$

where:

E – potential energy of impactor prior to drop, J;

C_E – specified ratio of impact energy to specimen thickness, 6.7 J/mm;

h – nominal thickness of specimen, mm.

2. Drop Height Calculation:

$$H = \frac{E}{m_d g}$$

where:

H – drop-height of impactor, m;

m_d – mass of impactor for drop height calculation, kg;

g – acceleration due to gravity, 9.81 m/s² [127].

5.1.7 Damage Resistance of sandwich panels ASTM D7766

Summary

This practice provides instructions for modifying laminate quasi-static indentation and drop-weight impact test methods to determine damage resistance properties of sandwich constructions. This practice provides supplemental instructions that allow for quasi-static indentation testing and for drop-weight impact testing to determine damage resistance properties of sandwich constructions. Three test procedures are distinguished:

Procedure A – In accordance with test method D6264, but with a sandwich specimen, perform a quasi-static indentation test of a rigidly-backed specimen. Damage is imparted through an out-of-plane, concentrated force applied by slowly pressing a displacement-controlled hemispherical indenter into the face of the specimen. The damage resistance is quantified in terms of the resulting size, location and type of damage in the specimen [140].

Procedure B – In accordance with test method D6264, but with a sandwich specimen, perform a quasi-static indentation test of an edge-supported specimen. Damage is imparted through an out-of-plane, concentrated force applied by slowly pressing a displacement-controlled hemispherical indenter into the face of the specimen. The damage resistance is quantified in terms of the resulting size, location and type of damage in the specimen [140].

Procedure C – In accordance with test method D7136, but with a sandwich specimen, perform a drop-weight impact test of an edge-supported specimen. Damage is imparted through an out-of-plane, concentrated impact using a drop weight with a hemispherical striker tip. The damage resistance is quantified in terms of the resulting size, location and type of damage in the specimen [140].

Procedure A is considered to be the most suitable procedure for comparison of the damage resistance characteristics of sandwich panels of varying material, geometry, stacking sequence and so forth. This is because the rigid backing plate resists out-of-plane deformation of the specimen, such that the sandwich flexural stiffness and support geometry have less influence on damage initiation and growth behavior than in edge-supported tests. However, it should be noted that damage resistance behavior observed using rigidly-backed specimens may not strictly translate to edge-supported applications. For example, sandwich constructions using cores with high compression stiffness or strength, or both (e.g., balsa wood) may exhibit superior performance in rigidly-backed tests, but that performance may not strictly translate to edge-supported tests in which the core shear stiffness, core shear strength and sandwich panel flexural stiffness have greater influence upon the test results. Consequently, it is imperative to consider the intended assessment and structural application when selecting a test procedure for comparative purposes, and as such the use of procedures B and C may be more appropriate for some applications [140].

Specimens

Procedures A and B – the specimen dimensions shall be in accordance with D6264M (150 × 150 mm), with the specimen thickness equal to the sandwich panel thickness. Procedure C – the specimen dimensions shall be in accordance with D7136 (100 × 150 mm) with the specimen thickness equal to the sandwich panel thickness [127, 140, 142].

Test setup

Specimen support:

Procedure A – General apparatus shall be in accordance with D6264 with flat rigid support [140].

Procedure B – General apparatus shall be in accordance with D6264, with edge support consisting of a single plate with a 125 mm diameter opening [140].

Procedure C – General apparatus shall be in accordance with D7136, with edge support utilizing a plate with a rectangular cut-out. The cut-out in the plate shall be 75 mm by 125 mm. Clamps shall be used to restrain the specimen during impact [140].

If the measured damage area exceed half the unsupported specimen width, it is recommended to examine alternative specimen and fixture designs, which are larger and can accommodate larger damage areas without significant interaction from edge support conditions [140].

Indenter or impactor:

Procedures A and B – the standard indenter tip shall be in accordance with D6264 (HS, 13 mm) [140].

Procedure C – The standard impactor tip shall be in accordance with D7136 (HS, 16 mm). Alternative tip geometries may be appropriate depending upon the core characteristics. For example, it may be necessary to use a tip of larger diameter to ensure that multiple honeycomb cells are indented or impacted. Conversely, the use of sharp tip geometries may be appropriate for certain facing penetration resistance assessments [140].

Testing speed

Procedure A – suggested standard crosshead displacement rate for honeycomb core is 1.25 mm/min. The test should be terminated before penetrating the back-side sandwich facing to avoid damaging the test apparatus. The unloading rate shall be the same as the loading rate [140].

Procedure B – suggested standard crosshead displacement rate is 1.25 mm/min. The unloading rate shall be the same as the loading rate [140].

Procedure C – impact energy shall be calculated using equation:

$$E = C_F t$$

where:

E – potential energy of impactor prior to drop, J;

C_F – specified ratio of impact energy to thickness of the impacted sandwich facing, 6.7 J/mm;

t – nominal thickness of impacted sandwich facing, mm.

Alternative impact energy levels may be appropriate depending upon the support geometry, support conditions, facing thickness, sandwich bending stiffness, etc. [140].

Failure

Possible damage locations shown in Figure 5.2. and commonly observed damage modes presented in Figure 5.3. [140].

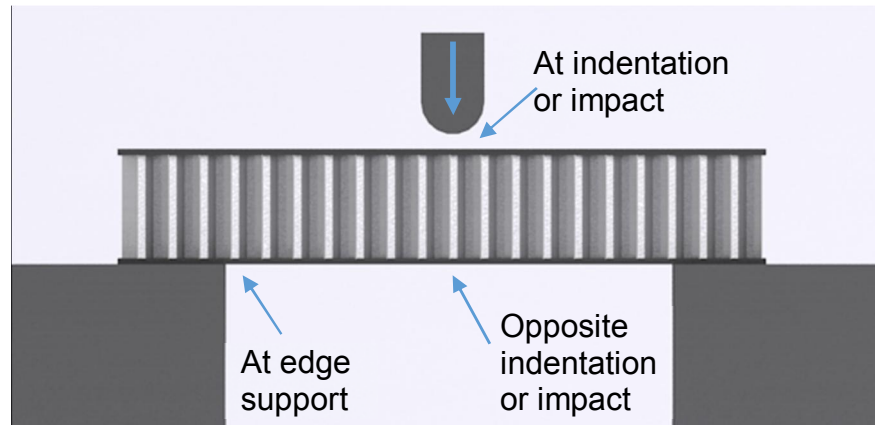


Figure 5.2. Indentation/impact damage locations [140]

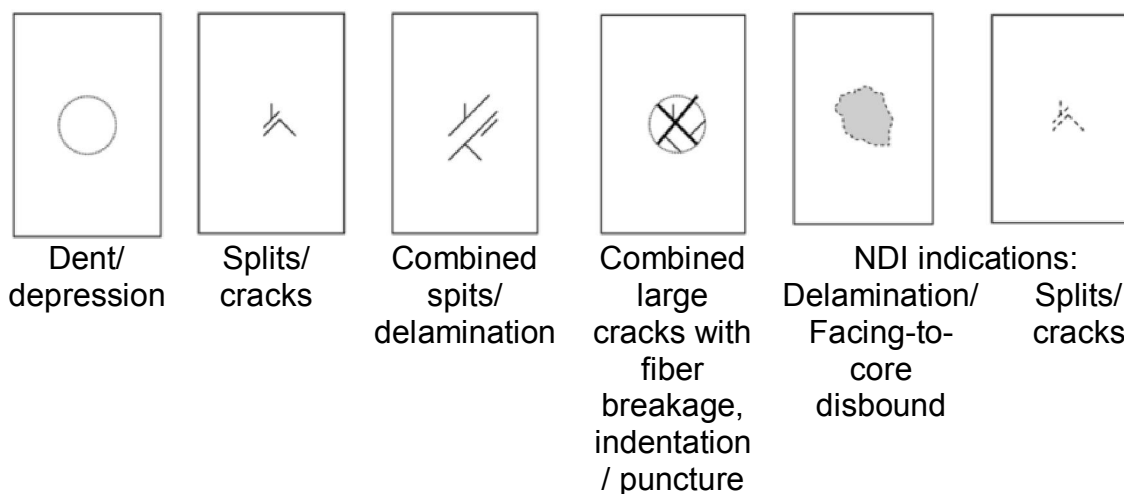


Figure 5.3. Commonly observed damage modes from out-of-plane indentation or drop-weight impact [140]

5.2 Step 2: Measurement of residual strength

5.2.1 Compression after impact summary

Reviewing literature it was seen that majority of researchers did not follow to any test methods, although many similarities were seen. Most of researchers uses compression test for residual strength and the strength-to-damage ratio determination because compressive loading represents the most critical loading scenario [7, 108]. It is apparent that no internationally approved compression after impact testing standards exist for composite sandwich structure [7].

Test methods

The two most common methods are those developed by Boeing (commonly referred to as SACMA) and NASA. A less common method was created by the Composites Research Advisory Group (CRAG). One other alternative method specific to the compression testing of sandwich specimens is ASTM C364 [7]. Most recent method is ASTM 7137. None of these methods are specified for sandwich panel compression after impact. NASA, SACMA, CRAG and ASTM 7137 are made and developed for laminate CAI, but ASTM C364 is preferred for intact sandwich panels compression. Table 5.7. summarizes CAI methods.

Table 5.7. Summary of compression after impact testing methods

Parameter	Unit	NASA	SACMA	CRAG	ASTM C364	ASTM 7136 & 7137	LU/IC
Specimen dimension (impact)	mm	254-317 × 178 × 6.35	152 × 102 × 4.6-5.6	Dia. ≥ 140 t ≤ 3	-	150 × 100 × 4-6	100-500 × 100-500 × 10-25
Impact test area	mm	127 × 127	127 × 76	Dia. 100	-	75 × 125	Dia. 100-500
Impactor mass	kg	4.55	5	-	-	5.5	Variable
HS impactor dia.	mm	12.7	16	10	-	16	10
Impact energy	J	27	Variable	Variable	-	Variable	Variable
Specimen dimensions (compression)	mm	254 × 125 × 6.35	152 × 102 × 4.6-5.6	180 × 50 × 3 (gauge length 100)	L ≤ 8t W ≥ 50 & ≥ 2t	150 × 100 × 4-6	350 × 250 × 10-25 or 150 × 100 × 1-604
End fixings	-	C between steel plates	C between steel plates	C using end tabs	C between steel bars	C between steel knife-shaped bars	C with epoxy end pots
Side fixings	-	SS	SS	SS	F	SS	SS
Loading rate	mm/min	1.27	1.27	To cause failure within 30-90 sec	0.5 or to cause failure within 3-6 min	1.25	1

Note:

Specimen size given by length × width × thickness (L×W×t) for rectangular geometries or diameter × thickness (d×t) for circular geometries.

Only ASTM C364 is specifically for sandwich panels.

C – compression, SS – simply supported,

F – free,

HS – hemispherical,

LU/IC – Loughborough University/Imperial College method,

CRAG – Composites Research Advisory Group (designed for coupon type laminate specimens rather than panels and therefore is not suitable for this research) [7].

Geometry of specimens

The lack of standardized and available method for honeycomb sandwich panel CAI testing explains the large difference in specimen’s dimensions used by different researchers. Length and width varies from 17.8 × 5.1 mm [12] to 1000 × 800 mm for rectangular specimens [138] and 1676 × 254 mm for beam shaped specimens [21]. Although there are some typical dimensions used by different researchers. They are summarized in Table 5.8. Little more often common are specimens with length 150 and width 100 mm. Second place is taken by 100 × 100 mm specimens. Also quite often occurs 500 × 500, 254 × 127 (which are 10 by 5 inches), 300 × 300 and 200 × 150 mm. In some cases large panels after impact event is then cut off to few smaller specimens for CAI. Overall thicknesses are between 25-30 mm. Large panels were less common due to the higher costs involved [7].

For the impact testing phase the overall specimen geometry is irrelevant if the panel is clamped as only the area inside the clamped region responds to the impact [7].

Table 5.8. Dimensions of specimens for CAI used by researchers

Ref.	Skin material	Core material	Length (mm)	Width (mm)	Test type
150 x 100 mm					
[143]	brass	Nomex HRH 78,1/ 4,3 Hauteur	150	100	I
[1]	T700S/12K roving (M77/42%/UD90/CHS)	CRIII 3/16 5052 4.4	150	100	I
[20]	T300/914 UD		150	100	I
[92]	CFRP UD	Aluminium 3/8- 5056-0.0007	150	100	I
[32]	AS4/35016 prepreg		150	100	I
[65]	T800H/3633		150	100	I
[50]	T300/914C UD		150	100	I
[98]	Aluminium 2024-T8	Aluminium 5056	152	101	I
[144]			152.4	101.6	I
[88]	IM7/8552	perforated 5052 aluminum	152.4	101.6	I

[145]	Hybrid composite: titanium alloy foils + graphite fiber reinforced plastics		152.4	101.6	I
[88]	IM7/8552-1 140 g/m ²	aluminum	152	102	I
100 x 100 mm					
[62]	200T 2x2 twill weave carbon (200 g/m ²)/Z105 epoxy resin		100	100	I
[8]			100	100	I
[26]	AS4/8553-40	glass/polyimide hone	100	100	I
[62]	CFRP & Kevlar mix	Foam	100	100	I
[29]	CFRP	Foam	101.6	101.6	I
500 x 500 mm					
[57]	FIBERITE 7714 D/XAS UD carbon epoxy prepreg	5052 aluminium	496	490	I
	Al2024-T3 aluminum alloy	Nomex			
[137]	Chopped strand mat and E glass		500	500	I
[79]	GFRP plain weave		500	500	I
[99]	A5083-H321 aluminium	A3003-H19 aluminium	500	500	I
[137]	Chopped strand mat and E glass	Foam	500	500	QS
[79]	GFRP plain weave	Foam	500	500	QS
500 x 500 mm					
[22]	AS4/8552 graphite-epoxy tape and woven fabric materials	Korex	254	127	I
[21]	tow AS4/8552	Phenolic (HRP) honeycomb	254	127	I
[23]	woven AS4	Last-A-Foam 6704; Stitches: Kevlar yarn of 400/4 ply	254	127	I
[48]	IM7/5260 (BMI resin)	Glass/phenolic	254	127	I
[22]	CFRP UD and woven AS4/8552	korex	254	127	I
300 x 300 mm					
[86]	CFRP NCF 0/90 & +-45	Foam	300	300	I
[139]	E glass woven roving (two types) polyester resin (top skin only)	Foam	300	300	I
[87]	CFRP	Foam	300	300	I
[139]	E glass woven roving (two types) polyester resin (top skin only)	Foam	300	300	QS
200 x 150 mm					
[11]	T700/LTM45	5052 Al HC (4.4-3/16-15)	200	150	I
[124]	T700/LTM45-EL UD	1) 5052 aluminium, 2) Nomex	200	150	I
[80]	CFRP	Foam	200	150	I
Smallest specimens					
[12]	IM7/8552 UD	CR-III 5052-H39 aluminum	17.8	5.1	I
			17.8	15.2	
[24]	1)quasi-isotropic IM7/8552 2) directional IM7/8552	aluminum	76.2	25.4	I

[34]	CFRP AS4/3501-6		101	25	I
[42]	CFRP AS4 carbon five harness satin weave		175	25.4	QS, I
[56]	CFRP, 4x4 twill weave - CF0111/LTM45-EL	HRH-10 Nomex	76.2	76.2	I
[84]	CFRP	Nomex	76.2	76.2	I
[56]	CFRP 4x4 twill weave - CF0111/LTM45-EL	CR-III 5052-H39 aluminium	76.2	76.2	QS
[82]	CFRP CF011/LTM45 EL 4x4 twill	aluminium	76.2	76.2	I
Largest specimens					
[57]	CFRP fiberite 7714D/XAS	Aluminium 4.5-1/8-10(5052)T	600	175	I
[31]	CFRP AS4/3501-6	Nomex	356	305	I
[39]	CFRP 69/GFE 3105H	Nomex HRH10-1/8	361	305	I
[85]	GFRP	Phenolic foam	450	250	I
[27]	Newport NB321/3K70 plain weave carbon fabric prepreg	Plascore PN2-3/16-3.0 Nomex	419	317	I
[53]	CFRP T300/914C	Aluminium honeycomb	1000	160	I
[77]	Glass epoxy 8 harness station	NomexHRH-10-1/8-3.0	720	320	I
[25]	IM7/5260	Titanium honeycomb	889	305	I
[83]	E-glass fabric	Foam	650	650	I
[21]	CFRP tow AS4/8552	Phenolic (HRP) honeycomb	1676	254	I
[138]	E glass woven roving polyester resin	Foam	1000	800	QS

Damage and dimensions

When the panel is tested in compression the diameter of the impact damage should not be greater than half the specimen width and penetration of the panel should not have occurred. If the damage is in excess of these limits then it is too extensive to meaningfully evaluate damage tolerance with a subsequent compression test. In these circumstances a bigger panel or lower energy level should be used [7].

Sample adjusting

In NASA CAI testing method is used a square panel for the impact testing phase which then is trimmed to make a smaller sized rectangular panel for the compression testing phase. This removed any damage induced by the clamps during impact testing and allowed for machining of the panel edges to obtain the flat and parallel/perpendicular edges required for compression testing [7].

Length to width ratio of CAI specimen

Length-to-width ratio otherwise known as the panel aspect ratio is typically 1 to 2.5, irrespective of the support conditions [7], about 73% of all reviewed articles had that value. The majority (23%) aspect ratio is 1, in second place (12%) is 1.5

and 28% are represented by 1.25, 1.33 and 2. The remaining part is beam like specimens with aspect ratio from 3 and up to 10.

The width-to-thickness ratio is generally below 5 for panels with clamped loaded edges and free unloaded edges but above 5 for panels with clamped loaded edges and simply-supported unloaded edges. As the width-to-thickness ratio approaches unity or the aspect ratio drops below 1 panel buckling becomes less likely. Therefore dimensions with these ratios should be avoided when studying the impact damage tolerance of realistic structural panels [7].

The effect of varying the panel aspect ratio has been studied by only a small number of researchers. For undamaged panels with simply-supported unloaded edges the increment of aspect ratio from 1 to 2 [99] and 1.33 to 2 [146] reduced the failure load despite the failure mechanisms being the same. In panels containing impact or artificial damage often very few comparisons could be made for panels with different aspect ratios, as despite a reduction in failure load with increasing aspect ratio, the level of impact/artificial damage also increased. One exception to this was in the study by Tomblin et al. [27] where the effect of panel aspect ratio was compared by normalizing the panel length and width by the damage diameter. Both length and width were varied for impact damaged panels with clamped loaded edges and simply supported unloaded edges. Increasing the width to give an aspect ratio between 1.6-0.64 tended to marginally increase the compressive strength, as was also observed by Moody et al. for panels with unsupported side edges [31], whilst increasing the panel length to give an aspect ratio between 0.84-1.32 caused a minor reduction in compressive strength. The latter was suggested to be due to an interaction between global buckling and the local indentation as a result of the impact damage. In addition the narrow specimens had higher strain levels within the damaged region, indicating a higher level of load was carried through the damaged region which resulted in higher levels of bending. Different failure mechanisms were also observed in narrow and wide panels, with wide panels exhibiting a dimple-growth arrest mechanism [7].

The dimensions of the monolithic laminates used in the NASA and SACMA standards vary but are designed to give a width-to-thickness ratio and specimen aspect ratio within a specific range. The width-to-thickness ratio is the dominant factor and ranges from 20-75 for 2-5 mm thick panels in the NASA standard and 16-100 for 1-8mm thick panels in the SACMA standard. The specimen aspect ratio is fixed at 2 and 1.5 in the NASA and SACMA standards respectively [7].

Residual strength estimation

After artificial damage is introduced in specimen, appropriate and robust method for residual strength estimation must be applied. Most of researchers were using compression type of loading, also bending was mentioned in some articles [4, 40, 101, 126, 141]. As there are no methods for sandwich panels residual strength estimation some existing methods which are related could be modified and applied. Probably the simplest method for sandwich panel edgewise compression is ASTM C364 (§ 4.4.1.) which is occasionally used in CAI testing. However, as it is a standard for uni-axial compression only with no support for the unloaded edges it could not be applied to large sandwich panels whose unloaded edges need to be supported. If the edges are free then compression of the panel can be compared to compression of a wide column. Other methods, such as NASA, SACMA, CRAG and ASTM 7137 provides supporting of unloaded sidewalls, although are designed

exclusively for laminate structures. In this case when the edges of the panel are simply-supported or clamped the panel must be treated as a plate. Clearly in the two-dimensional beam case the buckling modes and associated analysis is much simpler than for the three-dimensional plate case, with Timoshenko or Euler beam theory often applied in the former case. Additionally if the unloaded edges are free and the panel aspect ratio is moderate to large, global buckling of the specimen is likely to occur and the load required for failure will be much less than for that of a panel with simply-supported or clamped unloaded edges. McGowan et al [22] was found that the removal of the simple supports only affected the panel just before the point of failure when the panel suddenly bent, increasing the compressive strain in the impacted skin. The global axial stiffness of the panel was not affected by the absence of edge supports, and the panel failed in a similar way to the panel with simply-supported edges tested under the same conditions. Despite this observation caution must be taken when comparing panels with supported and free edges and all subsequent discussion will distinguish between the two support conditions, with focus on panels with supported unloaded edges where possible [7]. Although Adams et al reports that sides of the sandwich specimen must be supported to prevent buckling [108]. Hence the simple or clamped supports used on the unloaded edges are often termed anti-buckling supports, although contrary to what the name suggests local panel buckling can still occur but will be at a much higher load [7]. Such supports may take the form of knife edge supports or clamp-type supports, depending on the type of boundary condition desired; knife edge supports are used to replicate a pinned joint whereas clamped supports are used to minimize panel rotation at the edges [108].

Major part of researchers used testing method where loaded ends is clamped or potted and unloaded edges were free [10, 12, 24, 42, 93, 123, 124, 147, 148]. The lesser number of researchers used simply-supported unloaded edges and clamped loaded ends [1, 22, 65, 89, 108]. Clamped conditions prevent panel rotation and horizontal movement of the panel ends. This is created by either clamping the panel directly with metal blocks, as seen in the SACMA and NASA methods or potting the panel ends in epoxy resin. The potting material prevents direct rotation of the panel ends in a similar way to clamping the panel ends with metal blocks (grips). However, as the potting material is not fixed to the loading head a minimal amount of rotation of the potting material can occur. Potting the panels in epoxy resin or setting the panel ends into metal blocks eliminates the possibility of inflicting damage to the panel ends, as can occur when mechanically clamping or gripping the panel ends (§ 3.4). Irrespective of which method is used to clamp the loading ends it is vital that the ends are completely flat and parallel to the loading surface. If the loading ends and loading head are not in parallel an uneven stress distribution can be induced at the panel ends, which may lead to premature failure of the panel at the loaded ends [7]. Figure 5.4. gives a schematic comparison of compression supports.

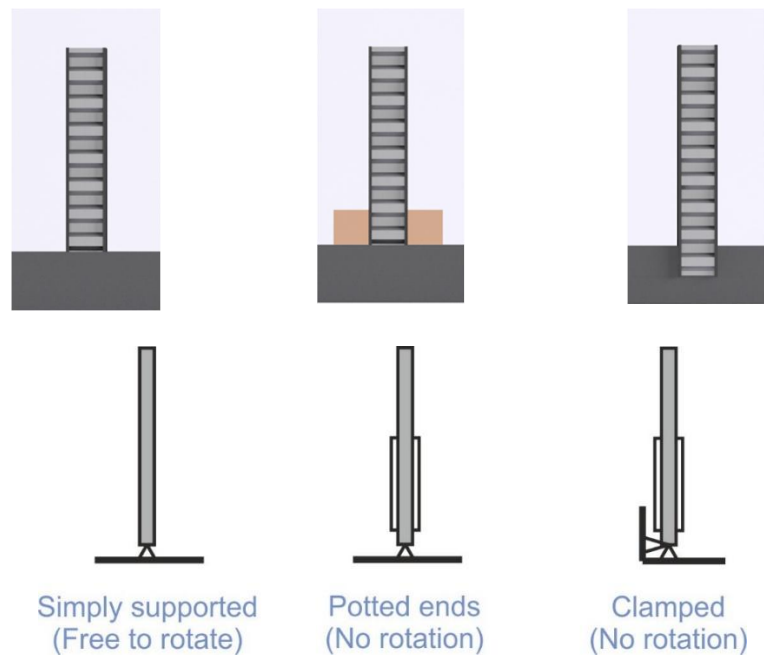


Figure 5.4. Comparison of compression supports [7]

Panel failure

Failure modes in edgewise compression:

- (1) core buckling,
- (2) delamination in the impacted face sheet,
- (3) core cracking,
- (4) matrix cracking,
- (5) fiber breakage in the facings [26].

* Failures that occur at or close to the supports, such as end crushing or brooming, are not true compressive failure modes, and are not representative when assessing residual compressive strength [7].

Failure modes of intact panels

Before the more complicated case of impact damaged panels can be understood the basic failure modes and strength of undamaged sandwich panels must be identified. A variety of failure modes have been identified for panels under in-plane compression; namely compressive failure of the skins, skin wrinkling or local buckling, skin dimpling and panel shear failure. All applicable to panels with both supported and unsupported unloaded edges. Global or Euler buckling is restricted to columns or panels with unsupported unloaded edges. The failure modes of sandwich panels under in-plane compression are much more dependent on the intrinsic and extrinsic variables, in particular the panel boundary conditions, than for transverse loading. The most common failure modes are discussed below and depicted in Figure 5.5. [7].

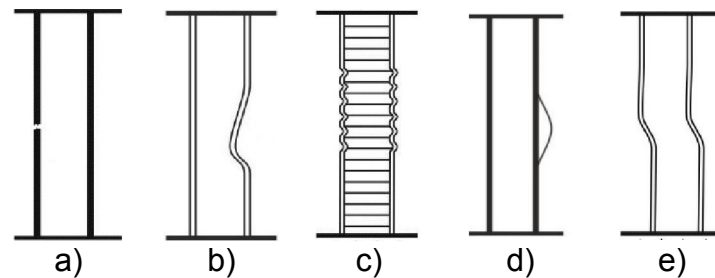


Figure 5.5. Failure modes of sandwich panels under in-plane compression with simply supported edges a) skin compressive failure, b) inward local buckling (dimpling), c) intra-cell buckling, d) face wrinkling e) panel shear failure

Compressive failure of the skins (Figure 5.5. (a)) applicable to panels with both supported and unsupported unloaded edges. Compressive skin failure depends purely upon the strength of the skins and will be the dominant failure mode provided the core is of sufficient stiffness and gives adequate support to the skins. Although for compressive skin failure the skins are assumed to support the entire load, the failure strength is generally lower than the compressive strength of the skin material as attained during mechanical property testing. The failure location can vary but ideally should be close to the panel mid-section. The compressive failure of one skin can lead to failure of the second skin nearly simultaneously in undamaged panels. In addition compressive skin failure often occurs in conjunction with local buckling type failure modes [7].

Singlesided buckling (Figure 5.5. (b)) is most common in experimental studies. Also can occur symmetric or asymmetric. Another type of well-known failure mode in honeycomb-cored sandwich panels with very thin faces and large honeycomb cells is “intra-cell buckling” or “dimpling” (Figure 5.5. (c)), where the skin buckles into each individual honeycomb cell, leading to panel failure via core crushing or skin-core debonding [7, 92]. This type of failure is comparatively uncommon compared to the other types of wrinkling failure.

Face wrinkling (Figure 5.5. (d)). The actual failure can occur if the tensile strength of the core or the adhesive joint is lower than the compressive strength of the core [149]. In the study by Shipsha et al. [128] whilst the residual indentation grew inwards the area surrounding the impact damaged area buckled outwards and it was this that led to a catastrophic skin-core debonding failure [7].

Both global buckling and panel shear failure are typically seen in columns or coupons with unsupported unloaded edges though wide columns can still fail in global buckling. Shear failure of panels with supported edges, as depicted in (Figure 5.5. (e)), typically occurs after global or local buckling if the core material has a relatively low shear strength and modulus [7].

Failure modes of damaged sandwich panels

Results of the CAI tests indicate that the global response of the panels was not affected by the presence of impact damage [11, 22]. Panels exposed to impact damage under compression load shows same failure modes as intact panels. Whilst it is widely recognized that increasing the impact energy and/or damage area reduces the RCS, the variation of either factor can also cause a change in failure mode. At low impact energies where the internal damage area is small the failure modes of the impact damaged panels were expected to be similar to those of the undamaged panels. However, in the majority of cases the introduction of even a low

level of impact damage generated stress concentrations at the impact site, leading to failure of the impacted skin. Failure of the back skin due to global buckling, debonding or compressive failure often occurred if loading was continued [7].

The way in which the damage propagates under compressive loading can either be progressive or catastrophic depending on the level of impact energy and size of the impact damage area:

1. Catastrophic failure is characterized by a sudden, instantaneous drop in the force vs. displacement curve and dramatic failure of the panel, often accompanied by a loud noise, with an abrupt loss of load carrying capability. Although this in itself implies the existence of an unstable failure mode the damage propagation in the early stages of loading is often stable [4, 7].
2. Progressive failure is signified by partial load loss or suspension of load increase prior to complete panel failure through the growth of delaminations or core crushing emanating from the impact damaged region [7].

The nature of the impact damage growth leading to failure is often a combination of the failure modes identified for the undamaged panels. Three varying types of impact damage propagation were identified, all of which were applicable to panels with both unsupported and simply-supported unloaded edges:

1. Panels with skin delamination caused by the impact the delamination was seen to propagate, which in turn led to compressive failure of the skin across the panel width [63].
2. The second and most common failure mode was due to growth of the residual indentation inwards causing further core crushing, leading to compressive skin failure across the panel width [44, 46, 57, 63, 86, 87, 150].
3. Thirdly, in addition to the residual indentation buckling inwards it was also seen to propagate perpendicular to the loading direction with failure due to the indentation spreading across the entire panel width [4, 57].

Each of the above failure modes initiates with the propagation of the impact damage [4, 7]. However, whether or not this develops into a compressive skin failure or dimpling/wrinkling failure depends upon the ability of the panel to resist the spread of the damage. In some instances for honeycomb sandwich panels the impact damage never spread and failure was purely due to the initiation of compressive skin failure emanating from the edge of the impact damage. In other instances although the residual indentation initially grew, upon reaching a certain distance from the impact center the dimple was arrested until the energy in the skin became large enough to either cause an unstable propagation of the existing dimple or compressive skin failure [7].

Strain gauges

The use of strain gauges at various locations across the panel skins can provide valuable information regarding the nature of the damage growth in impact damaged panels. It has been shown that the compressive load can be carried by the damage region at low loads but is redistributed around the impact damage location at higher loads, with large local stress concentrations forming around the impact site. Strain gauges positioned away from the damage site at a far-field

location often show a linear stress strain response until failure, indicating that the effect of the impact damage on the compressive response is insignificant away from the damage site [7, 22, 57].

Specimen alignments using strain gauges:

1. One possible alignment method is to place an undamaged sandwich panel into the fixture and use four alignment strain gages, placed near the bottom corners of the specimen, for alignment. The test configuration is aligned such that approximately equal strains are measured upon application of a preload. Such alignment can be performed using shims, or through the use of an alignment device, such as a hemispherical alignment stage placed under the test fixture. However, this method does not account for specimen-to-specimen variability in machining tolerances, and requires that the fixture not be displaced between tests [108].
2. A second method of alignment is similar to the method described above; however adjustments are made for alignment for each specimen tested. While side-to-side alignment generally can be obtained, front-to-back alignment is problematic, due to the impact damage on one surface of the sandwich panel [108].
3. A third approach, a mixture of the first two, is to use an undamaged specimen to set the front-to back alignment (which is “locked down”) followed by a test panel specific width-wise adjustment for side-to-side alignment [108].

Residual strength

The reduction in residual strength was found to be most severe for lightly damaged panels. Increasing levels of damage resulted in further reduction in residual strength, but the reduction between adjacent data points decreased in magnitude [4]. With low levels of impact damage the impact damaged panels fails in a similar mode to the undamaged panels and reduction in residual compressive strength still occurs. This is contrary to monolithic laminates where there is often no reduction in RCS for low impact energies. In the sandwich panels as the impact energy and damage size increases a definite reduction in RCS occurs, with reductions up to 60% common [7, 22, 63]. Further increases in impact energy can lead to a RCS of just 40% of the undamaged sandwich panel strength [7, 57, 63, 150].

Guidelines for impact damage tolerant design:

1. Sandwich panels should fail initially by facesheet compression (rather than facesheet buckling) so that the full strength of the composite facesheets can be realized [26].
2. Extensive core damage should not develop at a lower impact level than detectable facesheet damage since this can lead to local facesheet buckling at extremely low panel strain levels [26].

5.2.2 Compression-after-impact properties of oriented fibre-resin composites: SACMA SRM 2-88

Summary

SACMA SRM 2-88 was developed by Boeing and has been adopted by the Suppliers of Advanced Composite Materials Association (SACMA). It is the basis of the Airbus Industries test method and ASTM D7137. It is currently the most popular method for the compression-after-impact of monolithic laminates [7].

Specimens

Dimensions of laminate specimens required by current method are 152 mm x 102 mm x 4.6-5.6 mm [7].

Test setup

1. Impact: Sample is clamped to an aluminium support base, with a 76 mm x 127 mm cut out area, using 4 rubber tipped toggle clamp fixings. Indenter has hemispherical shape and diameter of 16 mm. Drop mass is 5 kg. The drop height can be adjusted to give the required impact energy of 6.7 J/mm, which is specified in terms of panel thickness [7].
2. CAI: Loading at a rate of 1.27 mm/min [7]. The specimen is supported along the four edges. The fixture is fully adaptable by the bolts for several specimen's sizes (Figure 5.6.). The plate on top, which is not linked directly to the lower part of the fixture, has a support function. The bars, arranged laterally, are sized to guarantee that there is always a certain gap between the top plate and the bars themselves [151].

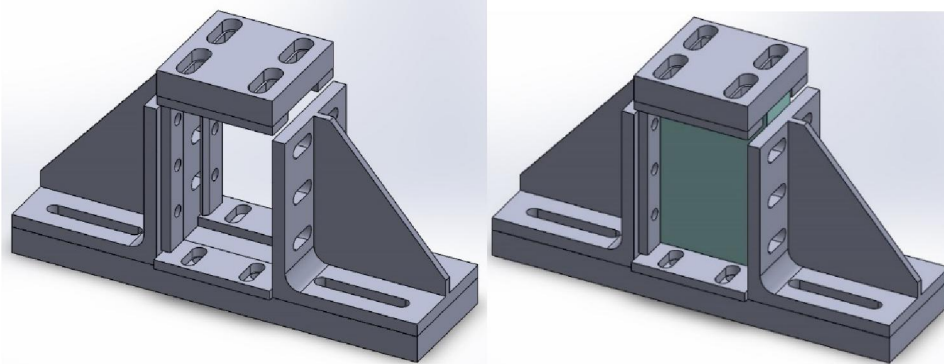


Figure 5.6. SACMA compression after impact test rig without and with specimen

Strain

Four axial strain gauges are used to measure the strain [7].

5.2.3 Standard tests for toughened resin composites: NASA 1 092

Summary

This method is similar to the SACMA method but utilizes bigger test specimens, making it less popular due to the larger associated testing costs [7].

Specimen

Dimensions of laminate specimens are different for impact 254-317 mm x 178 mm x 6.35 mm and for CAI tests are 178 mm x 125 mm [7].

Test setup

- 1) Impact: Specimens are clamped centrally between a steel base plate and top plate with 127 mm x 127 mm cut-outs. Impact damage is induced using a drop weight impact rig with a 4.55 kg, 12.7 mm diameter hemispherical indenter. The indenter drop height is 508 mm, producing fixed impact energy of 27 J. As with the SACMA method the test specimens should be visually checked and C-scanned before and after the impact, with the testing of three specimens for verification of results [7].
- 2) CAI: The impacted specimen must be trimmed to 178 mm x 125 mm to fit into the compression rig (Figure 5.7.). This also removes any damage to the panel induced through the clamping supports used in the impact phase and ensures each loading edge is perfectly square and flat. The 125 mm loading edges of the specimen are clamped between two steel plates to prevent local buckling of the specimen ends, whilst the 178 mm edges are simply-supported. The load is applied through the clamped edges at a crosshead speed of 1.27 mm/min and back to back axial strain gauges are used to monitor the load-strain response [7].



Figure 5.7. NASA compression after impact test setup, [152]

5.2.4 Compressive Residual Strength Properties: ASTM D7137

Summary

This test method covers compression residual strength properties of multidirectional, flat, rectangular polymer matrix composite plates, which have been subjected to quasi-static indentation per test method D6264 or drop-weight impact per test method D7136 prior to application of compressive force using a stabilization fixture.

Specimens

A uniaxial compression test is performed using a balanced, symmetric laminated plate, 150 × 100 mm, which has been damaged and inspected prior to the application of compressive force. The damage state is imparted through out-of-plane loading caused by quasi-static indentation or drop-weight impact.

It is recommended that the damage size be limited to half the unsupported specimen width (42 mm) to minimize interaction between damage and edge-related stress/strain fields; as the specimen has a small length-to-width aspect ratio of 1.5,

its stress/strain distribution is particularly sensitive to disturbances caused by impact or indentation damage.

Test set-up

The damaged plate is installed in a multi-piece support fixture (Figure 5.6.), that has been aligned to minimize loading eccentricities and induced specimen bending. The top and bottom supports provide no clamp-up, but provide some restraint to local out-of-plane rotation due to the fixture geometry. The side supports are knife edges, which provide no rotational restraint. Edge supports must be coplanar. The specimen/fixture assembly is placed between flat platens and end-loaded under compressive force until failure.

Results are affected by the geometry of the various slide plates local to the specimen. Results are also affected by the presence of gaps between the slide plates and the specimen, which can reduce the effective edge support and can result in concentrated load introduction conditions at the top and bottom specimen surfaces. Additionally, results may be affected by variations in torque applied to the slide plate fasteners; loose fasteners may also reduce the effective edge support.

Speed of Testing

Speed of testing should be enough to produce failure within 1 to 10 min. The suggested standard crosshead displacement rate is 1.25 mm/min.

Strain measurement

Strain measurement of the specimens is recommended, but not required. If strain measurement is performed, the longitudinal strain should be measured simultaneously at four locations (two locations on opposite faces of the specimen) to aid in ensuring application of pure compressive loading and to detect bending or buckling, or both, if any. The same type of strain transducer shall be used for all strain measurements on any single specimen. The gages, surface preparation, and bonding agents should be chosen to provide for optimal performance on the subject material for the prescribed test. A difference in the stress-strain or force-strain slope from opposite faces of the specimen indicates bending in the specimen.

Failure

All of the failure modes are acceptable, with the exception of end-crushing, edge-restrained delamination growth (for which delamination(s) grow prior to final failure and additional force-carrying capability results from edge restraint). Edge-restrained delamination growth and panel instability failures cannot be determined by visual inspection of the specimen during or after test; they must be determined through inspection of the stress-strain or force-strain curves.

Calculation

Ultimate compressive residual strength is calculated as shown:

$$F^{CAI} = \frac{P_{\max}}{A}$$

where:

F^{CAI} – ultimate compressive residual strength, MPa;

P_{\max} – maximum force prior to failure, N;

A – cross-sectional area = $h \cdot w$, mm².

Effective compressive modulus is calculated using equation:

$$E^{CAI} = \frac{P_{3000} - P_{1000}}{(\varepsilon_{3000} - \varepsilon_{1000}) \cdot A}$$

E^{CAI} – effective compressive modulus, MPa;

P_{3000} – applied force corresponding to ε_{3000} , N;

P_{1000} – applied force corresponding to ε_{1000} , N;

ε_{3000} – recorded strain value closest to 3000 microstrain,

ε_{1000} – recorded strain value closest to 1000 microstrain.

5.2.5 Bending after impact summary

As alternative for compression after impact is bending after impact. 4-point method usually is applied. Bending after impact is less popular but also is used for residual strength estimation. The subsequent 4-point bending tests are performed to assess the change in bending strength due to impact damages [141]. BAI also is sensitive as CAI. As reports Klaus et al. even damages which are almost invisible from outside and could be missed during a visual inspection are able to reduce the bending strength of such panels significantly [90].

For BAI tests due to fragility of thin skins and honeycomb walls, the sandwich panel in contact places with loading members should be reinforced as discussed in chapter 3.4. Also rubber pads could be placed between the loading cylinders and the sample [90].

Sandwich panels with different core heights and thus different bending stiffness, have approximately same level collapse loads [64]. Failure modes in flexure:

- (1) upper skin compression failure (Figure 5.8.) followed by either stable core crushing then lower skin tensile failure or core shear failure [26],
- (2) core shear failure [26],
- (3) two types of upper skin buckling with delamination (Figure 5.9.) [64].



Figure 5.8. Upper skin compression failure in 4-point bending [64]

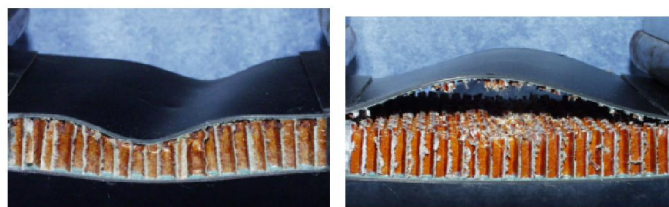


Figure 5.9. Upper skin buckling [64]

6 Damage & defect monitoring

For better quality control of manufactured panels and also for impact damage deep investigation nondestructive test methods are quite useful. Nondestructive inspection is defined as the examination of structural parts for surface and subsurface defects without damaging the structure. There are many different techniques in use. Some of these are: X-ray radiography, thermal neutron radiography, ultrasonic inspection, shearography and the coin tap test. A good NDI method should be able to locate, determine the size, and also classify the types of defects and damage. Sometimes this requires the use of several different procedures on one panel to get full “picture” because every method are sensitive only for some specific defects. A brief look is given in Table 6.1. [2].

The test equipment can be expensive to purchase and requires some operator skill to obtain reliable and repeatable results. Interpreting the data may be difficult and require a bit of experience; however, the new equipment is becoming less expensive and is much easier to use [2].

Table 6.1. Applicable inspection methods for various types of defects [111]

Type of Defect	Inspection method					
	Visual	Tapping	Ultrasonic	X-ray	Eddy current	Acoustic emission
External damage	X	X				
Core to skin delamination	X	X	X			
Internal Voids			X	X		
Distorted core			X	X		
Moisture				X		
Skin Cracks					X	
Corrosion						X

Visual inspection is the simplest and by far the oldest and most economical method. It is just the careful examination by eye of the panel surface that can be seen, and it is very limited as to the types of defects that can be identified [2].

Tapping inspection can be used for detecting voids or delaminations in bonded areas. A coin is normally used as a special tapping hammer, but there is a special tapping hammer available. When tapping a sandwich a ringing sound is produced. If a defect is encountered there is a difference in sound tone produced that can be detected by a trained ear. Sharp, clear tones indicate that adhesive is present and adhering to the substrate in some degree; dull, hollow tones indicate a void or unattached area. Some improvement in the tap test can be achieved by using a solenoid-operated hammer and a microphone pickup. The resulting electrical signal can be analyzed on the basis of amplitude and frequency This type of inspection must be conducted in a relatively quiet area [2, 94]. It can be difficult to distinguish for small areas of damage, furthermore it is not possible to distinguish

between different types of damage or obtain an accurate measurement of damage size [7, 114].

The Mitsui Engineering Company has produced an automatic hand-held tapping device called Woodpecker. This unit, with a built-in CPU and a sensor fitted to the battery-driven solenoid hammer, can detect and show delaminations on the LED display [2].

Ultrasonic inspection is the most popular and effective method for detecting damage in composite laminates. It is a very powerful tool for detecting delaminations, voids and inconsistencies in bonded sandwich structures. This method uses sound waves with a frequency above the audible range. The waves are induced into the part by a piezoelectric transducer transmitter. This sonic energy travels through the part, and any change in acoustic properties of the material will affect the sound traveling to a receiving transducer which displays the information on an oscilloscope or chart [2, 7].

There are three types of ultrasonic inspection instruments used for testing: high frequency (1 MHz to 5 MHz), low frequency (15 kHz to 50 kHz) and resonance:

1. The high frequency through-transmission procedure is quite commonly used for best defect definition. This method requires a couplant such as oil, grease or water between the interface of the transducer and the part. The main disadvantages are that it is time consuming and is not portable. However, this method is one of the most reliable and sensitive for inspecting honeycomb sandwich [2].
2. Low frequency equipment is portable and does not require a couplant; however, it is less accurate and typically does not provide a permanent record [2].
3. The resonant type equipment is also portable and does not require a couplant. [2].

There are two procedures for inspection, pulse-echo or through-transmission:

1. The pulse-echo method only requires access to one side of the panel. Sound waves are reflected back to the receiving transducer [2].
2. The through-transmission method has the transmitting transducer on one side and the receiving transducer on the panel other side. This procedure has the advantage of locating discontinuities throughout the depth of the panel. Voids, delaminations, crushed core or other anomalies in the structure attenuate the transmitted signal. The transducer alignment must be as nearly parallel to the cell axis as possible. Usually the output is coupled to a C-scan recorder [2, 114]. Research has shown that the damage area detected using through transmission C-scanning corresponds well with the honeycomb cell wall crushing area obtained through specimen cross-sectioning, but generally overestimates skin delamination [7].

Radiographic inspection uses X-rays or gamma rays to detect defects through differences in densities in the sandwich. It is a very useful NDI method in that essentially allows a view into the interior of the part [114]. Since this method records changes in total density through the thickness, it is best for detecting the presence of water in honeycomb core cells. Also it is very effective in finding core that has been dislocated or damaged. X-ray radiography provides another means of examining the internal damage and is particularly useful in determining core

defects and damage. The X-rays easily pass through the thin, low density composite skins and can detect irregularities in the core structure and skin-core debonding. Consequently conventional X-ray techniques cannot detect planar defects, such as core-to-facing delaminations because they are in a plane perpendicular to the ray direction. Detection of core crushing is possible, but as the X-rays are reflected by the vertical cell walls, unless the crushing is quite extensive it is difficult to identify on the radiograph. Additionally to obtain a clear picture of damage the X-ray needs to be collimated and motor driven, as the X-ray radiograph has a 3D distortion effect away from the damage sight [2,7]. Also this method is relatively expensive, and special precautions must be taken because of the potential radiation hazard. [114].

Neutron radiography is similar to X-ray radiography in that penetrating radiation is used to obtain visual images of the internal sandwich parts. This method is very time consuming; it takes 40 h for a neutron scan alone and 64 h for a complete X-ray and neutron scan. It also is extremely expensive [2].

Shadow moire interferometry can be used to measure dimple propagation during quasi-static testing and out-of-plane deformation/local buckling during compression loading. Typically a light-reflective line-grid film is adhered onto the panel surface and is calibrated prior to testing with a light source directed at the panel surface. During the test the moire fringe patterns associated with grid distortions are recorded with a camcorder. Selected images from the videotape can then be digitized and measured after the test. This method can only provide a measure of out-of-plane deformation, but does give a good indication of the deformation sequence with respect to load and time. For a sandwich panel indentation of the top skin is an important type of damage mechanism but still needs to be related to internal damage for complete understanding. Additionally this technique is only suited to compression tests where the face of the panel is unobstructed from the camera [7].

Shearography is sensitive to very slight changes in surface strain due to subsurface flaws and also is very applicable to sandwich structures. It is an advancement of shadow moire interferometry, using lasers to detect minute changes in surface strain during loading. A reference image is stored electronically using a video laser interferometer. Then a uniform stress is applied to the part via vibration, pressure or thermal means. Subsequent images of the test part are compared with the reference image resulting in flaw detections on the video monitor. This shearography method has a high inspection rate, inspects large areas at one time, does not touch the part and is not affected by part contours or shape. It can be used on metallic or nonmetallic honeycomb sandwich panels and can detect unbonds, delaminations, crushed core and corrosion [2, 7].

Thermal inspection is useful as a mean of detecting bonding discontinuities directly beneath relatively thin low thermal conductivity materials [114]. A pulse of heat is sent via a flash to the surface of material, which causes instantaneous heating of the material surface. As the heat flows through the thickness of the material variations in the local surface temperature can be seen using an infrared camera. These variations are due to defects and discontinuities in the internal material structure which affect the heat flow through the material. Single-sided or

through transmission measurements can be taken and a thermal diffusivity image produced. This response must then be fitted to a theoretical model for a quantitative measurement of thermal diffusivity to interpret the spread of damage through the thickness. All imaging is produced using an infrared camera and associated kit, which is quite expensive to purchase [7].

Eddy current is widely used for detecting defects in metallic components and can be used in detection of conductive composite material, like CFRP. Eddy current testing offers a number of advantages compared to other NDI techniques: it enables detection of surface and subsurface damage in contrast to dye penetrant inspection; it can be applied to non-magnetic metallic items in contrast to magnetic flux leakage; it does not require an acoustic couplant as is the case for ultrasonic inspection, and it is more economical, easily applied, and less hazardous than radiography [66]. The technique is most effective for detecting irregularities near the surface. It can, however, be used for greater depths with decreasing sensitivity [114].

7 Represent countries and departments. Foundation. Projects.

Within literature review also was paid attention to where researches and studies have been performed, within what projects and who gave financial support. In pie chart (Figure 7.1.) are show countries in which countries used literature articles were carried out. The absolute leader is United States of America, second place is divided by United Kingdom and People Republic of China. Also Germany and France in contrast to other not mentioned countries are quite more often participated.

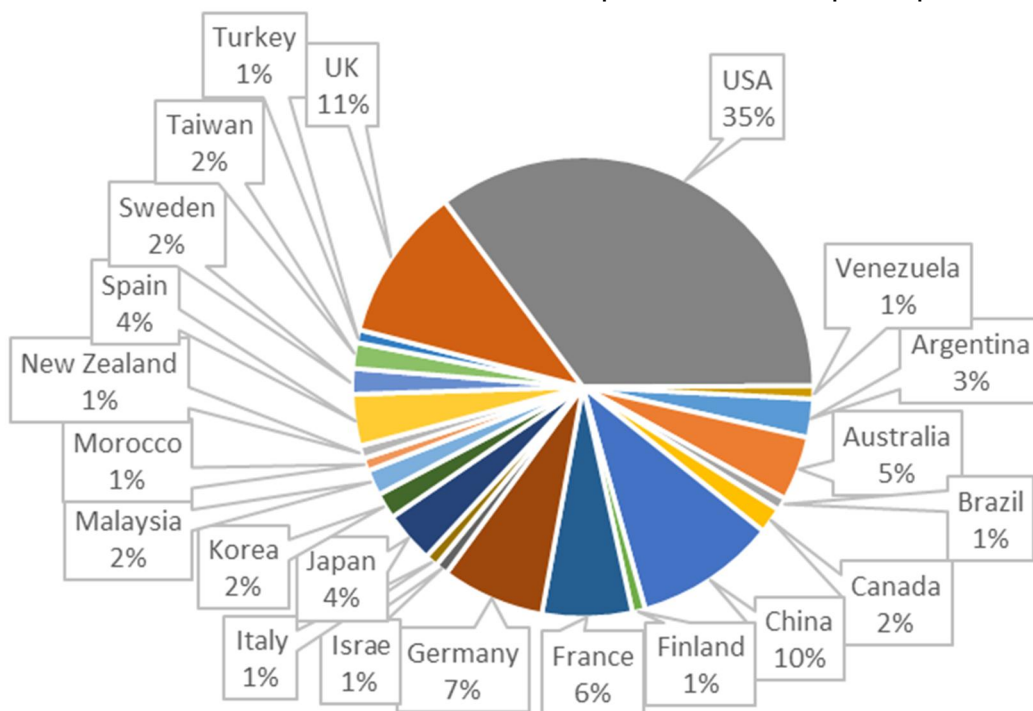


Figure 7.1. Countries where review researches were carried out

In

Table 7.1. are summarized financiers of researches reviewed. The most often representative of financiers related to aerospace industry is National Aeronautics and Space Administration (NASA), the second is Federal Aviation Administration (FAA) which parent agency is U.S. Department of Transportation, Boeing Commercial Aircraft Group and European Space Agency (ESA). Also were found Aviation Applied Technology Directorate (AATD) and Westland Aerospace. Other financiers are not specific to aerospace industry and they are Office of Naval Research (ONR), National Science Foundation of China, European Commission (EC), Major State Basic Research Development Program of China and Fundamental Research Funds for the Central Universities (China). Part of the rest are governments and government councils or programs. Also several grants were found (Table 7.2.). Although major part of financiers are not directly related to aerospace industry, the research departments almost entirely are. The list of departments and/or universities where reviewed articles were carried out is shown in Table 7.3.

Table 7.1. Summary of financiers of researches

Financier	Abbreviation	Country	Number of articles sponsored by
Financiers related to aerospace industry			
National Aeronautics and Space Administration	NASA	USA	13
Federal Aviation Administration	FAA	USA	6
European Space Agency	ESA	Sweden, UK	2
Boeing Commercial Aircraft Group	Boeing	USA	2
Aviation Applied Technology Directorate	AATD	USA	1
Westland Aerospace		UK	1
Bombardier and the Royal Academy of Engineering		Australia	1
Flight Dynamics Directorate		USA	1
EADS Space Transportation		France	1
Canadian Forces (Aerospace and Telecommunications Engineering Support Squadron)		UK, Canada	1
Financiers not related to aerospace industry			
Office of Naval Research	ONR	USA	5
National Science Foundation of China		China	4
European Commission	EC	Germany	3
Major State Basic Research Development Program of China		China, Argentina	3
Fundamental Research Funds for the Central Universities		China	3
Naval Surface Warfare Center, Carderock Division	NSWC-CD	USA	2
National Natural Science Foundation of China		China	2
National Sciences and Engineering Research Council of Canada	NSERC	Canada	2
Natural Scientific Research Innovation Foundation		China, Argentina	1
Human Resources Development of the Korea Institute of Energy Technology Evaluation and Planning	KETEP	Korea	1
Korea government Ministry of Knowledge Economy		Korea	1
Ministry of Construction and Transportation	MOCT	Korea	1
Engineering and Physical Sciences Research Council		UK	1
Spanish Comisión Interministerial de Ciencia y Tecnología		Spain	1

STA of Japanese Government		Japan, Australia	1
Fuji Heavy Industries	EPSRC	USA	1
Euro-Composites company	ECC	Morocco, France	1
National Science Council of the Republic of China		Taiwan	1
Fundacao de amparo a pesquisa do estado de sao paulo	FAPESP	Brazil	1
Ministério da Ciencia, Tecnologia e Inovacao	CNPq	Brazil	1
Rieter Automotive Management		Sweden	1
Australian Research Council		Australia	1

Table 7.2. Grant numbers founded in reviewed articles

Ref.	Foundation Company	Grant number	Country
[60]	FAA	01-C-AW- WSU-002	USA
[62]	NASA	82832	USA
[150]	NASA	82832	USA
[66]		EP/E005071	China, UK
[147]	Regione Lombardia	project "STIMA – Strutture Ibride per Meccanica ed Aerospazio"	Italy
[123]	1 Major State Basic Research Development Program of China; 2 National Science Foundation of China; 3 Fundamental Research Funds for Central Universities; 4 Natural Scientific Research Innovation Foundation	1) 2011CB610303; 2) 11222216, 11302060; 3) HIT.BRETIV. 201301, HIT.NSRIF.2014025 4) HIT.NSRIF.2014025	China, Argentina
[126]	EC	Project CELPACT ("Cellular Structures for Impact Performance")	Germany
[40]		Project TRA2004-03960	Spain, Venezuela
[67]	grant funded by the Korea government Ministry of Knowledge Economy	20124010203240	Korea
[71]	FAPESP; CNPq	02/01808-7; 02/01288-3; 02/02057-5; 300599/96	Brazil
[170]	National Natural Science Foundation of China	11172196; 10802055; 10972153;	China
[74]	ONR	N00014-07-1-0764	UK
[156]	Australian Research Council, National Natural Science Foundation of China	11102032	Australia, China
[176]	1 National Science Foundation of China;	1) 90816024 and 10872059;	China

	2 Major State Basic Research Development Program of China (973 Program); 3 Fundamental Research Funds for the Central Universities; 4 Fundamental Research Funds for the Central Universities	2) 2011CB610303; 3) HIT. NSRIF. 2010069	
[177]	1 Major State Basic Research Development Program of China 2 National Science Foundation of China	1) 2011CB610303; 2) 11222216, 11002041 and 11302060	Argentina
[87]	ESA	N00014001034	Sweden
[92]	ESA	N0001400103	UK

Table 7.3. List of departments where used articles are created

Ref.	University, Department, Country
[11]	Dept. of Aeronautical & Automotive Engineering, Loughborough University
[60]	Wichita State University
[143]	Dept. of IIUM, Laboratoire Structure Toulouse
[57]	Dept. of Aeronautics, Imperial College, London; QinetiQ, Cody Technology Park,
[62]	Dept. of Mechanical Engineering and Applied Mechanics, North Dakota State University
[38]	Aerospace Engineer, Structural Mechanics Branch
[107]	1 National Institute of Aerospace, Hampton, USA 2 Army research laboratory, Vehicle Technology Directorate, NASA Langley Research Center, USA 3 Sikorsky Aircraft, USA
[88]	NASA
[21]	NASA Langley Research Center
[51]	Dept. of Aeronautics and Astronautics at the Massachusetts Institute of Technology, Cambridge.
[24]	NASA Marshall Space Flight Center
[150]	Dept. of Mechanical Engineering and Applied Mechanics North Dakota State University Fargo
[33]	College of Astronautics, Northwestern Polytechnical University, China; Dept. of Aerospace Engineering, Mississippi State University, USA; Aviation Engineering Institute, Civil Aviation Flight University of China
[153]	University of Maryland Aerospace Engineering College Park
[154]	1 Université de Technologie de Compiègne, Laboratoire de Mécanique Roberval Dep GM - Polymères et Composites BP 20529 - 60205 Compiègne Cedex, France 2 L3M. IUT de Tremblay en France, France 3 STRUCTISO, France
[141]	RWTH Aachen University Dept. of Aerospace and Lightweight Structures Wuellnerstr, Germany

[35]	NASA Langel Research Center
[23]	Dept. of Mechanical Engineering, University of Utah,/ Graduate Research Assistant, Dept. of Mechanical Engineering, University of Utah
[155]	Key Laboratory of Eco-textiles Ministry of Education Jiangnan University
[61]	1 Université de Toulouse, UPS/LGMT (Laboratoire de génie mécanique de Toulouse), France 2 Mechanical Engineering Dept. of IIUM, Malaysia
[27]	Wichita State University
[51]	Technology Laboratory for Advanced Composites Dept. of Aeronautics and Astronautics, Massachusetts Institute of Technology, Cambridge, USA
[20]	1 LMS, IPPT PAN, E' cole Nationale Supérieure de l'Aéronautique et de l'Espace 10, France 2 LGMT, IGM, Université Paul Sabatier, Filie`re Ge'nie Me'canique, France 3 EADS Space Transportation rue du ge'ne'ral, France
[73]	Dept. of Continuum Mechanics and Structural Analysis, Carlos III University of Madrid, Spain
[144]	Dept. of Civil and Environmental Engineering, Vanderbilt University, USA
[32]	Helsinki University of Technology, Dept. of Applied Mechanics Aeronautical Engineering
[145]	1 Japan Aersopace Exploration Agency 2 Japan Aircraft Development Corporation
[50]	1 Aerospace Engineering Group, Cranfield University, United Kingdom 2 Aerospace and Telecommunications Engineering Support Squadron, Canadian Forces Base Trenton, Canada 3 Composite Design and Manufacturing, Applied Materials, United Kingdom
[43]	George C. Marshall Space Flight Center
[47]	George C. Marshall Space Flight Center
[65]	1 Japan Aerospace Exploration Agency, Tokyo, Japan 2 MAZDA Motor Corporation, Hiroshima, Japan
[89]	1 Airframe Division, National Aerospace Laboratory, Japan 2 Dept. of Aerospace Engineering, Royal Melbourne Institute of Technology(RMIT), Australia
[11]	1 Dept. of Aeronautical and Automotive Engineering, Loughborough University, UK 2 Composites Research Centre, GKN Aerospace Engineering Services, UK
[27]	Wichita State University
[41]	Mechanics of Advanced Materials Research Group, Dept. of Continuum Mechanics and Structural Analysis, University Carlos III of Madrid, Spain
[66]	1 College of Mechatronics Engineering and Automation, National University of Defense Technology, PR China 2 School of Electrical and Electronic Engineering, Newcastle University, UK
[156]	1 School of Mechanical and Chemical Engineering, University of Western Australia, Australia 2 State Key Laboratory of Structural Analysis for Industrial Equipment, Dalian University of Technology, China
[157]	1 Turkish Airlines, Turkey 2 Kocaeli University, School of Civil Aviation, Turkey 3 TUBITAK-MAM, Materials Institute, Turkey
[158]	1 Dept. of Mechanical Engineering, Stony Brook University, USA 2 Dept. of Materials Science and Engineering, Stony Brook University, USA
[147]	Politecnico di Milano, Dipartimento di Meccanica, Italy

[159]	1 Dept. of Civil and Environmental Engineering, , University of Wisconsin, USA 2 Kestrel Aircraft Company, USA
[4]	1 Shanghai Jiao Tong University, China 2 University of Michigan, USA 3 Shanghai Jiao Tong University, China
[123]	1 Center for Composite Materials and Structures, Harbin Institute of Technology, China 2 Research Institute of Material Science and Technology, National University of Mar del Plata, Argentina 3 Institute of Textiles and Clothing, The Hong Kong Polytechnic University, China 4 Science and Technology on Reliability and Environment Engineering Laboratory, Beijing Institute of Structure and Environment Engineering, China
[100]	Materials Science and Engineering, University of Liverpool, UK
[12]	1 Sibley School of Mechanical and Aerospace Engineering, Cornell University, USA 2 Dept. of Mechanical and Aerospace Engineering, Syracuse University, USA
[159]	1 Dept. of Civil and Environmental Engineering, College of Engineering & Applied Science, University of Wisconsin, USA 2 Kestrel Aircraft Company, USA
[90]	Dept. of Aerospace and Lightweight Structures RWTH Aachen University, Germany
[108]	Dept. of Mechanical Engineering University of Utah, USA
[26]	Wichita State University, USA
[1]	Dept. of Aeronautical and Automotive Engineering Loughborough University, United Kingdom
[7]	Dept. of Aeronautical and Automotive Engineering Loughborough University, United Kingdom
[21]	NASA Langley Research Center
[40]	1 Dept. of Continuum Mechanics and Structural Analysis, University Carlos III of Madrid, Spain 2 Dept. of Industrial Technology, Simón Bolívar University, Venezuela
[96]	1 Dept. of Mechanical and Mechatronic Engineering, National Taiwan Ocean University, Taiwan 2 Dept. of Mechanical Engineering, Chung Hua University Taiwan
[67]	1 High Speed Railroad System Research Center, Korea Railroad Research Institute, Republic of Korea 2 R&D Center, ILJIN Global, Republic of Korea 3 School of Mechanical Engineering, Kunsan National University, Republic of Korea
[49]	1 Ecole Polytechnique de Montr eal, Laboratory for Multi-Scale Mechanics (LM2), Dept. of Mechanical Engineering, Canada 2 Canadian Space Agency, Dept. of Space Science and Technology, Canada
[101]	a ENSA, Equipe de mécanique et calcul Scientifique, Morocco b Laboratoire de mécanique, Biomécanique, Polymère, Structures (laBPS), France
[8]	Division of Mechanical Engineering, HANBAT National University, Republic of Korea
[125]	1 Applied Physics Laboratory The Johns Hopkins University, USA; Dept. of Mechanical Engineering, The Johns Hopkins University, USA 2 The United States Naval Academy, USA

[42]	Robert R. McCormick School of Engineering and Applied Science, Northwestern University, United States
[5]	Dept. of Mechanical Engineering, Imperial College London, UK
[3]	Dept. of Mechanical and Systems Engineering, Japan
[160]	Institute of Structures and Design, German Aerospace Center, Germany
[71]	1 Materials Division, AMR, Instituto de Aeronáutica e Espaço, Centro Técnico Aeroespacial, Brazil 2 Fatigue and Aeronautic Material Research Group, Dept. of Material and Technology, Brazil 3 Centro Universitário Salesiano de São Paulo - UNISAL, Brazil
[70]	Aeronautical and Maritime Research Laboratory
[161]	Defence Science and Technology Organisation, Australia
[108]	Dept. of Mechanical Engineering University of Utah
[158]	1 Dept. of Mechanical Engineering, Stony Brook University, United States 2 Dept. of Materials Science and Engineering, Stony Brook University, United States
[162]	Laboratoire de Physique des Milieux Denses, Metz, France;
[72]	Private University of Applied Sciences c/o Standort Hansestadt Stade Airbus, Germany
[146]	1 Applied Physics Laboratory The Johns Hopkins University USA 2 Dept. of Mechanical Engineering, The Johns Hopkins University, USA 3 The United States Naval Academy, USA
[163]	Université de Bordeaux, France
[164]	Mork Family Dept. of Chemical Engineering and Materials Science, United States
[165]	Faculty of Civil Engineering, Technion, Israel Institute of Technology, Israel
[166]	Centre for Polymer and Composites Research, Dept. of Mechanical Engineering, The University of Auckland, New Zealand.
[167]	Dept. of Continuum Mechanics and Structural Analysis, University Carlos III of Madrid, Spain
[168]	Dept. of Mechanical Engineering, Chung Hua University, Taiwan
[90]	Lehrstuhl und Institut für Leichtbau, RWTH Aachen University, Germany
[64]	Institut für Leichtbau, Germany
[39]	1 Structures and Materials Group, UK 2 GKN Aerospace Services, Cowes, UK
[169]	Institute of Structural Analysis, Germany
[170]	Institute of Applied Mechanics and Biomedical Engineering, China
[148]	KTH Engineering Sciences Dept. of Aeronautical and Vehicle Engineering , SWEDEN
[171]	1 Liaoning Key Laboratory of General Aviation & Liaoning Key Laboratory of Composite Manufacture technology, Shenyang Aerospace University, China; 2 State Key Laboratory of Materials Modification by Beams & School of Chemical Engineering, Dalian University of Technology, China; 3 Haerbin Aircraft Industrial (Group) Co., Ltd., China
[10]	National Institute of Aerospace
[172]	Technical Engineering College
[25]	NASA Langley Research Center Hampton
[74]	Dept. of Engineering, University of Cambridge, UK
[173]	Institute of Product Development and Mechanical Engineering Design Technische Universität Hamburg, Germany
[156]	1 School of Mechanical and Chemical Engineering, University of Western Australia , Australia

	2 State Key Laboratory of Structural Analysis for Industrial Equipment, Dalian University of Technology, PR China
[174]	U.S. Dept. of Transportation Federal Aviation Administration
[175]	1 School of Mechanical and Aerospace Engineering, UK 2 Dept. of Mechanical and Aerospace Engineering, Monash University, Australia
[29]	Dept. of Aeronautics and Astronautics, Air Force Institute of Technology, USA
[93]	Dept. of Mechanical Engineering, USA
[176]	Center for Composite Materials, Harbin Institute of Technology, China
[177]	1 Center for Composite Materials and Structures, Harbin Institute of Technology, China 2 Research Institute of Material Science and Technology (INTEMA), 3 National University of Mar del Plata (UNMdP), Argentina
[87]	1 Dept. of Aeronautical and Vehicle Engineering, Division of Lightweight Structures, Sweden 2 Section for Structural Integrity and Laboratories, Norway
[92]	1 Institute of Mechanical Engineering, Aalborg University, Denmark 2 Dept. of Mechanical Engineering, University of Strathclyde, UK

8 Conclusions

Current literature review have scrutinized more than 170 literature sources including scientific peer review articles, handbooks, standards of test methods, reports, material data sheets and open access data available on world wide web pages. Even though residual strength estimation for aluminum honeycomb core and CFRP face sheet sandwich panels damaged by low velocity impact was the topical for studying a collateral knowledge from related research has been accumulated. An overall observation suggested that current field of research due to it is relatively high complexity is only partly addressed with scattered and low resemblance research. During review were found most critical aspects in selecting appropriate raw materials (fibers, adhesives and cores), sandwich panels manufacturing and testing, approaches for introduction of artificial damage, residual strength estimation methods and non-destructive inspection. Even though the ASTM standard stand as industry standard still there is a lack of coherent residual assessment methodology and recent standard does not include even a set up conditions for the tests, only definition of failure modes.

Besides technical research formerly funded projects in current domain were researches were examined to outline industrial/academia involvement and funding organization are summarized. This was done to map the main “players” in this field of research in order to establish the informal cooperation by participating similar workshops and conferences. This should enable broader further dissemination activity by conference attendance and industry exhibitions. In general the main aim of researchers was to make their own investment in reliable and robust test method development for residual strength estimation of honeycomb sandwich panels.

Reviewing literature it becomes apparent that some authors were cited more often than others, among those are Tomblin, Zhou, Hill and McGowan. These researchers can be considered as flagships in development of honeycomb sandwich panel’s damage tolerance estimation and will be considered for scientific review of current project.

9 References

1. James CT. Numerical Modelling of the Compression-After- Impact Behaviour of Composite Sandwich Panels. 2015.
2. Bitzer T. *Honeycomb Technology*. Dublin; 1997. doi:10.1007/978-94-011-5856-5.
3. Yamashita MÃ, Gotoh M. Impact behavior of honeycomb structures with various cell specifications — numerical simulation and experiment. 2005;32:618-630. doi:10.1016/j.ijimpeng.2004.09.001.
4. Wang J, Waas AM, Wang H. Experimental Study on the Low-velocity Impact. 2012;(April):1-13.
5. Dear JPÃ, Lee H, Brown SA. Impact damage processes in composite sheet and sandwich honeycomb materials. 2005;32:130-154. doi:10.1016/j.ijimpeng.2005.02.005.
6. Chanda M, K.Roy S. *PLASTICS TECHNOLOGY HANDBOOK*. New York: CRC Press; 2006.
7. Hill MD. Damage resistance and tolerance investigation of carbon / epoxy skinned honeycomb sandwich panels. 2007.
8. Shin KB, Youl J, Cho SH. An experimental study of low-velocity impact responses of sandwich panels for Korean low floor bus. 2008;84:228-240. doi:10.1016/j.compstruct.2007.08.002.
9. Ory H, Reimerdes H, Garcia JG. The design of shells and tanks in the aerospace industry : some practica . I i aspects. 1998.
10. McQuigg T. Compression After Impact Experiments and Analysis on Honeycomb Core Sandwich Panels with Thin Facesheets. 2011;(June). http://ntrs.nasa.gov/archive/nasa/casi.ntrs.nasa.gov/20110013136_2011013649.pdf
<http://ntrs.nasa.gov/search.jsp?R=20110013136>.
11. Zhou G, Hill M. Damage Characteristics And Residual Compressive Strength Of Composite Honeycomb Sandwich Panels. *16th Int Conf Compos Mater*. 2007;3.
12. Czabaj MW, Zehnder AT. Compression After Impact of Sandwich Composite Structures : Experiments and Modeling. 2010;(April):1-16.
13. Gorss J. High performance carbon fibers. *Am Chem Soc*. 2003. <http://onlinelibrary.wiley.com/doi/10.1002/pen.760150306/abstract>.
14. Mraz S. Basics of Aerospace Materials : Aluminum and Composites.
15. Department of Defense. *Composite Materials Handbook - Volume 2: Polymer Matrix Composites, Material Properties*. Vol 2.; 2002.
16. HexTow. *HexTow* ® AS4. Vol 000.; 2015.
17. Hexcel. *HexTow* ® IM7.; 2014.
18. Torayca. *T300 Data Sheet Carbon*.
19. Toray. T300. doi:10.1007/s13398-014-0173-7.2.
20. Petit S, Bouvet C, Bergerot A, Barrau J. Impact and compression after impact experimental study of a composite laminate with a cork thermal shield. 1978.
21. MCGowan DM, Ambur DR. Compression Response of a Sandwich Fuselage Keel Panel With and Without Damage. 1997;(February).
22. MCGowan DM, Ambur DR. Damage characteristics and residual strength of composite sandwich panels impacted with and without compression loading. In: *39th AIAA/ASME/ASCE/AHS/ASC Structures, Structural Dynamics and*

- Materials Conference.* ; 1998.
23. Singh P, Saponara V La. Experimental Investigation on Performance of Angle- Stitched Sandwich Structures. :1-14.
 24. Nettles AT, Jackson JR. Developing a Material Strength Design Value Based on Compression After Impact Damage for the Ares I Composite Interstage. 2009;(January).
 25. Walker S. Sandwich Loads of Composite Panels Under Honeycomb Compressive at Elevated Temperatures. 1998;(April).
 26. Tomblin J, Lacy T, Smith B, Hooper S, Vizzini A, Lee S. Review of Damage Tolerance for Composite Sandwich Airframe Structures. 1999:71. doi:DOT/FAA/AR-99/49.
 27. Tomblin JS, Raju KS, Arosteguy G. Damage Resistance and Tolerance of Composite Sandwich Panels — Scaling Effects. 2004;(February).
 28. Bernard ML, Lagace PA. Impact Resistance of Composite Sandwich Plates. *J Reinf Plast Compos.* 1989;8(5):432-445. doi:10.1177/073168448900800502.
 29. Herup EJ, Palazotto AN. Low-velocity impact damage initiation in graphite/epoxy/Nomex honeycomb-sandwich plates. *Compos Sci Technol.* 1997;57(12):1581-1598. doi:10.1016/S0266-3538(97)00089-4.
 30. Lagace PA, Williamson JE, Wilson Tsang PH, Wolf E, Thomas S. A Preliminary Proposition for a Test Method to Measure (Impact) Damage Resistance. *J Reinf Plast Compos.* 1993;12(5):584-601. doi:10.1177/073168449301200508.
 31. Moody RC. Scaling and Curvature Effects on the Damage Tolerance of Impacted Composite Sandwich Panels. *J Sandw Struct Mater.* 2002;4(1):71-82. doi:10.1177/1099636202004001037.
 32. Wallin M, Saarela O. COMPRESSION STRENGTH OF NOTCHED AND IMPACT DAMAGED COMPOSITE LAMINATES. :1-9.
 33. Zonghong X, Vizzini AJ. ON RESIDUAL COMPRESSIVE STRENGTH PREDICTION OF COMPOSITE SANDWICH PANELS AFTER LOW-VELOCITY IMPACT DAMAGE. *Acta Mech Solida Sin.* 2006;19(1):9-17. doi:10.1007/s10338-006-0602-z.
 34. Wu CL, Sun CT. Low velocity impact damage in composite sandwich beams. *Compos Struct.* 1996;34(1):21-27. doi:10.1016/0263-8223(95)00127-1.
 35. Portanova MA, Poe CC, Whitcomb JD. TECHNICAL OPEN OF POST-IMPACT AND COMPOSITES COMPRESSION FATIGUE STITCHED CARBON / EPOXY. 1990.
 36. P. Tsang, Lagace P. Failure mechanisms of impact-damaged sandwich panels under uniaxial compression (AIAA). <http://arc.aiaa.org/doi/abs/10.2514/6.1994-1396>. Accessed March 22, 2016.
 37. LAGACE PA, MAMORINI L. Factors in the Compressive Strength of Composite Sandwich Panels with Thin Facesheets. *J Sandw Struct Mater.* 2000;2(4):315-330. doi:10.1106/9A4Y-DB9D-QLUM-G6KK.
 38. McGowan DM, Ambur DR. Damage-Tolerance Characteristics of Composite Fuselage Sandwich Structures with Thick Facesheets. 1997;(February).
 39. Meo M, Vignjevic R, Marengo G. The response of honeycomb sandwich panels under low-velocity impact loading. *Int J Mech Sci.* 2005;47(9):1301-1325. doi:10.1016/j.ijmecsci.2005.05.006.

40. Buitrago BL, Santiuste C, Sánchez-sáez S, Barbero E, Navarro C. Modelling of composite sandwich structures with honeycomb core subjected to high-velocity impact. *Compos Struct.* 2010;92(9):2090-2096. doi:10.1016/j.compstruct.2009.10.013.
41. Ivañez I, Sanchez-Saez S. Numerical modelling of the low-velocity impact response of composite sandwich beams with honeycomb core. *Compos Struct.* 2013;106:716-723. doi:10.1016/j.compstruct.2013.07.025.
42. Schubel PM, Luo J-J, Daniel IM. Impact and post impact behavior of composite sandwich panels. *Compos Part A Appl Sci Manuf.* 2007;38(3):1051-1057. doi:10.1016/j.compositesa.2006.06.022.
43. Nettles AT, Hodge AJ, Jackson JR. Simplification of Fatigue Test Requirements for Damage Tolerance of Composite Interstage Launch Vehicle Hardware. 2010;(June).
44. Turner KM, Vizzini AJ. Response of Impacted Sandwich Panels with Integral Stiffeners. *J Sandw Struct Mater.* 2004;6(4):313-326. doi:10.1177/1099636204035394.
45. Macdonald CD, Vizzini AJ. Response of Indented Sandwich Panels. *J Thermoplast Compos Mater.* 2002;15(1):33-41. doi:10.1106/089270502022861.
46. Reifsnider K, Sendekyj G, Wang S, et al. Compressive Strength of Composite Sandwich Panels After Impact Damage: An Experimental and Analytical Study. *J Compos Technol Res.* 1988;10(2):65. doi:10.1520/CTR10131J.
47. Nettles AT, Lance DG, Marshall C. The Effects of Compressive Preloads on the Strength of Carbon / Epoxy. 1992.
48. Ambur D, Cruz J. Low-speed impact response characteristics of composite sandwich panels. In: *36th Structures, Structural Dynamics and Materials Conference*. Vol 4. Reston, Virginia: American Institute of Aeronautics and Astronautics; 1995. doi:10.2514/6.1995-1460.
49. Martin F, Houle D, Lanouette A, Therriault D. Residual mechanical properties of a carbon fibers / PEEK space robotic arm after simulated orbital debris impact. 2015;84:78-87. doi:10.1016/j.ijimpeng.2015.05.010.
50. Zhang X, Hounslow L, Grassi M. Improvement of low-velocity impact and compression-after-impact performance by z-fibre pinning. 2006;66:2785-2794.
51. Maria J, Antolin M, Spearing M, Edgerton HE. Damage Characterization and Modeling of Notched Graphite / Epoxy Sandwich Panels in Compression by by. 1999.
52. Nettles AT, Hodge AJ. Impact testing of glass/phenolic honeycomb panels with graphite/epoxy facesheets. 1990;35. https://www.researchgate.net/publication/4668505_Impact_testing_of_glass_phenolic_honeycomb_panels_with_graphiteepoxy_facesheets. Accessed March 22, 2016.
53. Levin K. *Developments in the Science and Technology of Composite Materials*. (Bunsell AR, Lamicq P, Massiah A, eds.). Dordrecht: Springer Netherlands; 1989. doi:10.1007/978-94-009-1123-9.
54. Ferri R, Sankar B V. A Comparative Study on the Impact Resistance of Composite Laminates and Sandwich Panels. *J Thermoplast Compos Mater.* 1997;10(4):304-315. doi:10.1177/089270579701000401.

55. Soutis C, Spearing SM. Compressive response of notched, woven fabric, face sheet honeycomb sandwich panels. *Plast Rubber Compos.* July 2002. <http://www.tandfonline.com/doi/abs/10.1179/14658010225006369>. Accessed March 22, 2016.
56. Anderson T, Madenci E. Experimental investigation of low-velocity impact characteristics of sandwich composites. *Compos Struct.* 2000;50(3):239-247. doi:10.1016/S0263-8223(00)00098-2.
57. Davies GAO, Hitchings D, Besant T, Clarke A, Morgan C. Compression after impact strength of composite sandwich panels. 2004;63:1-9. doi:10.1016/S0263-8223(03)00119-3.
58. Hiel C, Ishai O. Design of highly damage-tolerant sandwich panels. *Int SAMPE Symp Exhib.* 1992:1228-1242. <http://adsabs.harvard.edu/abs/1992sampeymp.1228H>. Accessed March 22, 2016.
59. Freeman B, Schwingler E, Mahinfalah M, Kellogg K. The effect of low-velocity impact on the fatigue life of Sandwich composites. *Compos Struct.* 2005;70(3):374-381. doi:10.1016/j.compstruct.2004.09.027.
60. Lacy TE, Hwang Y. Numerical modeling of impact-damaged sandwich composites subjected to compression-after-impact loading. 2003;61:115-128. doi:10.1016/S0263-8223(03)00034-5.
61. Castanié B, Aminanda Y, Bouvet C, Barrau J. Core crush criterion to determine the strength of sandwich composite structures subjected to compression after impact. 2003;33(0).
62. Gustin J, Mahinfalah M, Jazar GN, Aagaah MR. Low-velocity Impact of Sandwich Composite Plates. 2004;(6). doi:10.1177/0014485104046090.
63. Tomblin J.S., Raju K.S, Acosta J.F., Smith B.L. RN. Impact Damage Characterization and Damage Tolerance of Composite Sandwich Airframe Structures – Phase II. 2002;(October).
64. Klaus M. Bending Strength of Sandwich Panels With Different Cores After Impact.
65. Aoki Y, Yamada K, Ishikawa T. EFFECTS OF WATER ABSORPTION AND (CAI) STRENGTH OF CFRP LAMINATES. :1-7.
66. He Y, Tian G, Pan M, Chen D. Non-destructive testing of low-energy impact in CFRP laminates and interior defects in honeycomb sandwich using scanning pulsed eddy current. *Compos Part B Eng.* 2014;59(June):196-203. doi:10.1016/j.compositesb.2013.12.005.
67. Kim J, Lee S, Jin J, Kang K. Estimation for probabilistic distribution of residual strength of sandwich structure with impact-induced damage. *Renew Energy.* 2013;54:219-226. doi:10.1016/j.renene.2012.08.006.
68. Matyjaszewski K. *Encyclopedia Of Polymer Science and Technology - Wiley Online Library.*; 1999. doi:10.1002/0471440264.
69. Hexcel. *HexPly® F650.*; 2005.
70. Vodicka R. Thermoplastics for Airframe Applications A Review of the Properties and Repair Methods for Thermoplastic Composites. *Def Sci Technol Organ.* 1996.
71. Costa ML, Botelho EC, Paiva JMF De, Rezende MC. Characterization of cure of carbon/epoxy prepreg used in aerospace field. *Mater Res.* 2005;8(3):317-322. doi:10.1590/S1516-14392005000300016.
72. Arbelo MA. *Technischer Bericht Entwicklung.*; 2013.

73. Barbero E, Zaera R, Navarro C. Compression after impact of thin composite laminates. :1-9.
74. Russell BP, Liu T, Fleck NA, Deshpande VS. The soft impact of composite sandwich beams with a square-honeycomb core. *Int J Impact Eng.* 2012;48:65-81. doi:10.1016/j.ijimpeng.2011.04.007.
75. Raju K, Tomblin J. Damage characteristics in sandwich panels subjected to static indentation using spherical indentors. In: *19th AIAA Applied Aerodynamics Conference*. Reston, Virginia: American Institute of Aeronautics and Astronautics; 2001. doi:10.2514/6.2001-1189.
76. Sikdar S, Banerjee S, Subhani SM. Detection of Disbond in a Honeycomb Composite Sandwich Structure Using Ultrasonic Guided Waves and Bonded PZT Sensors Shirsendu Sikdar 1,.
77. Horrigan DPW, Aitken RR, Moltschaniwskyj G. Modelling of Crushing Due to Impact in Honeycomb Sandwiches. *J Sandw Struct Mater.* 2000;2(2):131-151. doi:10.1177/109963620000200203.
78. Shahdin A, Morlier J, Mezeix L. Evaluation of the impact resistance of various composite sandwich beams by vibration tests. *Shock Vib.* 2011;18:789-805. doi:10.3233/SAV-2010-0597.
79. Mines RAW, Worrall CM, Gibson AG. LOW VELOCITY PERFORATION BEHAVIOUR OF POLYMER COMPOSITE SANDWICH PANELS. *Int J Impact Eng.* 1998;21(10):855-879. doi:10.1016/S0734-743X(98)00037-2.
80. Fagerberg L. Wrinkling and Compression Failure Transition in Sandwich Panels. *J Sandw Struct Mater.* 2004;6(2):129-144. doi:10.1177/1099636204030475.
81. Rhodes MD. Impact fracture of composite sandwich structures. May 1975. <http://ntrs.nasa.gov/search.jsp?R=19750048601>. Accessed March 22, 2016.
82. Sburlati R. The Effect of a Slow Impact on Sandwich Plates. *J Compos Mater.* 2002;36(9):1079-1092. doi:10.1177/0021998302036009536.
83. Bull PH, S. Hallstrom. High-Velocity and Quasi-Static Impact of Large Sandwich Panels. *J Sandw Struct Mater.* 2004;6(2):97-113. doi:10.1177/1099636204030468.
84. Kim C-G, Jun E-J. Impact Resistance of Composite Laminated Sandwich Plates. *J Compos Mater.* 1992;26(15):2247-2261. doi:10.1177/002199839202601504.
85. Torre L, Kenny J. Impact testing and simulation of composite sandwich structures for civil transportation. *Compos Struct.* 2000;50(3):257-267. doi:10.1016/S0263-8223(00)00101-X.
86. Edgren F, Asp LE, Bull PH. Compressive Failure of Impacted NCF Composite Sandwich Panels - Characterisation of the Failure Process. *J Compos Mater.* 2004;38(6):495-514. doi:10.1177/0021998304040559.
87. ZENKERT D, SHIPSHA A, BULL P, HAYMAN B. Damage tolerance assessment of composite sandwich panels with localised damage. *Compos Sci Technol.* 2005;65(15-16):2597-2611. doi:10.1016/j.compscitech.2005.05.026.
88. Hodge AJ, Nettles AT, Jackson JR. Comparison of Open-Hole Compression Strength and Compression After Impact Strength on Carbon Fiber / Epoxy Laminates for the Ares I Composite Interstage. 2011;(March).
89. Ishikawa T, Matsushima M, Keng E, Lim G, Hayashi Y, Scott ML. COMPRESSION AFTER IMPACT (CAI) BEHAVIOR OF CF / PIXA

- STIFFENED PANELS FOR HSCT EMPENNAGE.
90. Klaus M a, Reimerdes HG a, Gupta NK a b. Experimental and numerical investigations of residual strength after impact of sandwich panels. *Int J Impact Eng.* 2012;44:50-58. doi:10.1016/j.ijimpeng.2012.01.001.
 91. Akay M, Hanna R. A comparison of honeycomb-core and foam-core carbon-fibre/epoxy sandwich panels. *Composites.* 1990;21(4):325-331. doi:10.1016/0010-4361(90)90347-Y.
 92. Thomsen OT, Banks WM. An improved model for the prediction of intra-cell buckling in CFRP sandwich panels under in-plane compressive loading. *Compos Struct.* 2004;65(3-4):259-268. doi:10.1016/j.compstruct.2003.11.002.
 93. Vadakke V, Carlsson LA. Experimental investigation of compression failure of sandwich specimens with face/core debond. *Compos Part B Eng.* 2004;35(6-8):583-590. doi:10.1016/j.compositesb.2003.10.004.
 94. Mil-Hdbk-141. Military Standardization Handbook, Optical Design. 1987:16-18 of section 4.
 95. Hexcel. HexWeb A1 and A10 High strength aramid honeycomb - Product Data. 2007:1-4.
 96. Jen Y, Teng F, Teng T. Two-stage cumulative bending fatigue behavior for the adhesively bonded aluminum honeycomb sandwich panels. *Mater Des.* 2014;54:805-813. doi:10.1016/j.matdes.2013.09.010.
 97. Hexcel Composites. Honeycomb Attributes and Properties, A comprehensive guide to standard Hexcel honeycomb materials, configurations, and mechanical properties. *Honeycomb Data Sheets.* 1999:1-40.
<http://scholar.google.com/scholar?hl=en&btnG=Search&q=intitle:Honeycomb+attributes+and+properties#4>.
 98. Nguyen MQ, Jacombs SS, Thomson RS, Hachenberg D, Scott ML. Simulation of impact on sandwich structures. *Compos Struct.* 2005;67(2 SPEC. ISS.):217-227. doi:10.1016/j.compstruct.2004.09.018.
 99. Kee Paik J, Thayamballi AK, Sung Kim G. The strength characteristics of aluminum honeycomb sandwich panels. *Thin-Walled Struct.* 1999;35(3):205-231. doi:10.1016/S0263-8231(99)00026-9.
 100. Akil Hazizan M, Cantwell WJ. The low velocity impact response of an aluminium honeycomb sandwich structure. *Compos Part B Eng.* 2003;34(8):679-687. doi:10.1016/S1359-8368(03)00089-1.
 101. Abbadi A, Tixier C, Gilgert J, Azari Z. Experimental study on the fatigue behaviour of honeycomb sandwich panels with artificial defects. *Compos Struct.* 2015;120:394-405. doi:10.1016/j.compstruct.2014.10.020.
 102. Tsotsis TK, Lee SM. Characterization of Localized Failure Modes in Honeycomb Sandwich Panels Using Indentation Testing. In: *ASTM 12th Symposium on Composite Materials: Testing and Design.* Vol 1274. ; 1994. https://www.researchgate.net/publication/216452630_Characterization_of_Localized_Failure_Modes_in_Honeycomb_Sandwich_Panels_Using_Indentation_Testing. Accessed March 22, 2016.
 103. Kiratisaevae H. Low-velocity Impact Response of High-performance Aluminum Foam Sandwich Structures. *J Reinf Plast Compos.* 2005;24(10):1057-1072. doi:10.1177/0731684405048205.
 104. Spearing SM. COMPRESSIVE FAILURE OF NOTCHED GRAPHITE /

- EPOXY-HONEYCOMB SANDWICH PANELS.
105. Toribio MG, Spearing SM. Compressive response of notched glass- ® ber epoxy / honeycomb sandwich panels. 2001;32.
 106. Baral N, Carti R, Partridge K, Baley C, Davies P. Improved impact performance of marine sandwich panels using through- thickness reinforcement : Experimental results. *Compos Part B Eng.* 2010;41(2):117-123.
 107. Ratcliffe J, Jackson W, Schaff J. IMPACT-DAMAGED SANDWICH PANELS.
 108. Adams DO, Kuramoto B. Damage Tolerance Test Method Development for Sandwich Composites. *Composite.* 2011:1-13.
http://depts.washington.edu/amtas/events/jams_12/papers/paper-adams_damage.pdf.
 109. Hexcel. HexPly Prepreg Technology. *Hexcel Regist Trademark.* 2013:28.
 110. Isola Group. Prepreg Storage and Handling. 2008.
 111. MIL-HDBK-349. *Military Standardization Handbook Manufacture and Inspection of Adhesive Bonded , Aluminum Honeycomb Sandwich Assemblies.*; 1994.
 112. Prepreg. Prepreg Manufacturing Processes. doi:10.1149/1.2428454.
 113. Park electrochemical corp. LAYUP AND CURE OF EPOXY PREPREG.
 114. DEFENSE D. *ADHESIVE BONDEDAEROSPACE STRUCTURE REPAIR.*; 1982.
 115. Hexcell. REDUX BONDING TECHNOLOGY. *J Chem Inf Model.* 2003.
 doi:10.1017/CBO9781107415324.004.
 116. Cytec. Vta ® 260. :1-4.
 117. Cytec. AEROSPACE MATERIALS. 2013;(October 2013).
 118. 3M. Structural Adhesive Film. 2007:1-15.
 119. Redux. Redux ® 312.
 120. ASTM Standard. ASTM C364-08 Standard Test Method for Edgewise Compressive Strength of Sandwich Constructions. *ASTM Int.* 2012;(Reapproved):1-8. doi:10.1520/C0364.
 121. Duemas Technology LTD. Alluminium Honeycomb Expander.
http://www.duemas.com/cm_alu_honey_expanders.html#. Accessed February 24, 2016.
 122. Hexcel Composites. Sandwich panel fabrication technology. 2001;(May):1-16. doi:10.1016/0010-4361(78)90736-X.
 123. Xiong J, Zhang M, Stocchi A, et al. Mechanical behaviors of carbon fiber composite sandwich columns with three dimensional honeycomb cores under in-plane compression. *Compos Part B Eng.* 2014;60:350-358.
 doi:10.1016/j.compositesb.2013.12.049.
 124. Zhou □ G, Hill MD. Impact Damage and Energy-absorbing Characteristics and Residual In-plane Compressive Strength of Honeycomb Sandwich Panels.
 125. Roberts JC, Boyle MP, Wienhold PD, White GJ. Buckling, collapse and failure analysis of FRP sandwich panels. *Compos Part B Eng.* 2002;33(4):315-324. doi:10.1016/S1359-8368(02)00017-3.
 126. Klaus M, Structures L. Residual Strength Simulations of Sandwich Panels After Impact.
 127. D7136 A. Standard Test Method for Measuring the Damage Resistance of a

- Fiber-Reinforced Polymer Matrix Composite to a Drop-Weight Impact Event. *Analysis*. 2005;i:1-16. doi:10.1520/D7136.
128. Shipsha A, Zenkert D. Compression-after-Impact Strength of Sandwich Panels with Core Crushing Damage. *Appl Compos Mater*. 2005;12(3-4):149-164. doi:10.1007/s10443-005-1119-1.
 129. ASTM C365-03. ASTM C365-03 Standard Test Method for Flatwise Compressive Properties of Sandwich Cores 1. 2011:1-8. doi:10.1520/C0365.
 130. ASTM C363. Standard Test Method for Delamination Strength of Honeycomb Core Materials. 2009:1-4. doi:10.1520/C0363.
 131. ASTM Standard. ASTM C393-06 Standard Test Method for Core Shear Properties of Sandwich Constructions by Beam Flexure. *ASTM Int*. 2010;i(C):1-7. doi:10.1520/C0273.
 132. MIL-STD-401B. SANDWICH CONSTRUCTIONS AND CORE MATERIALS; GENERAL TEST METHODS. 1956;(September 1967).
 133. ASTM D5467. Standard Test Method for Compressive Properties of Unidirectional Polymer Matrix Composite Materials Using a Sandwich Beam. *ASTM Stand*. 2010:1-9. doi:10.1520/D5467.
 134. ASTM C297. Standard Test Method for Flatwise Tensile Strength of Sandwich Constructions 1. 2015;1(1):1-8. doi:10.1520/C0297.
 135. TH115. Climbing Drum Peel Test Fixture. 2015.
 136. D7137. Standard Test Method for Compressive Residual Strength Properties of Damaged Polymer Matrix Composite Plates. *ASTM Int*. 2012;i:1-17. doi:10.1520/D7137.
 137. Kepler J. Impact Penetration of Sandwich Panels at Different Velocities - An Experimental Parameter Study: Part I - Parameters and Results. *J Sandw Struct Mater*. 2004;6(4):357-374. doi:10.1177/1099636204038217.
 138. Davies P, Choqueuse D, Vemiolle P, Prevosto M, Genin D, Hamelin P. *Impact and Dynamic Fracture of Polymers and Composites*. Wiley. (Williams JG, Pavan A, eds.); 1995. <http://eu.wiley.com/WileyCDA/WileyTitle/productCd-0852989466.html>. Accessed February 12, 2016.
 139. Roach AM, Jones N, Evans KE. The penetration energy of sandwich panel elements under static and dynamic loading. Part II. *Compos Struct*. 1998;42(2):135-152. doi:10.1016/S0263-8223(98)00062-2.
 140. D7766. Standard Practice for Damage Resistance Testing of Sandwich Constructions 1. *Annu B ASTM*. 2013;i:1-9. doi:10.1520/D7766.
 141. Klaus M, Reimerdes H. Numerical investigation of different strength after impact test procedures. *Aerospace*. 2010.
 142. D6264. Standard Test Method for Measuring the Damage Resistance of a Fiber-Reinforced Polymer-Matrix Composite to a Concentrated Quasi-Static. 2014;(May):1-11. doi:10.1520/D6264.
 143. Aminanda Y, Castanie B, Barrau J-J, Thevenet P. Experimental and numerical study of compression after impact of sandwich structures with metallic skins. 2009;69:50-59. doi:10.1016/j.compscitech.2007.10.045.
 144. Yan H, Oskay C, Krishnan A, Xu LR. Compression-after-impact response of woven fiber-reinforced composites. *Compos Sci Technol*. 2010. doi:10.1016/j.compscitech.2010.08.012.
 145. Takatoya T, Sato Y, Susuki I, Tsuda N, Agency E, Corporation D.

- COMPRESSION AFTER IMPACT PROPERTIES OF.
146. Boyle M., Roberts J., Wienhold P., Bao G, White G. Experimental, numerical, and analytical results for buckling and post-buckling of orthotropic rectangular sandwich panels. *Compos Struct.* 2001;52(3-4):375-380. doi:10.1016/S0263-8223(01)00028-9.
 147. Gilioli A, Sbarufatti C, Manes A, Giglio M. Compression after impact test (CAI) on NOMEX™ honeycomb sandwich panels with thin aluminum skins. *Compos Part B Eng.* 2014;67:313-325. doi:10.1016/j.compositesb.2014.07.015.
 148. Lindström A. Strength of Sandwich Panels Loaded in In-plane Compression. 2007.
 149. Zenkert D. *An Introduction to Sandwich Construction.*; 1995. https://books.google.lv/books/about/An_Introduction_to_Sandwich_Construction.html?id=zc-GQgAACAAJ&pgis=1. Accessed March 16, 2016.
 150. Gustin J, Joneson A, Mahinfalah M, Stone J. LOW VELOCITY IMPACT OF COMBINATION KEVLAR / CARBON FIBER SANDWICH COMPOSITES.
 151. Sòphia High Tech s.r.l. <http://www.sophiahightech.com/en/fixtures-standard.php>. Accessed March 3, 2016.
 152. Innovative Test Solutions. <http://www.its-inc.com/subpageH.cfm?subPageID=38&mainPageID=2>. Accessed March 3, 2016.
 153. Moody RC, Vizzini AJ. Test and Analysis of Composite Sandwich Panels With Impact Damage.pdf.
 154. Lascoup B, Aboura Z, Khellil K, Benzeggagh M, Maquet J. On the interest of stitched sandwich panel. :1-10.
 155. Luklu BOŞ, Sandv Yİ, Tler İÇKİ, Sonrasi D, Tirmasi SŞ, Cao H. COMPRESSION AFTER IMPACT OF 3-D INTEGRATED HOLLOW CORE SANDWICH COMPOSITES. 2011:16-21.
 156. Shi S, Sun Z, Hu X, Chen H. Flexural strength and energy absorption of carbon-fiber–aluminum-honeycomb composite sandwich reinforced by aluminum grid. *Thin-Walled Struct.* 2014;84:416-422. doi:10.1016/j.tws.2014.07.015.
 157. Akatay A, Bora MÖ, Çoban O, Fidan S, Tuna V. The influence of low velocity repeated impacts on residual compressive properties of honeycomb sandwich structures. *Compos Struct.* 2015;125:425-433. doi:10.1016/j.compstruct.2015.02.057.
 158. Alkhader M, Iyer S, Shi W, Venkatesh TA. Low frequency acoustic characteristics of periodic honeycomb cellular cores: the effect of relative density and strain fields. *Compos Struct.* 2015;133:77-84. doi:10.1016/j.compstruct.2015.07.102.
 159. Yang P, Shams SS, Slay A, Brokate B, Elhajjar R. Evaluation of temperature effects on low velocity impact damage in composite sandwich panels with polymeric foam cores. *Compos Struct.* 2015;129:213-223. doi:10.1016/j.compstruct.2015.03.065.
 160. Aktay L, Johnson AF, Holzapfel M. Prediction of impact damage on sandwich composite panels. *Comput Mater Sci.* 2005;32(3-4):252-260. doi:10.1016/j.commatsci.2004.09.044.
 161. Wang J, Callinan R. Residual strengths of composite structures subjected to ballistic impact. *Compos Struct.* 2014;117:423-432.

- doi:10.1016/j.compstruct.2014.07.006.
162. Arbaoui J, Schmitt Y. NUMERICAL SIMULATION AND EXPERIMENTAL BENDING BEHAVIOUR OF MULTI-LAYER SANDWICH STRUCTURES Jamal Arbaoui. 2014:431-442.
 163. Catapano A, Montemurro M. A multi-scale approach for the optimum design of sandwich plates with honeycomb core. Part I: homogenisation of core properties. *Compos Struct.* 2014;118:664-676.
doi:10.1016/j.compstruct.2014.07.057.
 164. Centea T, Grunenfelder LK, Nutt SR. A review of out-of-autoclave prepregs – Material properties, process phenomena, and manufacturing considerations. *Compos Part A Appl Sci Manuf.* 2015;70:132-154.
doi:10.1016/j.compositesa.2014.09.029.
 165. Frostig Y. Classical and high-order computational models in the analysis of modern sandwich panels. *Compos Part B Eng.* 2003;34(1):83-100.
doi:10.1016/S1359-8368(02)00073-2.
 166. Horrigan D, Aitken R. Finite element analysis of impact damaged honeycomb sandwich. *FEA Ltd Surrey UK.* 1998;(1):1-14.
http://lusas.co.uk/pdf/CS503_FEA_of_Impact_Damaged_Honeycomb_Panels.PDF.
 167. Ivañez I, Moure MM, Garcia-Castillo SK, Sanchez-Saez S. The oblique impact response of composite sandwich plates. *Compos Struct.* 2015;133:1127-1136. doi:10.1016/j.compstruct.2015.08.035.
 168. Jen YM, Chang LY. Effect of thickness of face sheet on the bending fatigue strength of aluminum honeycomb sandwich beams. *Eng Fail Anal.* 2009;16(4):1282-1293. doi:10.1016/j.engfailanal.2008.08.004.
 169. Kriegesmann B, Hilburger MW, Rolfes R. The Effects of Geometric and Loading Imperfections on the Response and Lower-Bound Buckling Load of a Compression-Loaded Cylindrical Shell. *53rd AIAA/ASME/ASCE/AHS/ASC Struct Struct Dyn Mater Conf 20th AIAA/ASME/AHS Adapt Struct Conf 14th AIAA.* 2012:1-10. doi:10.2514/6.2012-1864.
 170. Li X, Zhang P, Wang Z, Wu G, Zhao L. Dynamic behavior of aluminum honeycomb sandwich panels under air blast: Experiment and numerical analysis. *Compos Struct.* 2014;108(1):1001-1008.
doi:10.1016/j.compstruct.2013.10.034.
 171. Lu C, Zhao M, Jie L, et al. Stress Distribution on Composite Honeycomb Sandwich Structure Suffered from Bending Load. *Procedia Eng.* 2015;99:405-412. doi:10.1016/j.proeng.2014.12.554.
 172. Mohammed F. Experimental and Numerical Analysis of AA3003 Honeycomb Sandwich Panel with Different Configurations. 2015;(6):25-32.
doi:10.5251/ajsir.2015.6.2.25.32.
 173. Seemann R, Krause D. Numerical modelling of nomex henoycomb cores for detailed analysis of sandwich panel joints. *16th Eur Conf Compos Mater.* 2014;(Wccm Xi).
 174. Stanley L, Adams D. Damage Tolerance of Composite Sandwich Structures. *Int SAMPE Symp.* 2001;46(May):1947-1957.
 175. Tan W, Falzon BG, Chiu LNS, Price M. Predicting low velocity impact damage and Compression-After-Impact (CAI) behaviour of composite laminates. *Compos Part A Appl Sci Manuf.* 2015;71:212-226.
doi:10.1016/j.compositesa.2015.01.025.

176. Wang B, Wu L-Z, Ma L, Feng J-C. Low-velocity impact characteristics and residual tensile strength of carbon fiber composite lattice core sandwich structures. *Compos Part B Eng.* 2011;42(4):891-897.
doi:10.1016/j.compositesb.2011.01.007.
177. Xiong J, Ma L, Stocchi A, Yang J, Wu L, Pan S. Bending response of carbon fiber composite sandwich beams with three dimensional honeycomb cores. *Compos Struct.* 2014;108(0):234-242.
doi:<http://dx.doi.org/10.1016/j.compstruct.2013.09.035>.